DEVELOPMENT OF FRAGILITY FUNCTIONS FOR CODE CONFORMING LOW-RISE REINFORCED CONCRETE BUILDINGS

by

Erkan Şenol

B.S., Civil Engineering, Kocaeli University, 2016

Submitted to Kandilli Observatory and Earthquake Research Institute
in partial fulfillment of the requirements for the degree of
Master of Science

Graduate Program in Earthquake Engineering

Boğaziçi University

2021

ACKNOWLEDGEMENTS

This study has been possible with the help and support of a few valuable people. Firstly, I would like to express my gratitude to my thesis supervisor Ufuk Hancılar for his support, guidance, direction, and friendly approach during the preparation of my thesis and also for all opportunities which he provided to me during my master education.

Secondly, I would like to express my deepest thanks to my close friend and second brother Mahir Çetin for his wise support in all my master education. He is a great engineer and always helps me with every aspect of my life. His most important feature is his approach to problems in school and life-related issues and his ability to offer solutions in accordance with the level of the person in front of him.

I wish to thank my teacher and friend Aylin Ünaldı for her motivation and patience during the learning of English.

I also thank my valuable and wise friend Yasin Yorulmaz for his motivation and help since 2008.

Finally, I should also thank Eray Şenol, Ali Osman Bingöl, Hakan Süleyman, Zeynep Eda Önder, Şahin Özdoğan Dede, Aslıhan Yolcu, and Esra Huriye Koç.

ABSTRACT

DEVELOPMENT OF FRAGILITY FUNCTIONS FOR CODE CONFORMING LOW-RISE REINFORCED CONCRETE BUILDINGS

In this study, fragility functions are developed and compared for low-rise (2 and 3-story), reinforced concrete (RC), moment-resisting frame (MRF) buildings, which are designed per the Turkish Seismic Codes (TSC) released in 1998 and 2018, at eight different locations in Istanbul, Turkey.

In the preliminary design of each building, the minimum conditions defined in the corresponding seismic code are followed. Moreover, the capacity design principles are taken into consideration as defined in the seismic codes. To increase the representativeness of the dimensions (i.e., footprint, structural member dimensions, story height) of the buildings, the past studies about the characteristics of the low-rise buildings in Turkey, and the structural drawings belonging to the existing buildings designed per the corresponding seismic codes are examined and used.

Considering eight different locations, two different story numbers, and two seismic codes, a total of 32 buildings are designed and analyzed. The nonlinear analyses of the buildings are conducted by using the OpenSees Software (Open System for Earthquake Engineering Simulation Pacific Engineering Research (PEER) Center Version 3.0.3). The structural elements (beams and columns) are modeled with frame elements. The distributed plasticity (fiber) is considered for the columns whereas lumped plasticity (plastic hinge) is considered for beams.

To generate the fragility functions for the buildings, multiple stripe analysis (MSA) together with the maximum likelihood estimation (MLE) method is utilized. Spectral displacement (Sd) and spectral acceleration (Sa) are selected as the intensity measure (IM) parameters whereas the maximum inter-story drift ratio (MIDR) and top displacement (Dtop) are used as engineering demand parameters (EDP). The fragility functions are developed for four damage states which are slight damage, moderate damage, extensive damage, and complete damage. While deciding the limit values of the EDPs for each damage state, we perform pushover analysis to decide the limit values of top displacements from the idealized pushover curves. With regards to the limit values of MIDR, they are taken from Hazus MR4 Technical Manuel, which is defined for low-rise, high-code MRF structures. For MSA, eleven intensity measure levels (stripes) are defined, and for each stripe, 22 pairs of ground motion records are selected and used. To select the ground motion records for each stripe, a code-based target response spectrum is developed for each IM level. By making use of the developed response spectra for each IM, 22 pairs of ground motion records are selected from PEER Ground Motion Database for each IM level (stripe).

The fragility functions based on the different types of IMs (Sa and Sd) and the different types of EDPs (MIDR and Dtop) are developed and compared for the 2 and 3-story low-rise RC buildings designed per TSC1998 and TSC2018.

ÖZET

DEPREM YÖNETMELİKLERİNE GÖRE TASARLANMIŞ AZ KATLI BETONARME BİNALARIN KIRILGANLIK FONKSİYONLARININ TÜRETİLMESİ

Bu çalışmada, İstanbul ilinde bulunan 8 farklı konum için iki farklı deprem yönetmeliği (1998 Türk Deprem Yönetmeliği ve 2018 Türkiye Bina Deprem Yönetmeliği) kullanılarak, az katlı (2 ve 3 katlı) moment aktaran betonarme çerçeve binalar tasarlanıp kırılganlık eğrileri oluşturulup karşılaştırılmıştır.

Bina modellerinin, İstanbul'daki az katlı moment aktaran betonarme çerçeve binaların geometrik ve malzeme özelliklerini temsil edebilmesi için Türkiye'de yapılmış bina stoğunun karakteristiğini araştıran daha önce yapılmış çalışmalar ve mevcut az katlı binaların proje çizimleri incelenmiştir. Binaları tasarlarken yeniden ön boyutlandırma yapılarak kontrolleri yapılmış ve iki farklı yönetmeliğin minimum malzeme ve tasarım koşulları dikkate alınmıştır.

İki farklı kat sayısı, 8 farklı konum ve 2 farklı yönetmelik dikkate alınarak toplamda 32 adet bina tasarlanmıştır. Binaların, doğusal olmayan dinamik analizleri OpenSees v3.0.3 yazılımında 3 boyutlu çubuk elemanlar kullanılarak gerçekleştirilmiştir. Kolon elemanları yayılı plastik davranış modeliyle, kiriş elemenları ise yığılı plastik mafsal modeli kullanılarak modellenmiştir.

Doğrusal olmayan dinamik analizler için maksimum olabilirlik fonksiyonu (MLE) kullanılarak çoklu çizgi analizi (MSA) tercih edilmiştir. Şiddet ölçüsü olarak spektral ivme (Sa) ve spektral yer değiştirme (Sd) kullanılırken binaların davranışlarını ölçmek

için mühendislik talep parametresi olarak maksimum göreli kat ötelenmesi (MIDR) ve çatı yer değiştirmesi (Dtop) kullanılmıştır. Binalarda meydana gelen hasarlar; hafif, orta, şiddetli ve yıkıcı hasar olmak dört kademede sınıflandırılmıştır. Hasar ölçülerinin limit değerlerini tanımlamak için iki farklı parametre kullanılmış olup, çatı yer değiştirmesi için limit değerleri belirlerken statik itme analizi, maksimum göreli kat ötelenmesi için limit değerleri belirlerken ise Hazus MR4 teknik el kitabından elde edilen maksimum göreli kat ötelenmesi limit değerleri kullanılmıştır. Çoklu çizgi analizi (MSA) için 11 adet şiddet ölçü (IM) düzeyi belirlenip her bir IM seviyesine uygun olarak 11 adet tasarım spektrumu oluşturulmuştur. Ardından her bir tasarım spektrumu düzeyine uygun 22 adet yer hareketi çifti PEER Yer Haraketi Veritabanı kullanılarak seçilmiştir.

Bu tez kapsamında 1998 ve 2018 yönetmeklerine göre tasarlanmış 2 ve 3 katlı binalar için iki farklı şiddet ölçüsü (Sa ve Sd) ve iki farklı mühendislik talep paratmetresi (Dtop ve MIDR) kullanılarak kırılganlık eğrileri elde edilip karşılaştırılmıştır.

TABLE OF CONTENTS

LIST OF FIGURES

LIST OF TABLES

LIST OF SYMBOLS

g	gravitational acceleration, 9.80665 m/s^2
$\phi(\ )$	Standard normal cumulative distribution function (CDF)
β	Standard deviation of lnIM
Θ	median of the fragility function (the IM level with 50 percent probability of collapse)
Π	Mathematical constant, approximately equal to 3.14159
Ss	Coefficient of map spectral acceleration corresponding to the T=0.2-second-short period
S_1	Coefficient of map spectral acceleration corresponding to the T=1.0-second-long period
T_1	First-mode period
$(V_s)_{30}$	Shear wave velocities at 30 m below the top of the soil layer

LIST OF ACRONYMS/ABBREVIATIONS

2-D	Two Dimensional
3-D	Three Dimensional
AI	Arias intensity
ASCE	American society of civil engineers
ATC	Applied Technology Council
CAV	Cumulative absolute velocity
C1L	Low-rise concrete moment frame
CDF	Cumulative distribution function
CP	Collapse prevention
DS	Damage state
EDP	Engineering demand parameter
ELF	Equivalent Lateral Force
EMS98	European Macroseismic Scale
FE	Finite element
FL	Failure limit
FEMA	Federal Emergency Management Agency
G	Dead load
HAZUS	Hazards United States
IDA	Incremental dynamic analysis
IM	Intensity measure
IO	Immediate occupancy
kN	Kilonewton
LS	Life safety
m	Meter
MFA	Maximum floor acceleration
MIDR	Maximum interstory drift ratio
MLE	Maximum likelihood estimation
ML	Minimum damage limit

MPR	Maximum plastic end rotation
MMI	Modified Mercalli Intensity
MRF	Moment resisting frame
MPa	Megapascal
MSA	Multiple stripe analysis
M_W	Moment magnitude
NAFZ	North Anatolian Fault Zone
NRHA	Nonlinear response history analysis
PEER	Pacific Earthquake Engineering Research
PGA	Peak ground acceleration
PGV	Peak ground velocity
Q	Live load
RC	Reinforced concrete
R_{JB}	Joyner-Boore distance
SL	Safety limit
s	Second
S_a	Spectral acceleration
S_d	Spectral displacement
S_v	Spectral velocity
SCWB	Strong column weak beam
S_{D1}	Design spectral acceleration coefficient for long period
S_{DS}	Design spectral acceleration coefficient for short period
TSC	Turkish Seismic Code

1. INTRODUCTION

Earthquake is one of the natural disasters that have big effects on social and economic life. In cities with high populations, earthquakes can cause severe consequences such as life and monetary losses due to structural damages. Turkey has several active faults which are very close distance to metropolitan cities like Istanbul and Izmir. North Anatolian Fault Zone (NAFZ) under the Sea of Marmara threatens the metropolitan city of Istanbul which is such a city that provides educational, economical, and social opportunities which, in turn, give rise to migrations from all over the country. This situation makes governments take precautions against the possible natural hazards, particularly against large earthquakes. Since the buildings, particularly those constructed before the 2000s, did not take enough engineering service at the design and construction phases, the capacities of these structures are thought not to satisfy the possible large seismic demands. Governments want to decrease the hazardous effect of large earthquakes and want to be prepared in case one occurs.

In Turkey, urban transformation and retrofit of buildings are seen, by the government, as two important options to decrease the effects of seismic hazards. With the help of urban transformation, first, risky buildings are demolished, and new buildings are constructed. At this phase, research on structures to assess their earthquake performance comes into prominence especially when the seismic gap at NAFZ is considered.

Earthquake risk assessment has an important role for governments that want to be prepared for earthquakes. With the help of earthquake risk assessment, locations, where losses may be seen with a high percentage, are determined, and measures for reducing the seismic risks are taken to decrease the big losses such as monetary loss and casualties. Earthquake hazard, fragility, and inventory of assets that are subjected to hazards are major determinants of seismic risk assessment [1].

Fragility function is a cumulative distribution function that shows the probability of exceeding an unwanted damage limit such as safety and failure limits against

an intensity measure (IM) like peak ground acceleration (PGA), peak ground velocity (PGV), spectral acceleration (Sa), and spectral displacement (Sd). Fragility functions (curves) help authorities to detect risky structures and to take decisions to minimize the effects of future hazardous earthquakes. Derivation and comparison of fragility functions (curves) for low-rise reinforced concrete (RC) buildings, which are designed according to the 1998 and 2018 Turkish seismic codes (TSC) considering various locations in Istanbul, is the subject of this thesis.

This section continues with a short description of the four methods to develop fragility functions and gives the main elements of them. Then a literature survey is summarized by considering the studies about seismic risk assessment in Turkey. Finally, this chapter completes with the scope and objectives of the thesis.

1.1. Four Methods for Obtaining Fragility Functions

Fragility function (curve) is a cumulative distribution function (CDF) that shows the probability of a building exceeding a damage limit such as safety and failure limits against a ground motion intensity measure (IM) like Sd and Sa or peak ground motion intensity parameters (PGA, PGV, etc.). There are four methods to obtain a fragility function, which are, in decreasing reliability, empirical, analytical, expert opinion or judgmental, and hybrid methods [2].

Empirical (observational) fragility functions are generated by using post-earthquake results and observations. Although the most realistic results are obtained from this method, it has some disadvantages such as the lack of real earthquakes with high magnitudes that the analysts can exploit.

Analytical (predicted) fragility functions are obtained by analyzing the mathematical analytical models of buildings. Analysts can scale the ground motions to represent large earthquakes or can simulate ground motions when there are not enough recorded accelerograms. Analysts can make some assumptions when using this method, but they must be careful not to include unrealistic parameters in the analyses.

The judgmental fragility functions are generated by making use of expert opinions. Experts know failure. Their thoughts about failures are collected in a pool and used. The main drawback of this method is its lack of credibility.

In the hybrid methods, fragility functions are generated by using the combination of the methods explained above. For instance, the analytical method can be used to generate fragility functions for collapse limit state while the empirical method is used to generate fragility function for light limit damage state.

1.2. Elements of Fragility Functions

Structural model, damage state, and intensity measure are the three main elements of fragility functions [3]. Typology of structures is also an important parameter since the structures' features play a crucial role in obtaining the correct fragility function. The geometry of the building, the height of the story, material properties, seismic code, and structural system also affect the fragility function's character. For example, for the same building, different design parameters due to earthquake codes differentiate the fragility functions. Moreover, region-to-region fragility functions show big changes due to soil and design parameters. Story number is also an important factor and is considered by the analysts to obtain its effect on the structures. Buildings with high story numbers have high damage levels [4].

Damage state (DS) is an important element of fragility function. For instance, minimum damage limit (ML), safety Limit (SL), and failure limit (FL) are damage limits defined by the Turkish seismic codes (TSC) 2007. Damage states are classified as minor, moderate, substantial, or complete, according to FEMA 356 [5]. Limit values of damage states are related to the level of engineering demand parameters (EDPs) that are used to measure the response. EDPs are classified as global and local demand parameters. While base shear, top displacement, roof drift ratio, maximum inter-story drift ratio (maximum inter-story drift normalized by story height) are examples of global engineering demand parameters, strain and chord rotation are examples of local demand parameters. EDPs should be appropriate with the structure's behavior. The

analyst should be careful not to select ill-defined EDPs. For example, while base shear force is not an appropriate EDP for structures with high periods, the inter-story drift ratio is a meaningful measure for ductile structures.

Intensity measure (IM) is another important element of fragility function. Peak ground motion intensity values (PGA, PGV, etc.), spectral values (Sa, Sd) for the first natural vibration period, arias intensity (AI), cumulative absolute velocity (CAV) are the examples of intensity measures [6]. AI and CAV are energy-based parameters. IM should be efficient and sufficient. Intensity measures should be selected attentively, and the response of structures (EDP) should be well correlated with the intensity measures. For instance, low-rise and brittle structures' EDPs are convenient with peak ground acceleration (PGA) whereas spectral displacement (Sd) and spectral acceleration (Sa) are good IMs for ductile structures. Sa(T1) is a very prevalent intensity measure in developing fragility curves.

Spectral acceleration with the five percent damping ratio for the first mode is not fully sufficient when an analyst uses the high scale factor for ground motion records to obtain collapse state especially for the structures that are designed according to high codes [7].

In a fragility plot, the vertical axis indicates the cumulative probability of structural damage reaching or exceeding the threshold of a given damage state and the horizontal axis shows the ground motion intensity measure [6]. An example of a fragility curve is shown in Figure 1.1.

1.3. Literature Survey

There are plenty of studies about the derivation of fragility functions to evaluate the probabilistic structural assessment of structures. The literature survey at this study is focused on the studies that are related to the structures in Turkey.

Duran (2020) developed fragility functions (curves) for mid-rise, no-code RC

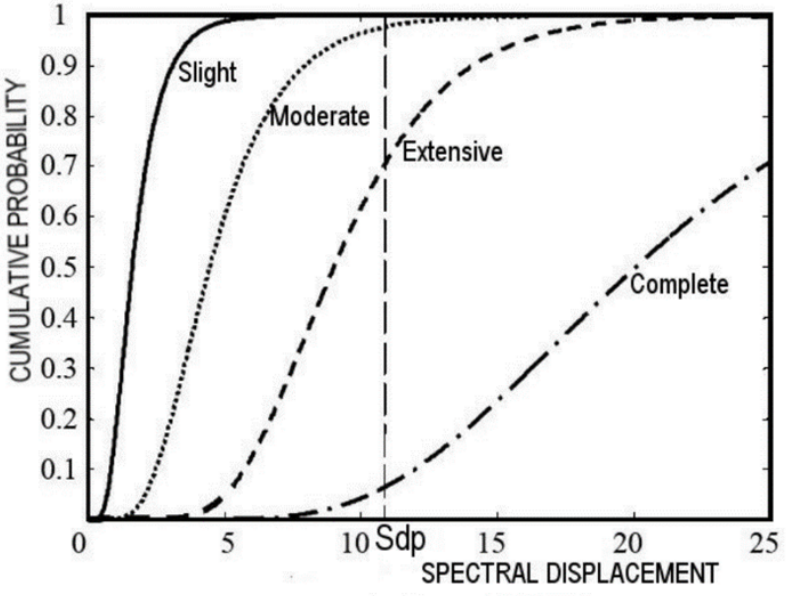

Figure 1.1. Example of fragility curves.

frame structures. He used sixteen different types of buildings to represent the typologies of 800 buildings that are located in the district of Zeytinburnu in Istanbul. He classified the buildings into two groups according to the confinement conditions of their structural members, namely, confined and unconfined. He used the maximum interstory drift ratio (MIDR) as engineering demand parameter (EDP), and peak ground acceleration (PGV) as intensity measure (IM). He utilized incremental dynamic analysis (IDA) and nonlinear static analysis (pushover) to evaluate the responses of the buildings, he compared the responses that are obtained from these two types of analyses. He used the maximum likelihood method to obtain the fragility curves [3].

Akkar et al. (2005) generated fragility functions for low and mid-rise reinforced concrete buildings. Thirty-two reinforced concrete buildings with 2 and 3-stories were analyzed. These buildings represent the typology of buildings that were affected by the 1999 Düzce earthquake in Turkey. Fragility functions were obtained by using the hybrid method. When generating fragility functions, the lateral deformation capacity, strength, and stiffness of the buildings are obtained from the field observation database.

He performed nonlinear response history analysis (NRHA). He used the global(roof) drift ratio as EDP and PGV as intensity measures because of its good correlation with the response of these types of buildings. The author indicated that the story number of buildings is an important parameter when developing fragility function [4].

Hancılar et al. (2014) generated fragility functions for mid-rise RC frames and RC shear buildings that were constructed in the 1990s. Fifty-five public school buildings in Istanbul were examined in this study and a standardized school building was modeled. Material and geometrical properties and dimensions of the structural elements were considered aleatory uncertainty, while the direction of ground motion excitation was considered epistemic uncertainty. The Monte Carlo approach was used in the study to see the effects of these uncertainties. The analytical method was used for generating the fragility functions. 107 earthquake records were utilized for the nonlinear dynamic analyses of the buildings. Five damage states (no damage, slight, moderate, extensive, complete) and three intensity measures (PGA, PGV, Sd (T1)) were used to develop fragility curves. The maximum inter-story drift ratio was also selected as the engineering demand parameter. This study showed that the uncertainties and control mechanisms to implement the standards have big effects on the fragility functions of buildings [8].

Kırçıl and Polat (2006) developed fragility functions for mid-rise RC frame buildings which were designed according to the 1975 Turkish seismic code (TSC 1975). Buildings were classified by their story numbers. (3-, 5-, 7- story). Yielding and collapse limits were chosen for damage levels. Maximum inter-story drift ratio (MIDR) was used as the engineering demand parameter to measure structures' response and first mode spectral acceleration, spectral displacement, and peak ground acceleration were used as the intensity measures. Incremental dynamic analyses were performed. The limit of yield capacity was defined as a point when the linear IDA curve became nonlinear, while the limit of collapse capacity was defined as a point when little increment of spectral acceleration leads to infinite MIDR. Fragility curves were developed based on Sa, Sd, and PGA as IM [9].

Tüzün (2008) developed analytical fragility curves for RC-MRF structures with story numbers ranging between two to seven. Building data were gathered from the existing RC frame buildings in Bolu, Turkey. He classified these structures into six groups according to their story numbers. Fragility curves were developed by using the analytical method. Spectrum-based ground motions were used for nonlinear dynamic analysis. He scaled the records with 0.05 g increments up to 1.00 g fır IDA. The Park-Ang damage index was used to define the damage levels. Sa(T1) and Sd(T1) were used as intensity measures. He showed that the near-field effect of ground motion, material uncertainty, and structural geometry has important effects on the fragility curves [10].

Dolağan (2019) generated fragility functions for mid-rise RC frame buildings which do not conform to any seismic code released after 1975. She used sixteen different types of buildings to represent the typologies of 800 buildings which are located in the district of Zeytinburnu in Istanbul. Nonlinear time-history analyses of the buildings were conducted with the use of OpenSees. She utilized incremental dynamic analysis (IDA) to evaluate the responses of the buildings. PGA was chosen as the intensity measure due to its convenience with pre-code structures' responses, and the maximum inter-story drift ratio was used as the engineering demand parameter. Damage levels were defined as strain values of structural members by considering TSC 2018. She indicated that structure's low geometrical and material quality cause early dynamic instability [11].

Hancılar and Çaktı (2015) studied the correlation between the engineering demand parameters (EDPs) and ıntensity measures (IMs). Buildings were classified by their story numbers as 5-, 10-, 15-, and 20- stories in this study. Unscaled ground motion records were used for nonlinear time history analysis (NRHA) to develop fragility curves. In this study, peak ground acceleration, velocity, and displacement (PGA, PGV, PGD), spectral acceleration, velocity, and displacement for first mode vibration period (Sa(T1), Sv(T1), Sd(T1)), arias intensity (AI), cumulative absolute velocity (CAV) were used as intensity measures. Maximum plastic end rotation (MPR), strain, maximum inter-story drift ratio (MIDR), maximum floor acceleration (MFA) were used as engineering demand parameters by the authors. According to this study, maximum

inter-story drift ratio and plastic end rotation are well correlated with the first mode spectral acceleration for 5,10-story buildings, while for 15, 20-story buildings, maximum inter-story drift ratio, and plastic end rotation demand parameters show a good correlation with PGV. For low-rise buildings, peak ground acceleration is also well correlated with MFAs [6].

From the literature surveys, we conclude that there are various ways to develop fragility functions (curves). Intensity measure, engineering demand parameter, structure typology, material properties, geometrical configuration, ground motion selection, design code rules, etc. are the factors that affect fragility functions. Difference, deficiency, and uncertainty of any of these components can lead to different results when creating the fragility function. While defining damage states, analysts can prefer global or local engineering demand levels according to their time and effort. Some researchers may define the limit of engineering demand parameters by using capacity curves by converting the capacity curves to bilinear elastic-perfectly curves with the equal energy principle. Damage thresholds can be obtained by using yield and ultimate spectral displacement values.

Methods that are used to generate fragility functions are another factor that leads to different results. Most accurate results are obtained from the empirical method which does not give reliable results for high magnitude earthquakes. The analytical method is the second most chosen method to develop an accurate fragility curve.

Different building's finite element (FE) models also lead to different fragility functions. Since 2D models are easy to develop, analysts often prefer to use them but, they cause more uncertainties than 3D models.

1.4. Scope and Objective of Thesis

RC frame buildings are the most prevalent structure type in Turkey due to the high speed and low cost of construction. With the rapid urbanization, the number of RC-MRF structures in the metropolitan city of Istanbul increased quickly in the

last three decades. North Anatolian Fault Zone (NAFZ) threatens a lot of buildings in Istanbul. Buildings constructed before the 2000s should be carefully analyzed in terms of their earthquake performances because most of these structures did not take engineering service or were not controlled by the technical people who check the conformity of earthquake codes. For these reasons, earthquake risk assessment of RC-MRF buildings needs to be determined and the results should be shared with governments to take precautions for future earthquakes.

This study aims to develop fragility curves for low-rise RC-MRF buildings at eight different locations in Istanbul. These buildings are designed with minimum requirements in TSC 1998 and TSC 2018, and the results are compared. Two and three-story buildings are taken into consideration to represent the low-rise buildings. Considering eight different locations, two different story numbers, and two seismic codes (TSC 1998, TSC 2018), 32 buildings are modeled and designed. These structures are classified into four groups: 2-story designed per TSC 1998, 2-story designed per TSC 2018, 3-story designed per TSC 1998, 3-story designed per TSC 2018.

To conduct nonlinear analyses, the 3-D mathematical building models are generated by using OpenSees 3.0.3 version (Open System for Earthquake Simulation). Distributed plasticity is considered along the columns, whereas lumped plasticity is used at the end of the beams to represent the nonlinear behavior of members. Cross-sections of members are modeled by using fibers. Multiple stripe analysis (MSA) is performed to obtain the response of the buildings for the defined intensity levels. For every building model, 11 stripes are defined by using code-based spectra. Twenty-two real ground motion record pairs are selected from PEER Strong Motion Database (https://peer.berkeley.edu/) for each stripe. Spectral displacement (Sd) and spectral acceleration (Sa) are used as intensity measures, while maximum inter-story drift ratio (MIDR) and top displacement are used for engineering demand parameters.

Although this study is done for a specific region (Istanbul), the results of the study reflect the properties of the buildings all over the country.

2. STRUCTURAL SYSTEMS AND GROUND MOTION SELECTION

2.1. Definition of Structural Models

In this study, we develop and compare the fragility functions for low-rise RC buildings designed per 1998 TSC and 2018 TSC. The buildings are designed by the author considering the corresponding seismic codes. In the phase of the development of generic building types, examples of structural drawings for low-rise RC buildings, which are designed per 1998 TSC, are taken from Kadıköy Municipality. The structural dimensions and the material properties in these drawings are used to develop the generic building types. Moreover, the past studies about the characteristics of the low-rise buildings in Turkey are examined [12].

To increase the representativeness of the dimensions (i.e., footprint, structural member dimensions, story height, slab thickness) of the buildings, the past studies about the characteristics of the low-rise buildings in Turkey, and the structural drawings belonging to the existing buildings designed per the corresponding seismic codes are examined and used.

Eight locations in the city of Istanbul, which are shown with red bubbles in Figure 2.1, are selected, and 2 and 3-story buildings are designed according to the seismic hazard parameters in these locations. Location coordinates and the corresponding shear wave velocities to 30 meter ,$(Vs)_{30}$, are listed in Table 2.1. A total of 32 buildings (2 different story numbers, 2 different seismic design codes, and 8 different locations) are modeled and designed. The plans of the buildings with 2 and 3-stories are given in Figure 2.2. The 3D finite element (FE) models of the buildings are given in Figure 2.3.

Buildings are modeled and designed according to the minimum conditions of 1998

Figure 2.1. Eight locations in Istanbul.

Table 2.1. Location parameters.

Location ID	Coordinates	$(\mathrm{Vs})_{30}[m/s]$
1	28.705, 41.045	178
2	28.125, 41.070	313
4	29.050, 40.990	666
5	29.130, 40.870	514
6	29.235, 40.890	784
7	28.910, 41.050	293
8	29.155, 41.085	619
10	29.030, 41.115	1250

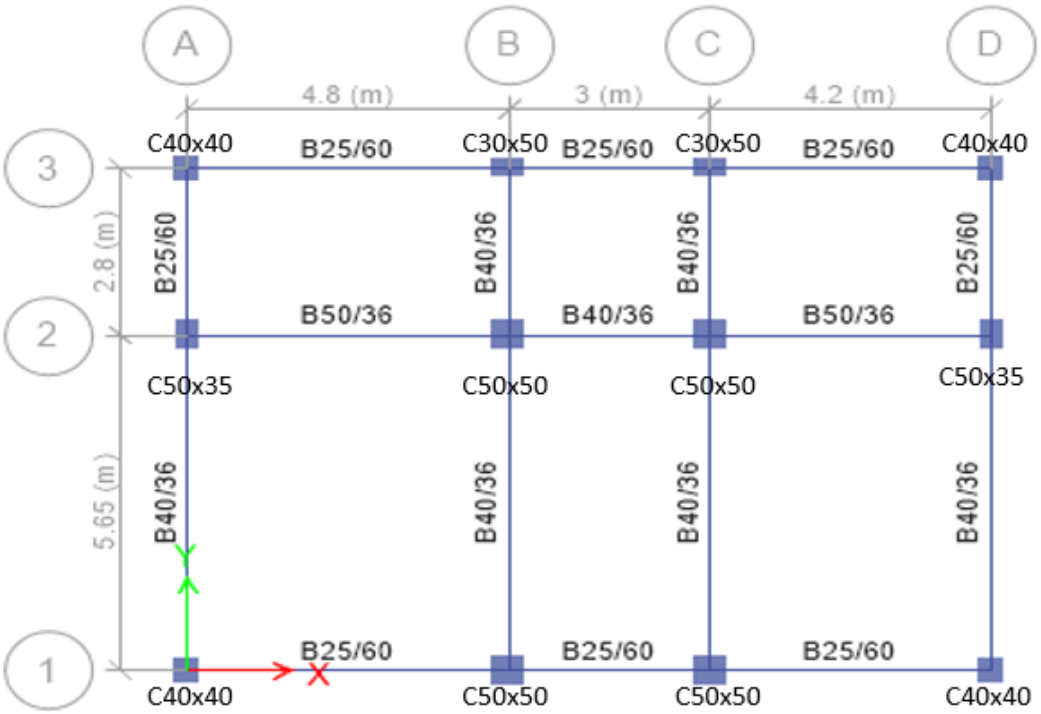

(a)

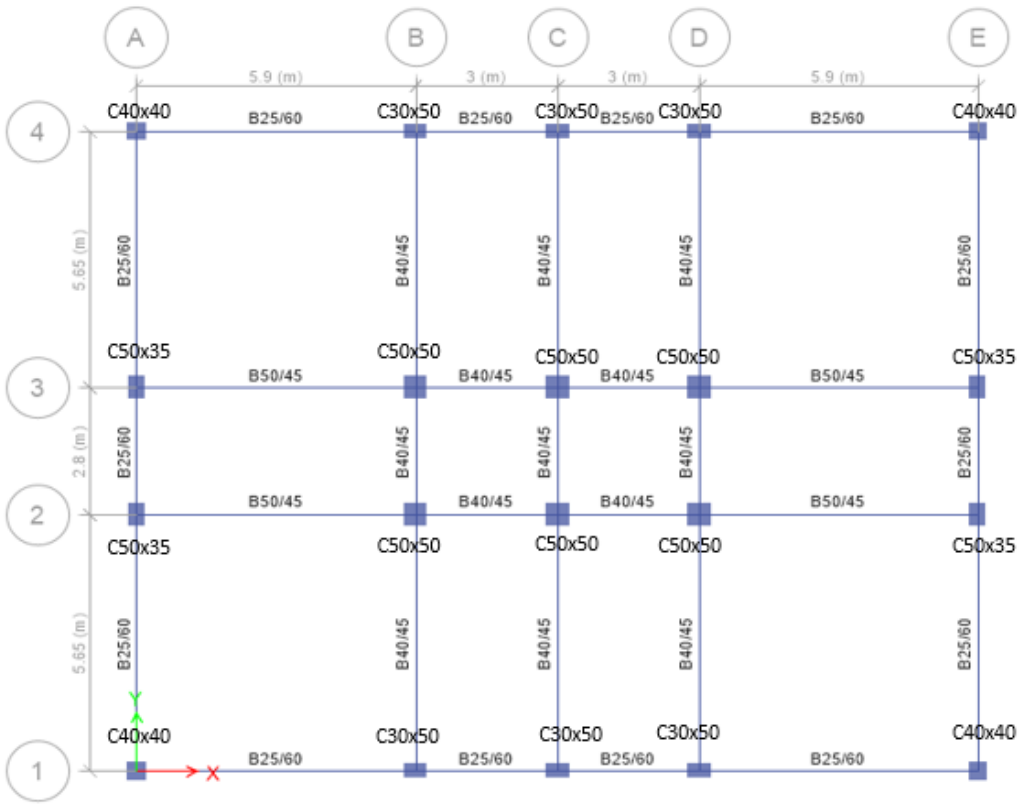

(b)

Figure 2.2. (a) Plan of 2-story buildings, (b) Plan of 3-story buildings.

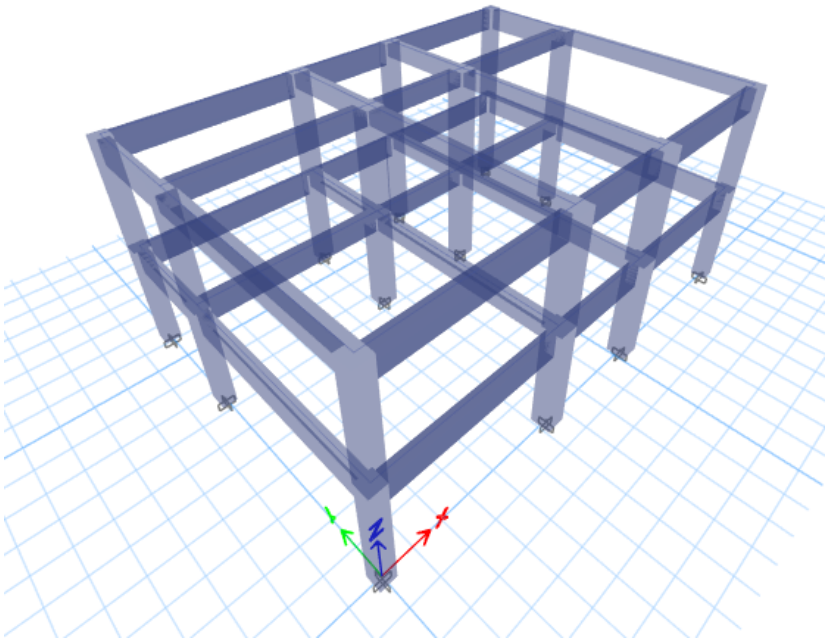

(a)

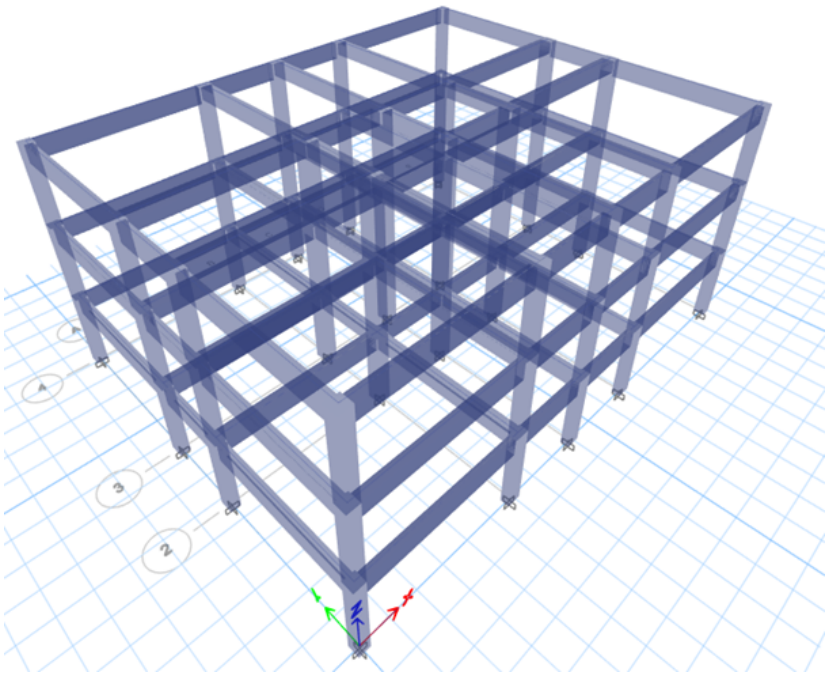

(b)

Figure 2.3. (a) The representative FE model of 2-story buildings, (b) The representative FE model of 3-story buildings.

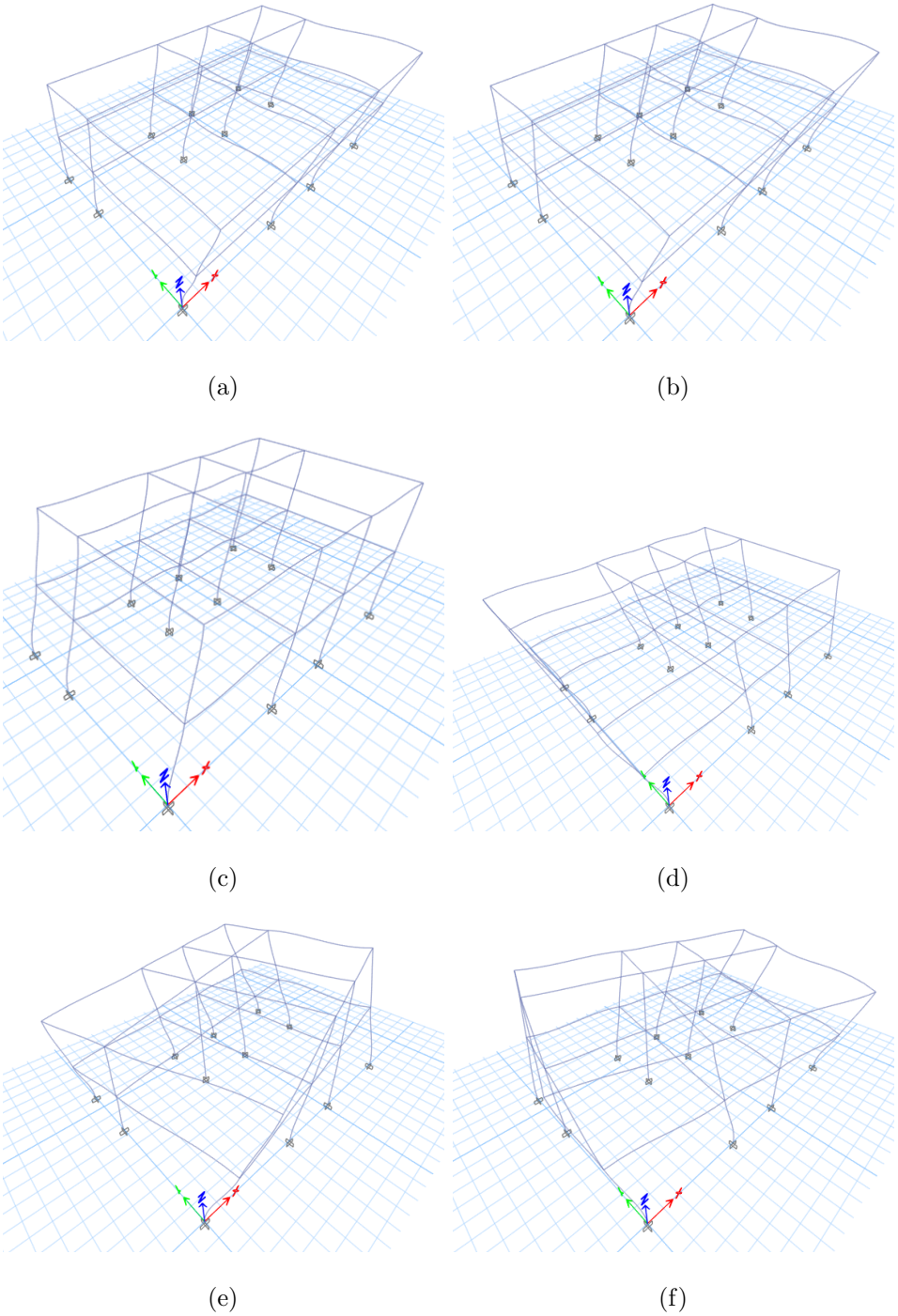

(a) (b)

(c) (d)

(e) (f)

Figure 2.4. The first three mode shapes of 2-story buildings designed per 1998 TSC (left) and 2018 TSC (right). The top row shows the first modes, the last row shows the third modes.

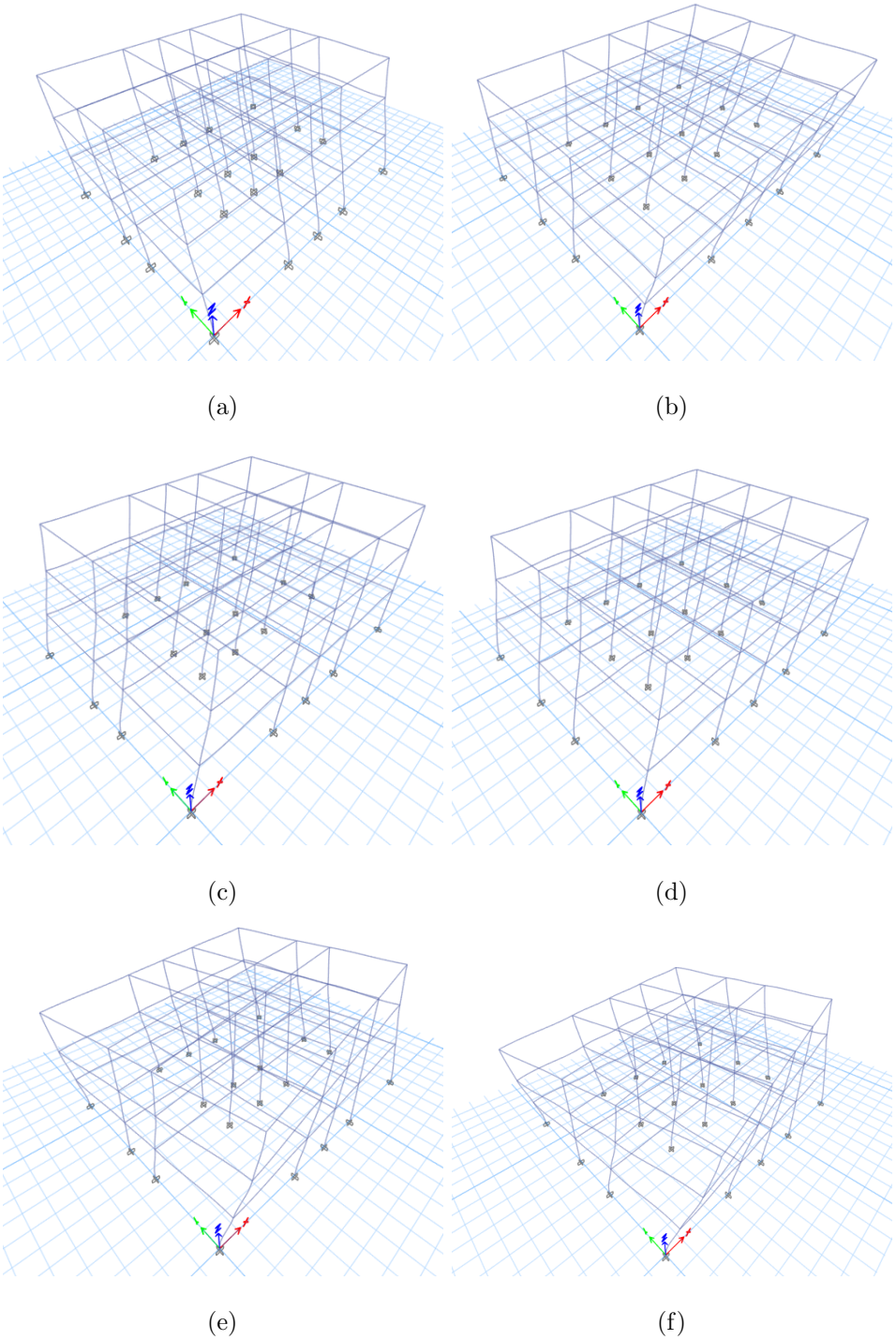

(a) (b)

(c) (d)

(e) (f)

Figure 2.5. The first three mode shapes of 3-story buildings designed per 1998 TSC (left) and 2018 TSC (right). The top row shows the first modes, the last row shows the third modes.

TSC and 2018 TSC. Design parameters for two earthquake codes are given in Table 2.2. ETABS software is utilized for modeling and analyzing the buildings in the preliminary design phases [13]. The equivalent lateral force (ELF) method is utilized for the linear analyses of the buildings. The first three mode shapes of 2 and 3-story buildings are shown in Figures 2.4 and 2.5. The free vibration periods of the 2 and 3-story buildings are given in Table 2.3. In the TSC 1998, the use of the cracked section stiffness of elements is not compulsory. Thus, the buildings which are designed according to the TSC 1998 have shorter free vibration periods although their concrete strength and the corresponding elasticity modulus values are lower than the buildings which are designed according to the TSC 2018.

The capacity design principles are taken into consideration at the design phase. By considering the capacity design approach, the nonlinear ductile behavior at the load-carrying system is ensured so the energy of an earthquake is damped with the deformation of structural members that are designed as ductile. Failures from shear deformations are sudden and non-ductile, while failures due to bending are slow and ductile. By increasing the shear capacity of the structural members, failure from brittle forces is avoided. During an earthquake, the structural internal-forces increase but thanks to the capacity design principles, the structural members safely respond in a ductile manner by using their inelastic deformation capacities. The shear force capacity of the structural members should be designed so that the bending type yielding is ensured.

The principle of the strong column-weak beam (SCWB) is satisfied. Furthermore, beam-column joints are designed to have sufficient shear capacity to transfer moments between frame members.

2.2. Differences Between 1998 TSC and 2018 TSC for Low-Rise RC MRF Buildings

There are some differences between these two seismic codes and in this section, the differences, which are encountered during the design phases of the buildings, are

Table 2.2. Design parameters.

Design Parameters	TSC,1998	TSC,2018
Concrete Class	C20	C25
Reinforcing Steel Grade	S420	S420
Building usage purpose	Residential	Residential
h basement, m	2.9	2.9
h normal, m	2.9	2.9
Footprint Area, m^2	101.4(for 2-story)	101.4(for 2-story)
Footprint Area, m^2	250.98(for 3-story)	250.98(for 3-story)
Slab thickness, mm	120.0(for 2-story)	120.0(for 2-story)
Slab thickness, mm	150.0(for 3-story)	150.0(for 3-story)
Type of The Lateral Load Resisting System	MRF	MRF
Super-imposed Dead Load, kN/m^2	2	2
Peripheral wall load, kN/m^2	4.325	4.325
Interior wall load, kN/m^2	2.5	2.5
Live Load, kN/m^2	2	2
Super-imposed Dead Load (roof), kN/m^2	4	4
Live Load (roof), kN/m^2	1.5	1.5
Analysis Type	ELF method	ELF method

Table 2.3. The free vibration periods of the buildings in seconds.

	First Mode	Second Mode	Third Mode
2-story,1998	0.234	0.210	0.192
2-story,2018	0.309	0.277	0.245
3-story,1998	0.399	0.375	0.358
3-story,2018	0.540	0.506	0.496

emphasized.

The first important difference is the updated seismic hazard map of Turkey. For each location in Turkey, with the new seismic hazard map, instead of the seismic zones, Ss and S_1 values, which are the spectral acceleration coefficients corresponding to the T=0.2-second-short period and T=1.0-second-long period, respectively, are defined. By multiplying the spectral acceleration coefficients with the soil effect coefficients, design spectral acceleration coefficients (S_{DS} and S_{D1}) are obtained and the lateral elastic design spectrum is developed depending on these values. However, in TSC 1998, a single acceleration coefficient (A_0) depending on the earthquake zone is used.

The second important difference is the definition of the local soil class. In the 2018 seismic code, five soil classes are defined as ZA, ZB, ZC, ZD, ZE to represent the soils from best to worst, while according to the 1998 earthquake code, the soils are classified from Z1 to Z4 and these soil classes are determined according to the soil groups (A, B, C, D) which represents the soil properties from best to worst.

The third major difference is the building performance objective and design approaches. In the TSC 2018, according to the seismic design category and building height class, building performance objective is determined, then design approach is selected for new buildings. Strength-based design and deformation-based design are the two design approaches in the TSC 2018. Considering the strength-based design approach, a new factor that is named the over-strength factor is added to TSC 2018. According to the structure's feature, the over-strength factor is determined and with the use of the over-strength factor, forces on members that behave as non-ductile are multiplied with the over-strength factor, and so the behavior of these members is limited to be elastic. With the strength-based design approach in the TSC 2018, the use of the cracked section stiffness of elements has become compulsory.

At the phase of the design of RC structural members, there are also some differences between the two seismic codes. One of them is the minimum concrete class. According to the TSC 2018, the minimum allowed concrete class is C25, whereas C20

is the minimum concrete class in TSC 1998. The other one is the column section dimensions; according to the TSC 2018, the minimum column section dimension is 300 mm, while 250 mm is used as the minimum column section dimension in TSC 1998.

2.3. Nonlinear Modelling

The 3-D FE models of the buildings are generated by the use of OpenSees Software (Open System for Earthquake Engineering Simulation Pacific Engineering Research Center Version 3.0.3) for nonlinear analyses. Columns are modeled by using the "nonlinearBeamColumn" element of the software. nonlinearBeamColumn command considers distributed plasticity along the line element, and distributed plasticity methods allow yielding at any integration point along the element length. Five number of Gauss integration points along the column elements are considered. Beams are modeled by using the "beamWithHinges" element of the software. "beamWithHinges" command makes plasticity spread along the plastic hinge regions. The examples of stress-strain histories generated using the concrete04 and steel02 models are shown in Figure 2.6.

The cross-sections of the structural members are divided into several numbers of fibers (20x20 fibers for core and cover concrete, 1 fiber for longitudinal reinforcement). For the concrete model, the "Concrete04" material of OpenSees software is used for the core and cover concrete. This command "Concrete04" is used to generate the same concrete model proposed by Mander et al. (1988). The tensile strength of the concrete model is neglected. For the reinforcement model, the "Steel02" material of OpenSees software is used. This reinforcing material command constructs a uniaxial Giuffre-Menegotto-Pinto steel material object with isotropic strain hardening [14].

The fiber section is used for modeling the inelastic behavior of elements and by using the "section Aggregator" OpenSees software command, torsional and shear behavior of sections are considered as elastic and are implemented in the analyses.

The slab and foundation are not modeled in this study, but the weight of slabs is

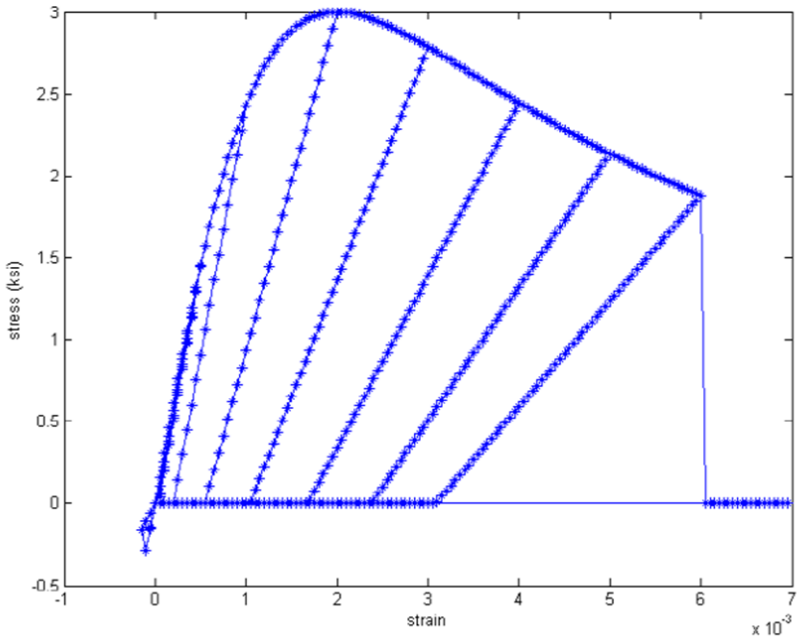

(a)

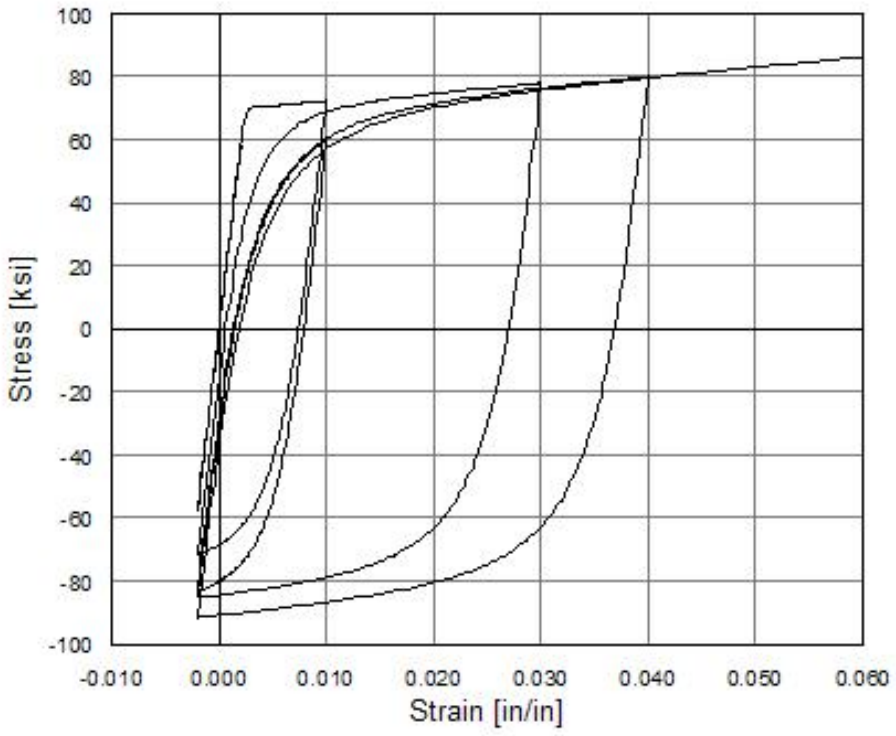

(b)

Figure 2.6. (a) Stress-strain model for concrete04 (Opensees 3.0.3 user command -language manuel), (b) Hysteretic behavior of steel02 model w/o isotropic hardening (Opensees 3.0.3 user command -language manual).

considered in gravity analysis. Degrees of freedom of columns at the foundation level are fixed. A rigid diaphragm is assigned to floors to consider the in-plane behavior of slabs and to transmit the seismic loads to the columns.

Masses are considered as dead load and 30 percent of live load (G+0.3Q) and implemented at nodes at every floor level. Rayleigh damping is used as a five percent damping ratio for the 1st and 3rd modes.

The P-Delta effect is taken into account in the analyses to consider the second-order effects.

2.4. Ground Motion Selection and Scaling

In this study, to generate fragility functions, multiple stripe analysis is used. A sufficient number of ground motions records are needed to get a credible structural response. For non-linear dynamic analysis, the use of 11 pairs of ground motions has been recommended as per ATC-58 [7] [15]. In this study, to generate one of the fragility curves for each building, eleven stripes are defined to represent intensity measure levels, Sa(T1). Each of these stripes consists of 22 pairs of ground motion records. To select the ground motion records for each stripe, firstly, a code-based target response spectrum is developed for each IM level. Secondly, with the help of each defined target response spectrum, 22 pairs of ground motion records are selected from PEER Ground Motion Database (https://peer.berkeley.edu/).

According to earthquake ground motion levels with 43, 72, 475, and 2475 years return periods, 4 design spectra have been obtained considering the location and the soil class of the buildings from the Disaster and Emergency Management Authority (AFAD) (https://www.afad.gov.tr/). Then the spectral acceleration values for the fundamental periods of the buildings are determined for 4 design spectra (DD4,Sa(T1) = 0.525 g, DD3,Sa(T1) = 0.756 g, DD2,Sa(T1) = 1.08 g, DD1,Sa(T1) = 1.314 g). Four lateral elastic design spectra are illustrated in Figure 2.7.

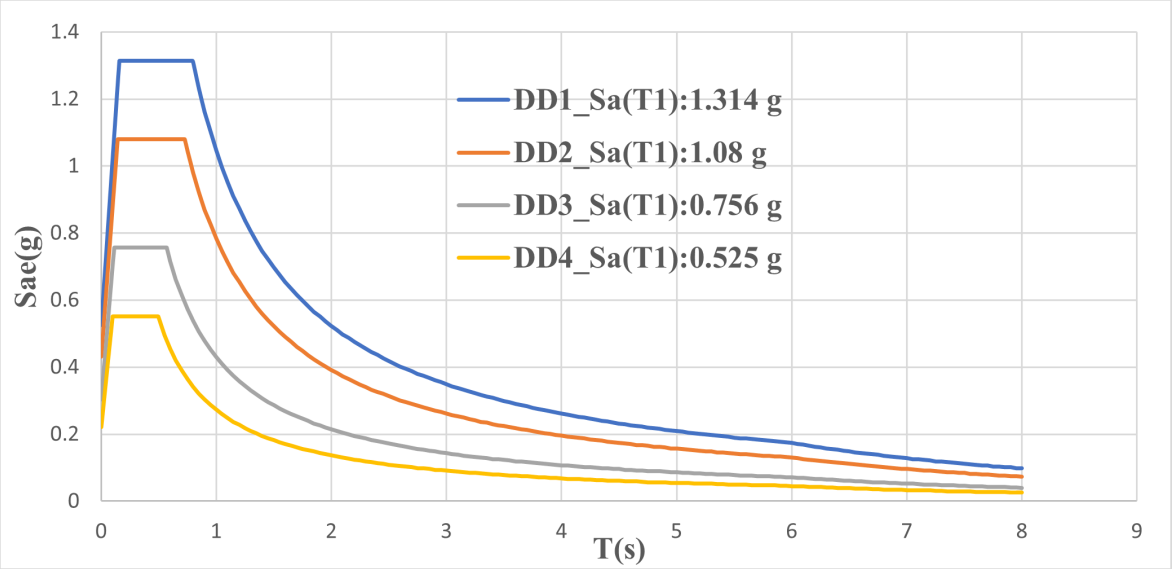

Figure 2.7. 5% damped horizontal elastic design spectra.

11 stripes (IM levels) are created between 0.1 g and 2.90 g with the increments of 0.30 g (0.1 g, 0.25 g, 0.50 g, 0.8 g, 1.10 g, 1.40 g, 1.70 g, 2.00 g, 2.30 g, 2.60 g, and 2.90 g). To select ground motions, a design spectrum for each IM level is created. While creating the 11 design spectra for each IM level, DD1, DD2, DD3, and DD4 earthquake ground motion levels are scaled to obtain eleven IM levels (0.1 g, 0.25 g, 0.50 g, 0.8 g, 1.10 g, 1.40 g, 1.70 g, 2.00 g, 2.30 g, 2.60 g, and 2.90 g). Eleven scaled lateral elastic design spectra are given in Figure 2.8.

When creating the design spectra for the eleven IM levels, the design spectrum for the intensity measure of Sa(T1)=0.1 g is developed by scaling the DD4 spectrum whose Sa(T1) value is 0.525 g, the design spectrum for the intensity measure of Sa(T1)=0.25 g is developed by scaling the DD4 spectrum whose Sa(T1) value is 0.525 g, the design spectrum for the intensity measure of Sa(T1)=0.50 g is developed by scaling the DD4 spectrum whose Sa(T1) value is 0.525 g, the design spectrum for the intensity measure of Sa(T1)=0.80 g is developed by scaling the DD3 spectrum whose Sa(T1) value is 0.756 g, the design spectrum for the intensity measure of Sa(T1)=1.10 g is developed by scaling the DD2 spectrum whose Sa(T1) value is 1.08 g, the design spectrum for the

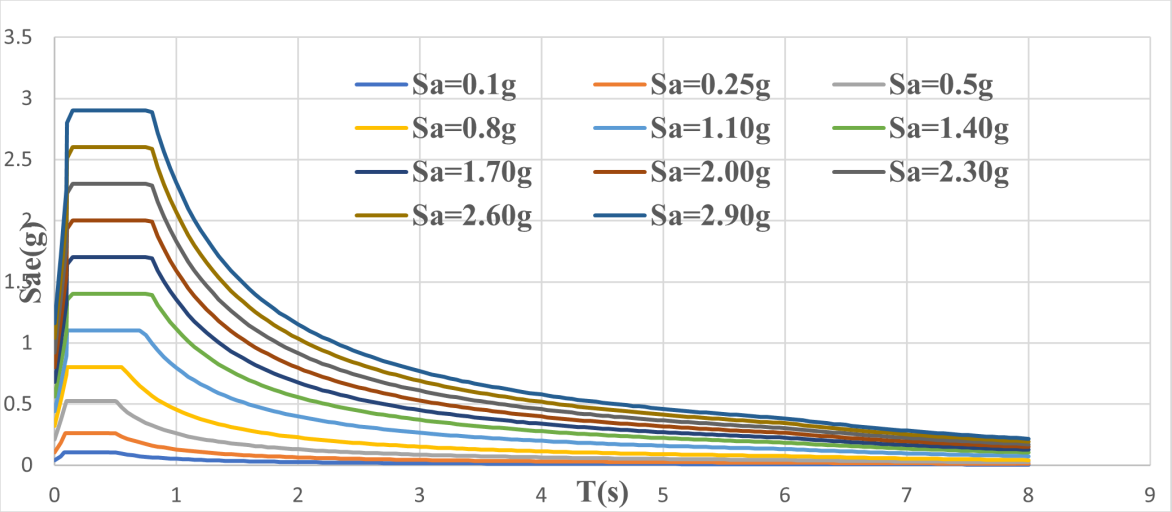

Figure 2.8. Scaled lateral elastic design spectra.

intensity measure of Sa(T1)=1.40 g is developed by scaling the DD1 spectrum whose Sa(T1) value is 1.314 g, the design spectrum for the intensity measure of Sa(T1)=1.70 g is developed by scaling the DD1 spectrum whose Sa(T1) value is 1.314 g, the design spectrum for the intensity measure of Sa(T1)=2.00 g is developed by scaling the DD1 spectrum whose Sa(T1) value is 1.314 g, the design spectrum for the intensity measure of Sa(T1)=2.30 g is developed by scaling the DD1 spectrum whose Sa(T1) value is 1.314 g, the design spectrum for the intensity measure of Sa(T1)=2.60 g is developed by scaling the DD1 spectrum whose Sa(T1) value is 1.314 g, and the design spectrum for the intensity measure of Sa(T1)=2.90 g is developed by scaling the DD1 spectrum whose Sa(T1) value is 1.314 g.

The selected ground motions are scaled by the factor of 1.3 to account for the directional uncertainty in the perpendicular components of the records. For the ground motion selection, the magnitudes (M_w) and source to site distances (R_{JB}) range between 6.0-8.0 and 16-300 km, respectively, are used as the input parameters for PEER. An example of the search parameters to select the ground motions for the analyses of 3-story buildings that are located in location-1 is listed in Table 2.4. An example of the spectra of scaled ground motions for the second stripe is given in Figure 2.9.

Table 2.4. Ground motion search parameters for 3-story buildings.

Fault type	Strike-Slip
Magnitude	6.0 - 8.0
R_{JB} (km)	15 - 300
Vs (m/s)	150 - 240
Spectral Ordinate	Geomean
ScaleFactor	0.8 - 9.0
Scaling Period	0.52

Two horizontal components of each 22 pairs of ground motion records are applied to the 3D structural models at the same time.

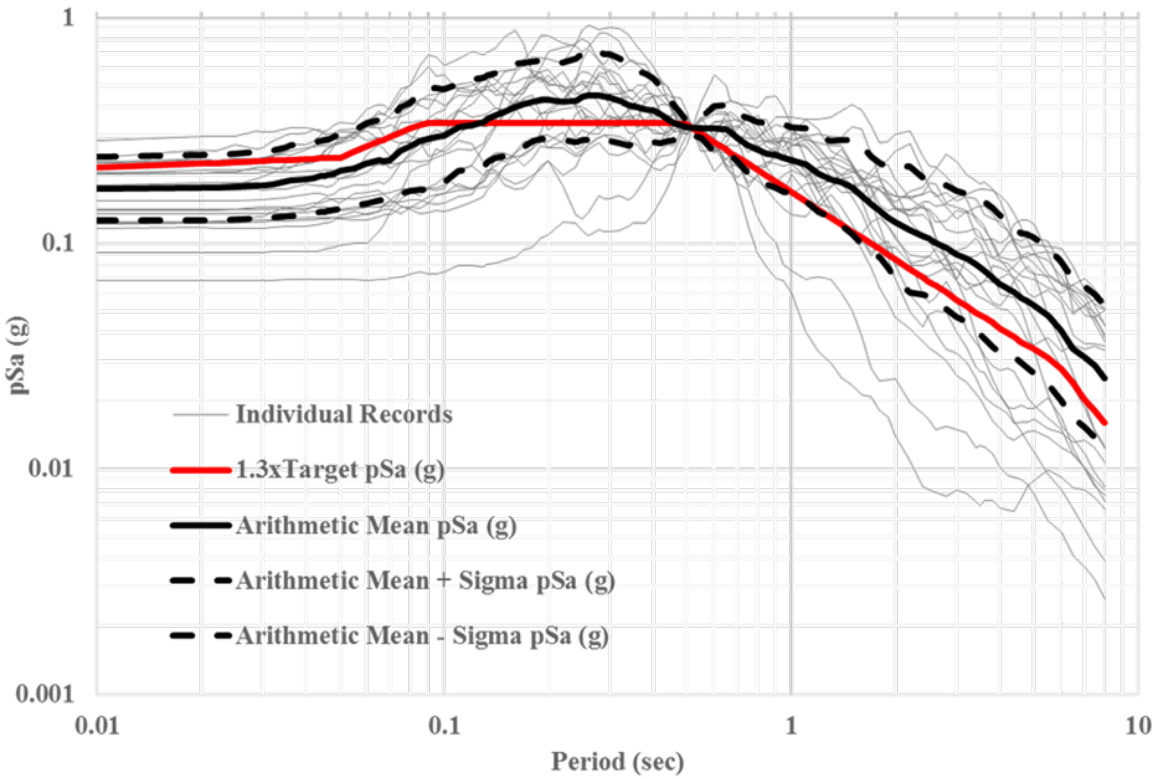

Figure 2.9. Response spectra of the scaled ground motions for the second stripe(Sa=0.25 g) used for the analyses of 3-story buildings.

3. DETERMINATION OF DAMAGE STATE LIMITS AND INTENSITY MEASURES

To generate the fragility functions for the buildings, we need to specify the damage states and their EDP limits for which the fragility functions are developed. Also, depending on the buildings' lateral behavior types (ductile or brittle), the convenient EDP and IM types should be decided so that the fragility functions represent the corresponding buildings coherently. This chapter continues with the determination of the damage state limits and the selection of the intensity measures.

3.1. Determination of the Damage State Limits

The limit values of damage states need to be defined for the performance levels of the buildings. Engineering demand parameters (EDPs) are used to measure structures' response for a given level of intensity measure (IM). There are various types of EDPs but they are divided into two groups as global and local EDPs. Roof displacement, maximum inter-story drift ratio (MIDR), and permanent deformation are used for global EDPs, while end rotation and strain of structural members are used for local EDPs. If the number of buildings increases, local EDPs are not time efficient. For this study, there are 32 buildings and for each building, a large number of nonlinear dynamic analyses have been carried out. Thus, in this study, top displacement and MIDR are used as EDP parameters.

To define the limit values of top displacement, we performed pushover analysis and obtained a pushover curve for each building. We selected the limit values by idealizing and examining the pushover curves. While deciding the limit value of top displacement for one building type (i.e., 2-story, 3-story), and for one damage state, the mean of the limit values from all pushover curves is selected as the limit value for that building type and for that damage state. With regards to the limit values of MIDR, they are taken from Hazus MR4 Technical Manuel which is defined for low-rise,

high-code MRF structures.

Lagomarsino and Giovinazzi (2006) identified the following four damage states (Slight, Moderate, Extensive, and Complete) by using the global capacity curve in Equation 3.1 [7]. An example of a pushover curve and an idealized pushover curve are given in Figure 3.1. Global damage threshold values that are taken from pushover curves are listed in Tables 3.2 and 3.3.

$$\begin{aligned} S_{slight} &= S_{dy} \\ S_{moderate} &= 1.5 \times S_{dy} \\ S_{extensive} &= 1.5 \times (S_{dy} + S_{Sdu}) \\ S_{complete} &= S_{du} \end{aligned} \tag{3.1}$$

Hazus MR4 Technical Manual is used to define the global damage threshold values for MIDR. In this manual, the MIDR threshold values are determined considering building height class, load carrying system, and code class [16]. C1L-High code is selected to represent the low-rise RC MRF systems from this technical manual. Global damage threshold values (MIDR) that are taken from Hazus MR4 Technical Manual are listed in Table 3.1. Pushover and capacity curves for 2 and 3-story buildings are given in Figures 3.2 to 3.13. The explanations written over the figures (i.e., Loc6-2st-PushoverX-dir-2018) denote the location of the building, the number of stories, the direction of the analysis, and the seismic design code year (Loc6: Location 6, 2st: 2-story building, PushoverX-dir: Pushover analysis in the x-direction, 2018: Turkish seismic code 2018).

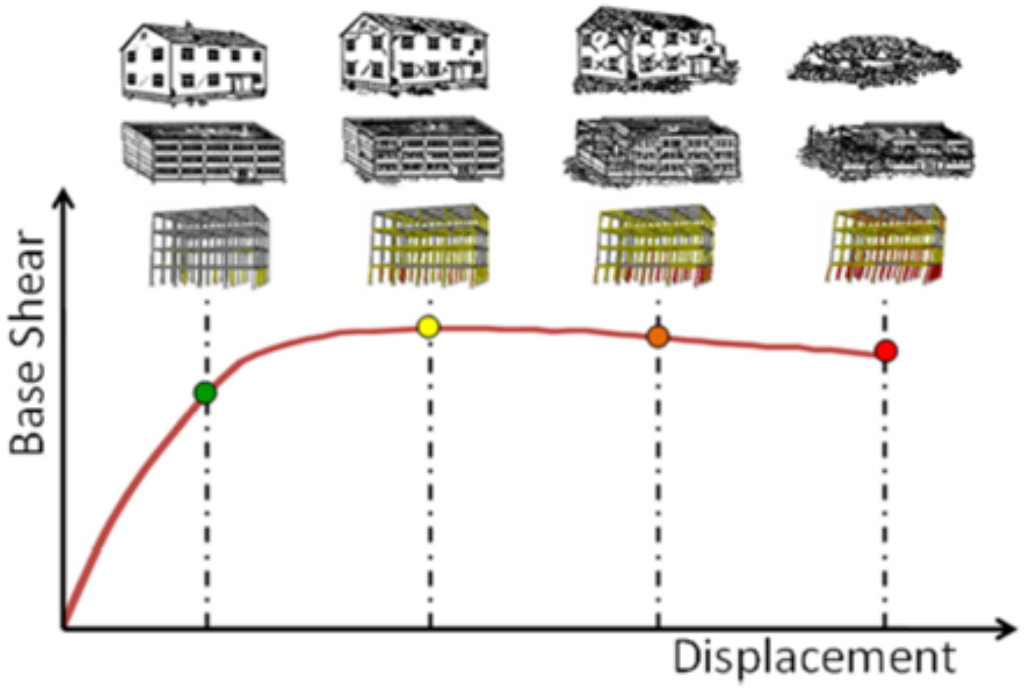

(a)

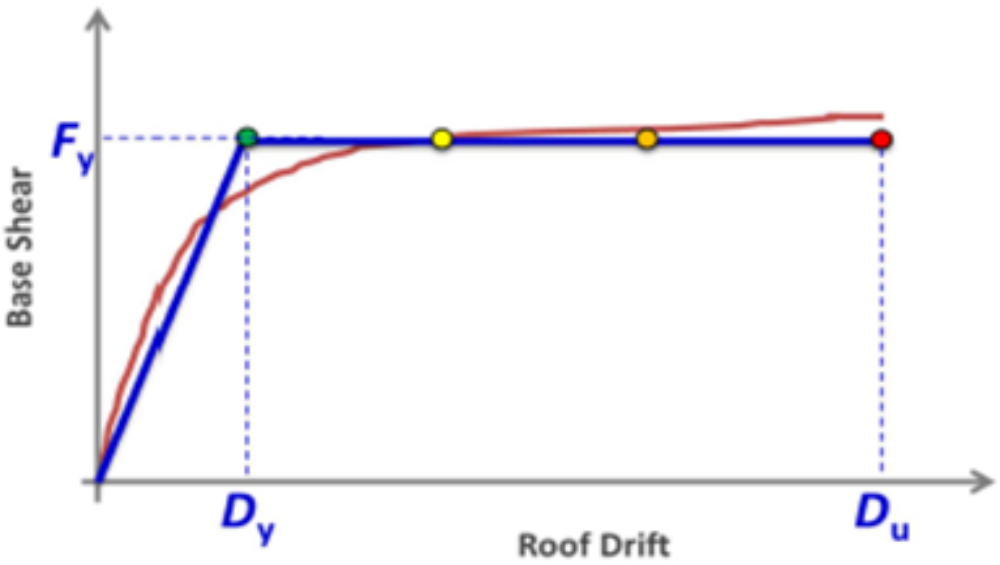

(b)

Figure 3.1. (a) Example of pushover curve and damage thresholds (Source: GEM Technical Report 2014-12 V1.0.0)), (b) Idealized pushover curve. (Source: GEM Technical Report 2014-12 V1.0.0).

Table 3.1. Limit values for the maximum inter-story drift ratio (MIDR)

Building Properties	Interstory Drift at Tresholds of Damage State			
	Slight	Moderate	Extensive	Complete
C1L	0.005	0.01	0.03	0.08

Table 3.2. Mean of limit values for top displacements taken from the pushover curves in the x-direction. They are given in millimeters.

Building Type	Slight	Moderate	Extensive	Complete
2-story,1998	38.50	57.75	106.24	173.98
2-story,2018	46.50	69.75	84.14	121.78
3-story,1998	44.40	66.60	128.41	212.43
3-story,2018	47.88	71.81	107.13	166.39

Table 3.3. Mean of limit values for top displacements taken from the pushover curves in the y-direction. They are given in millimeters.

Building Type	Slight	Moderate	Extensive	Complete
2-story,1998	42.00	63.00	122.53	203.06
2-story,2018	45.38	68.06	107.18	168.98
3-story,1998	39.33	59.00	135.67	232.00
3-story,2018	36.63	54.94	127.61	218.59

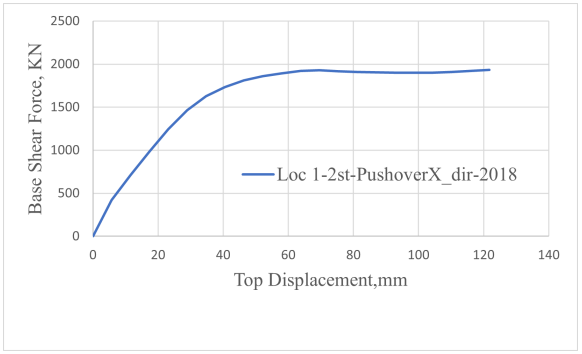

(a)

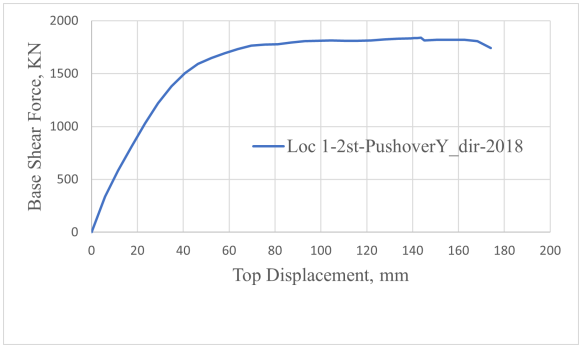

(b)

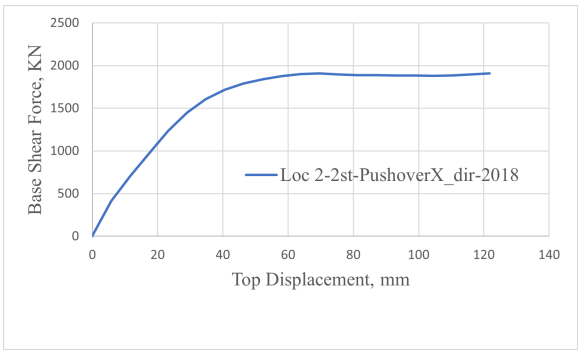

(c)

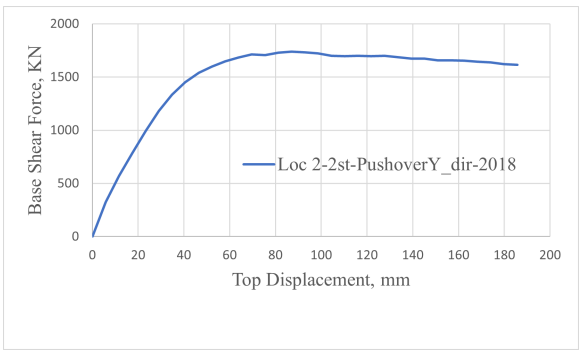

(d)

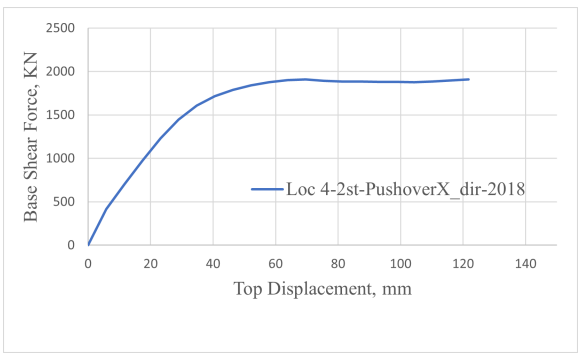

(e)

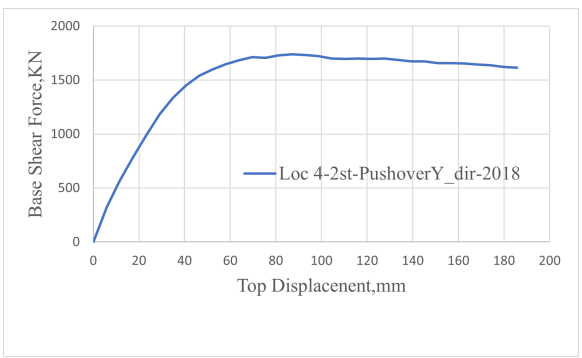

(f)

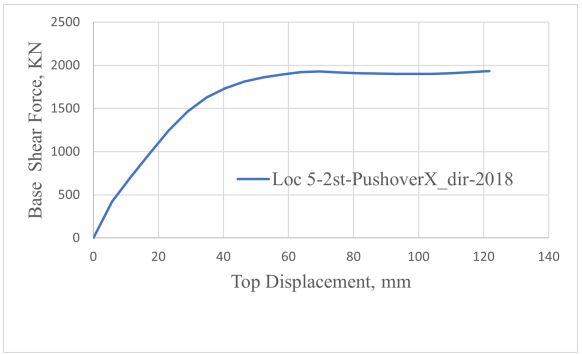

(g)

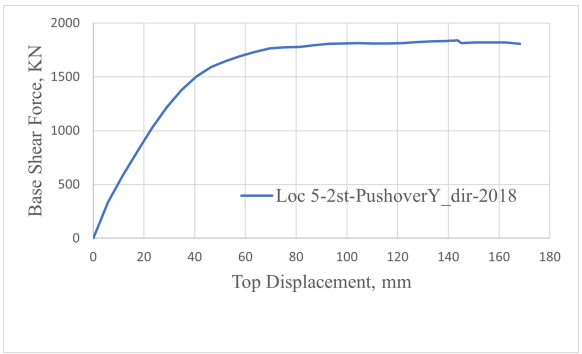

(h)

Figure 3.2. Pushover curves for 2-story buildings. cont.

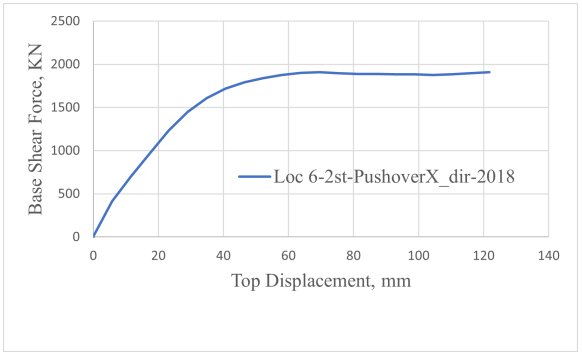

(a)

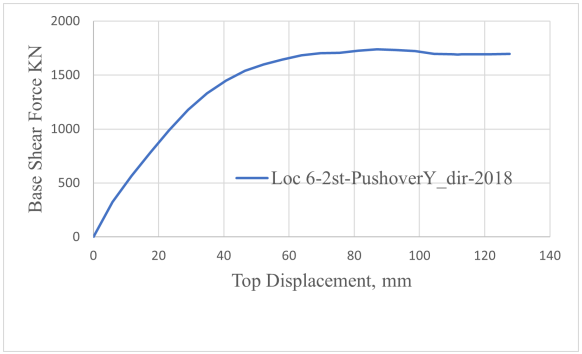

(b)

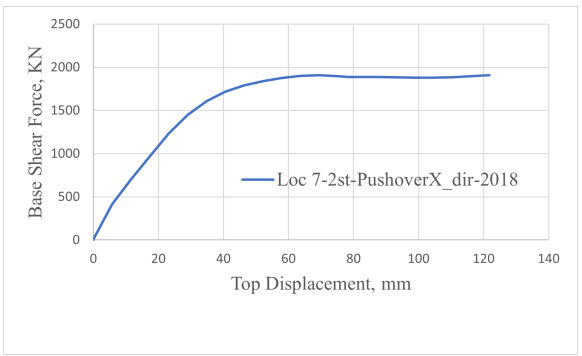

(c)

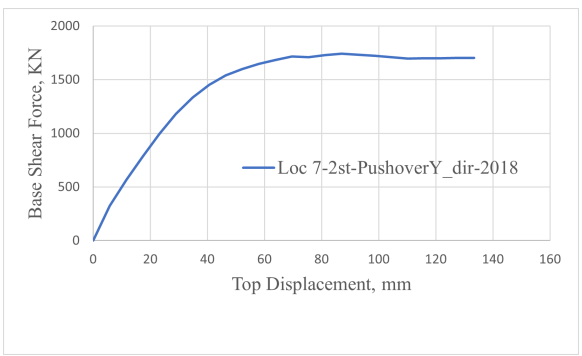

(d)

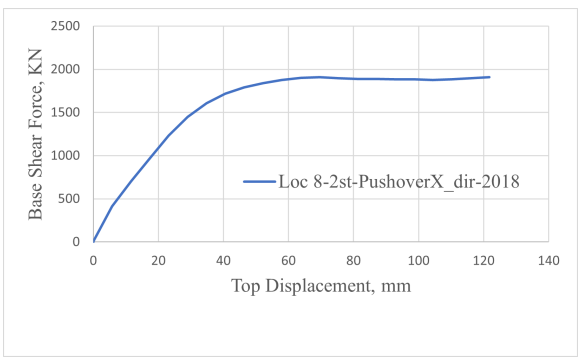

(e)

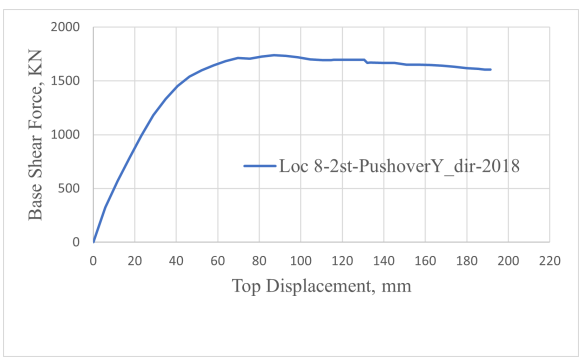

(f)

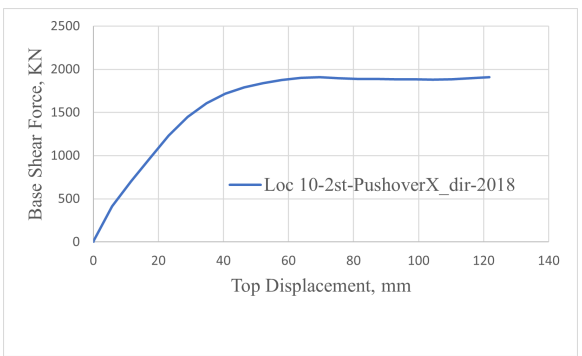

(g)

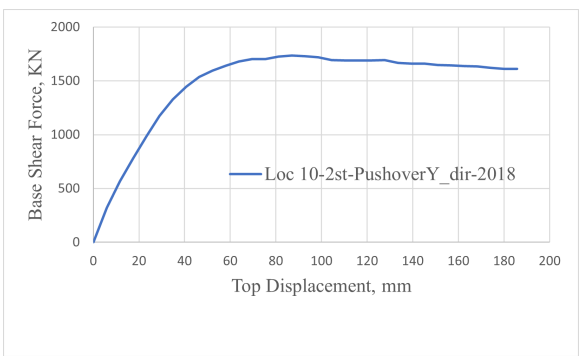

(h)

Figure 3.3. Pushover curves for 2-story buildings. cont.

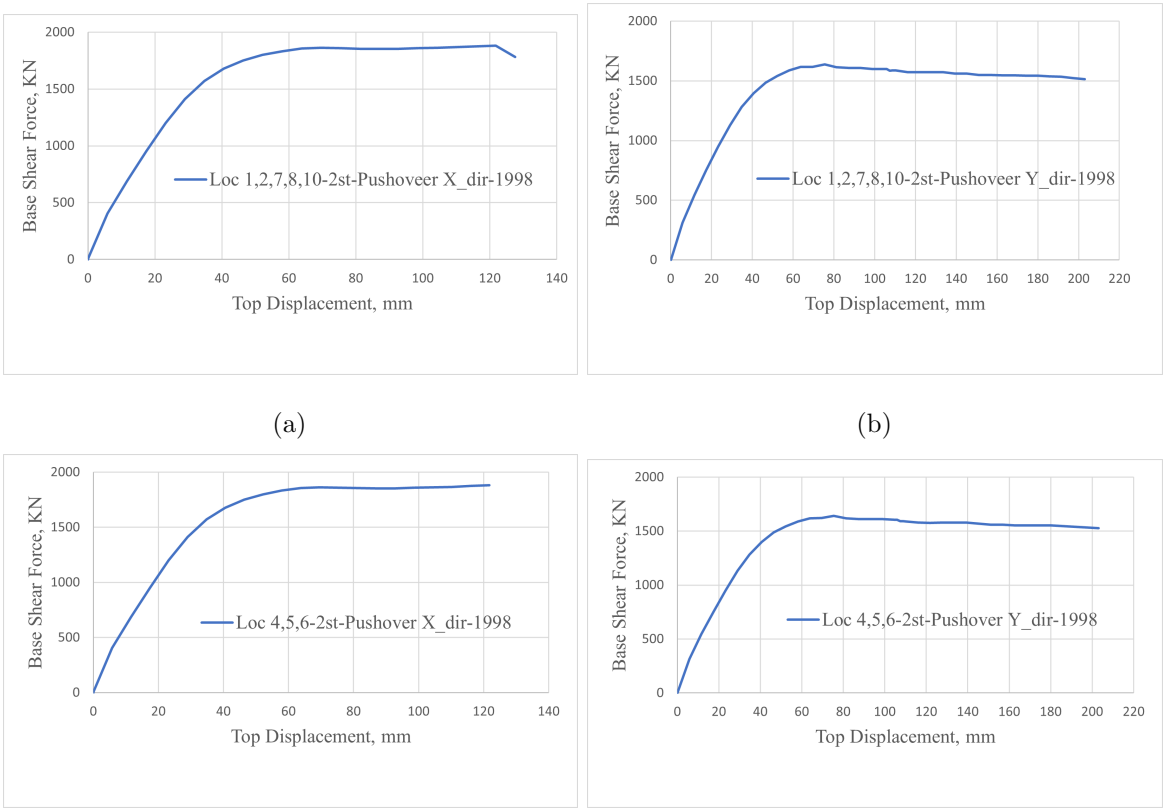

Figure 3.4. Pushover curves for 2-story buildings.

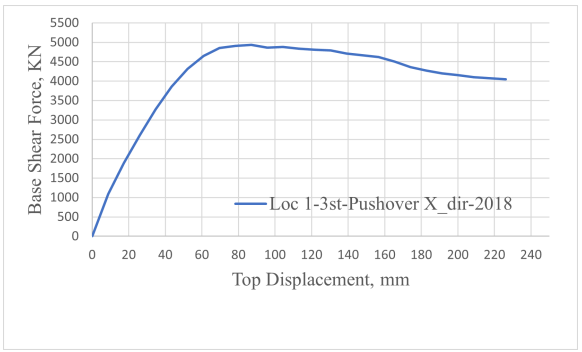

(a)

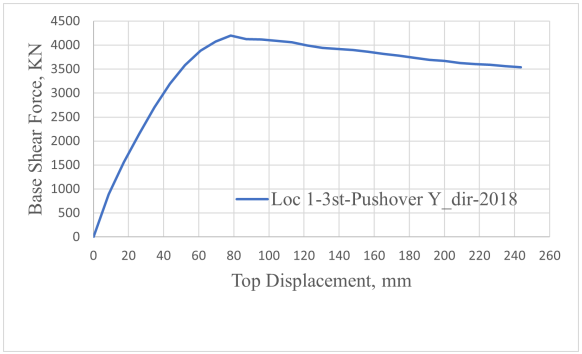

(b)

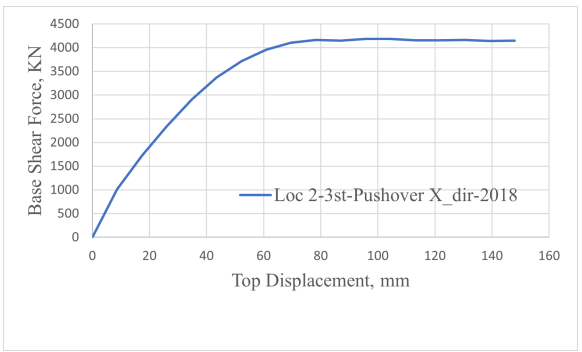

(c)

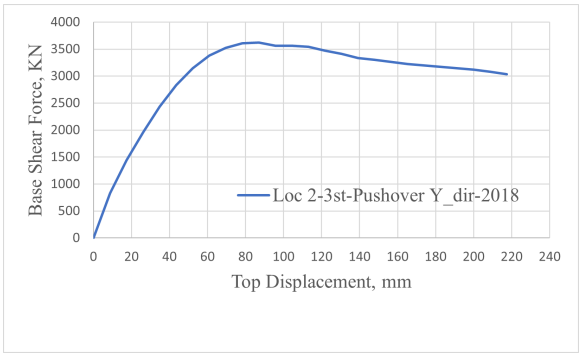

(d)

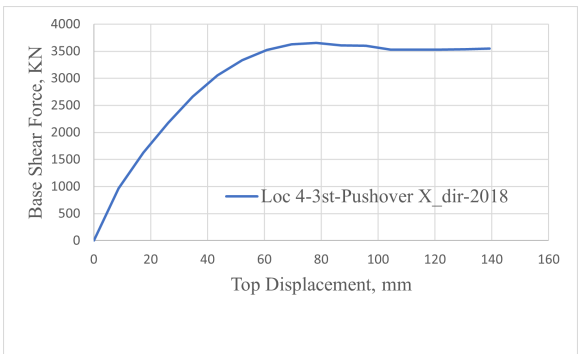

(e)

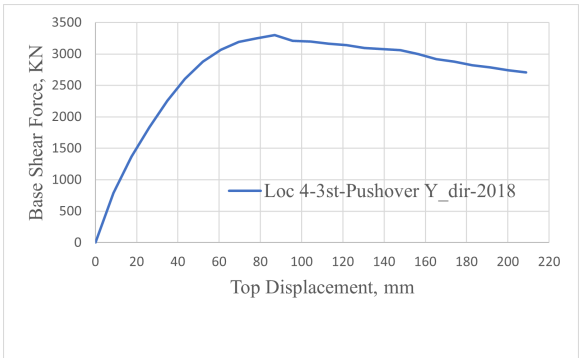

(f)

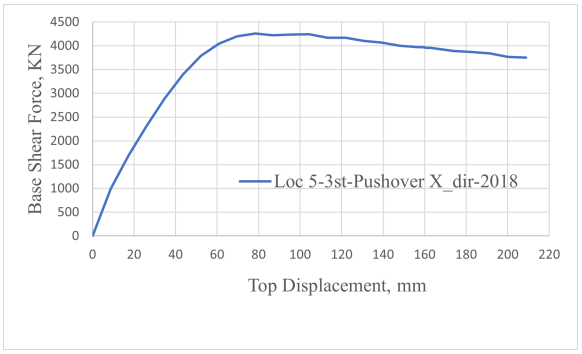

(g)

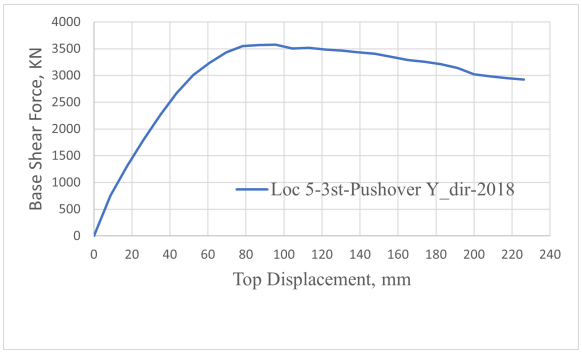

(h)

Figure 3.5. Pushover curves for 3-story buildings. cont.

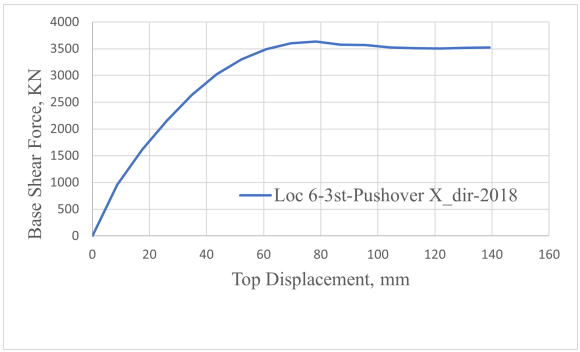

(a)

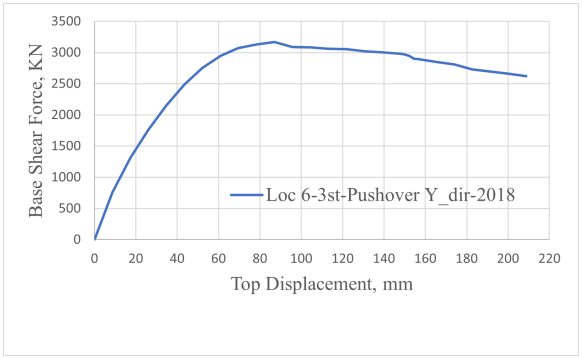

(b)

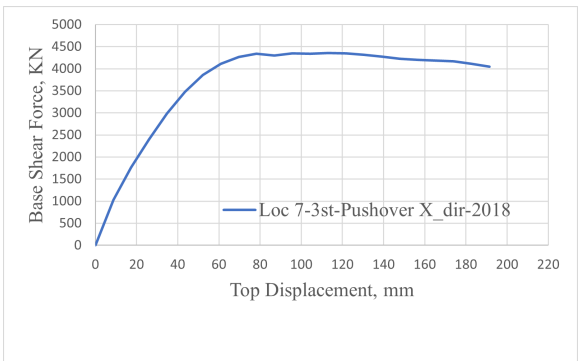

(c)

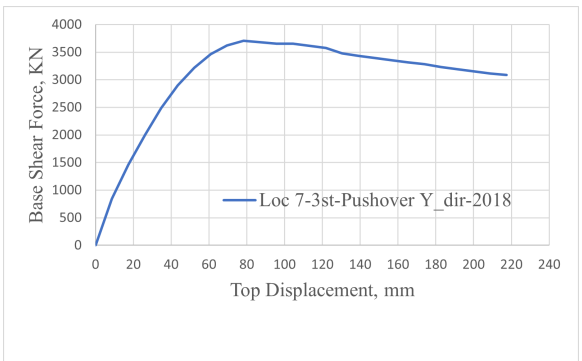

(d)

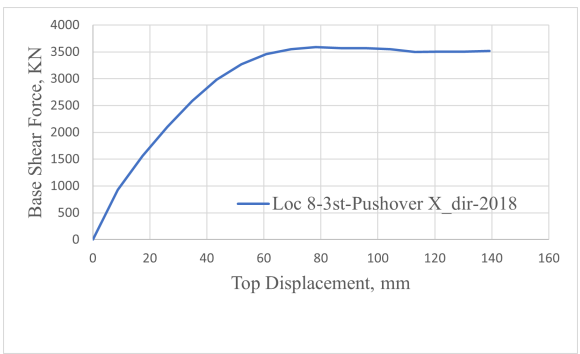

(e)

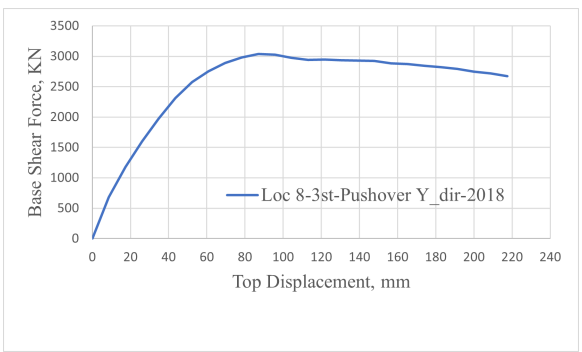

(f)

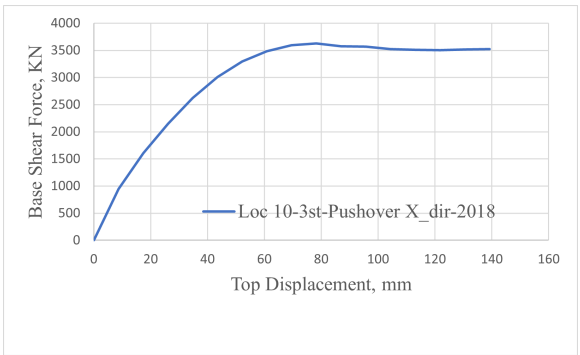

(g)

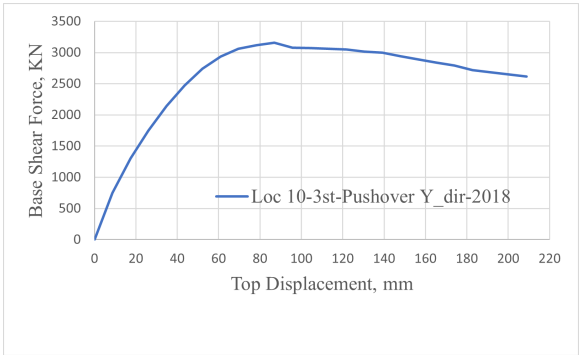

(h)

Figure 3.6. Pushover curves for 3-story buildings. cont.

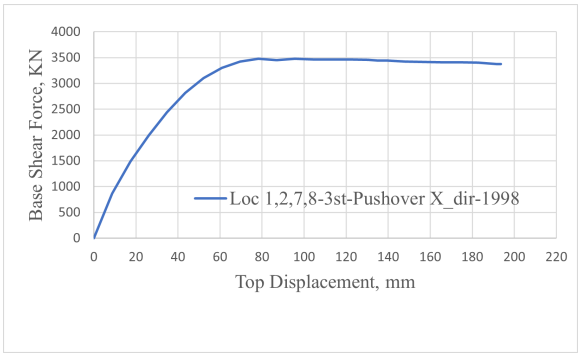

(a)

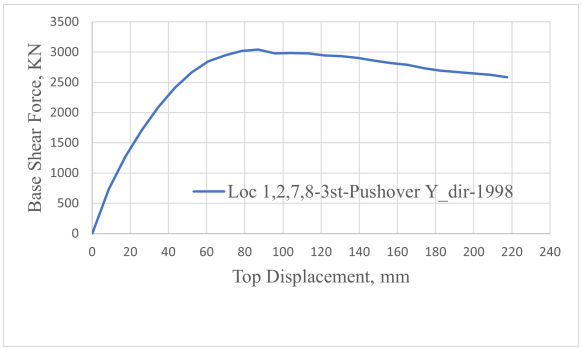

(b)

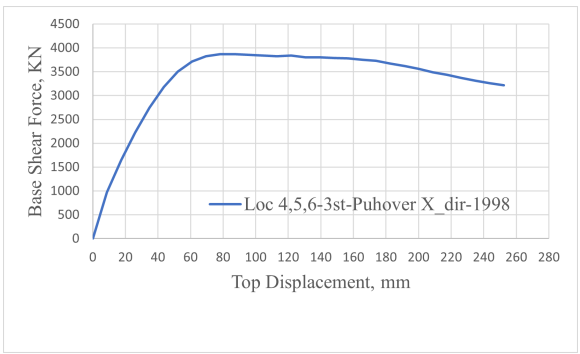

(c)

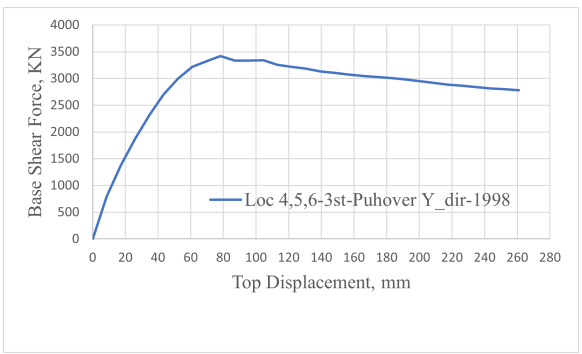

(d)

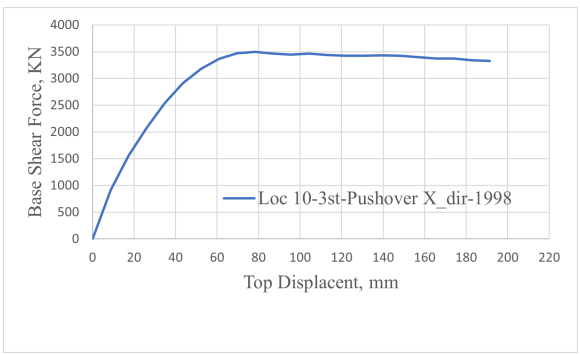

(e)

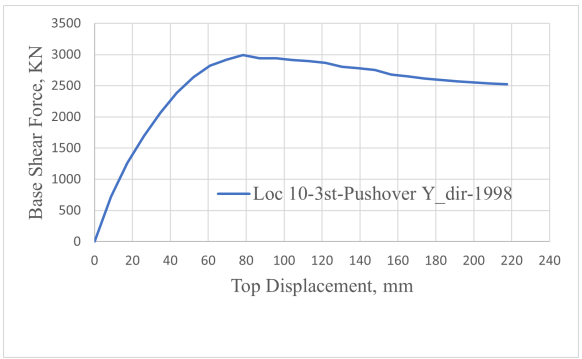

(f)

Figure 3.7. Pushover curves for 3-story buildings.

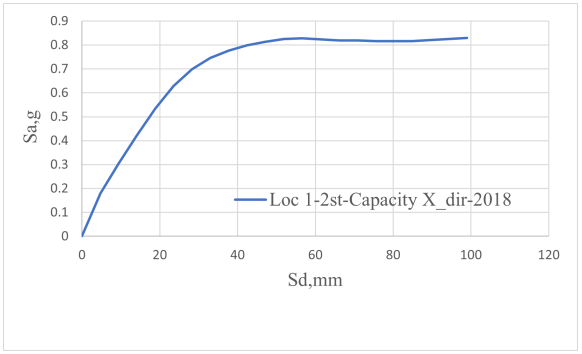

(a)

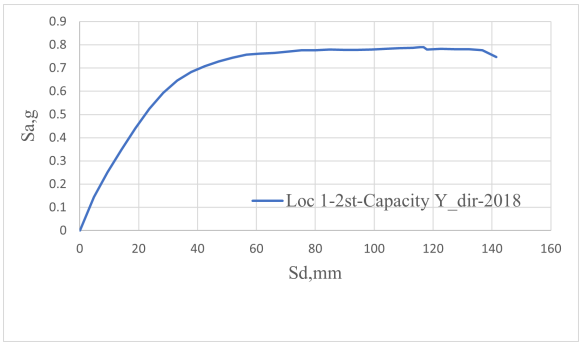

(b)

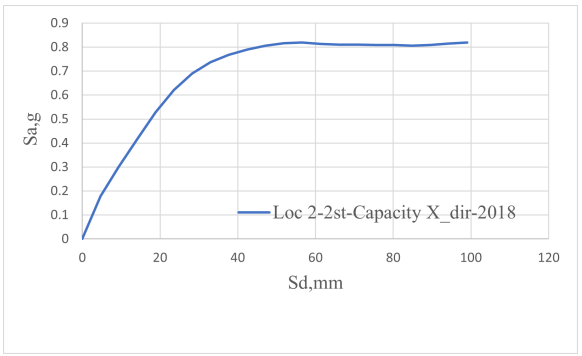

(c)

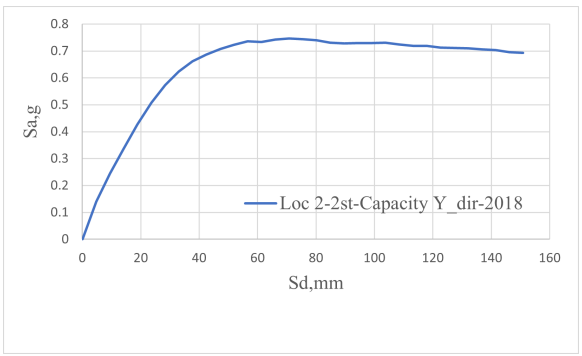

(d)

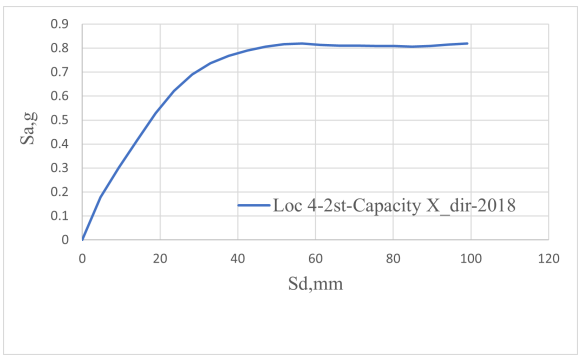

(e)

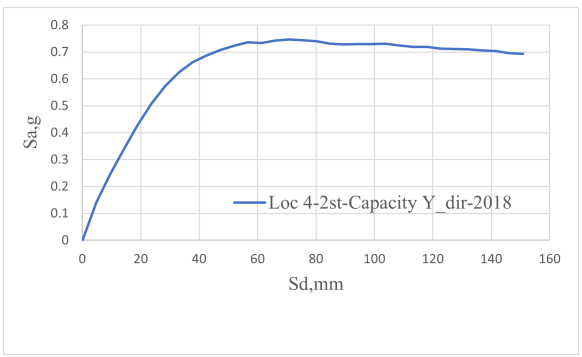

(f)

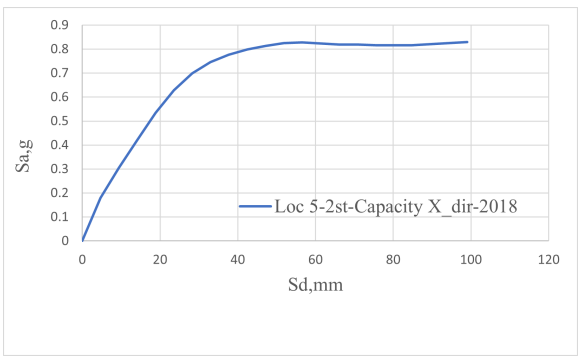

(g)

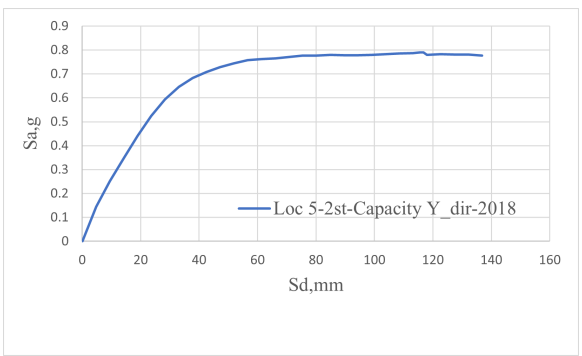

(h)

Figure 3.8. Capacity curves for 2-story buildings. cont.

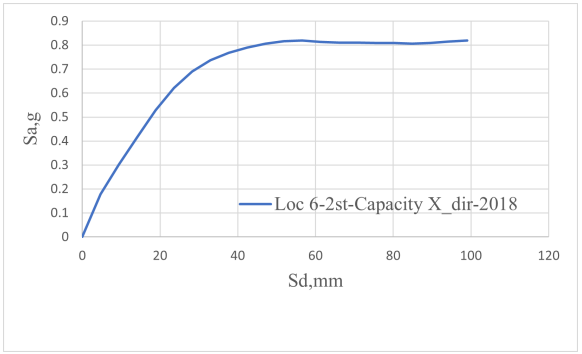

(a)

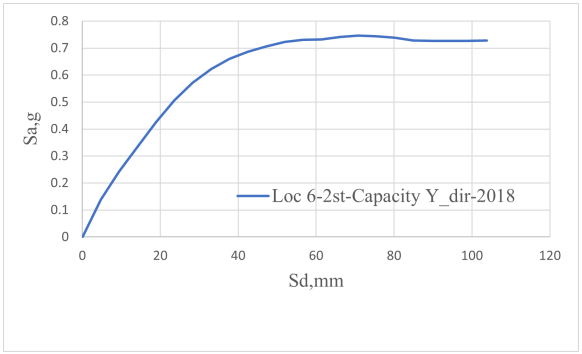

(b)

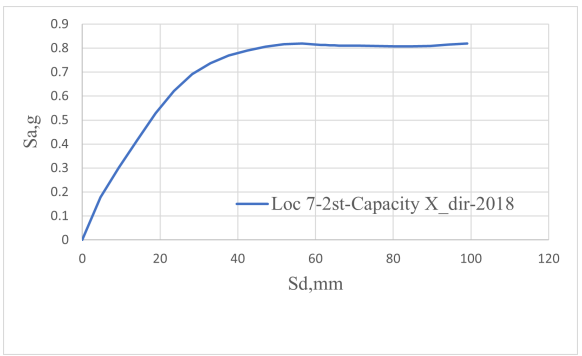

(c)

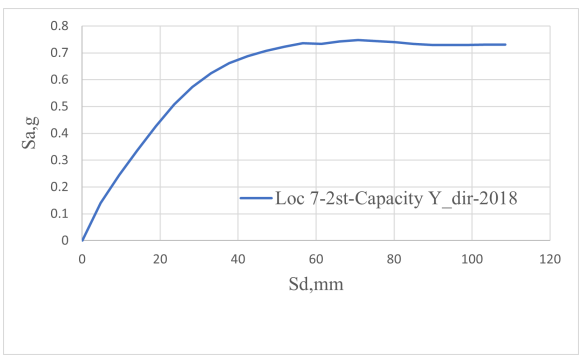

(d)

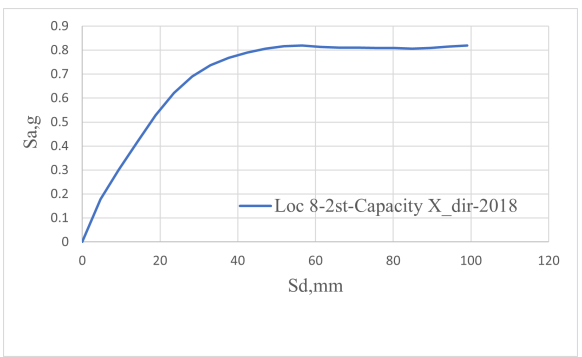

(e)

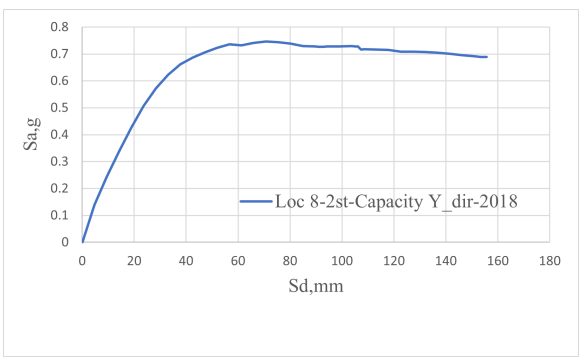

(f)

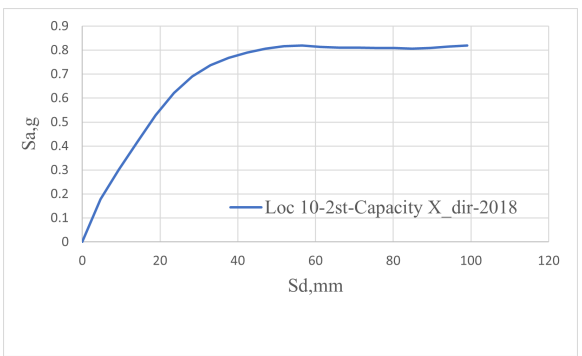

(g)

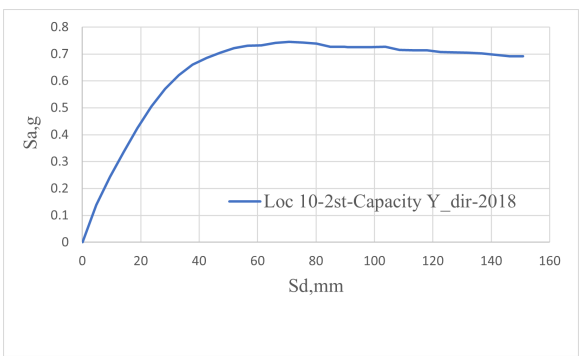

(h)

Figure 3.9. Capacity curves for 2-story buildings. cont.

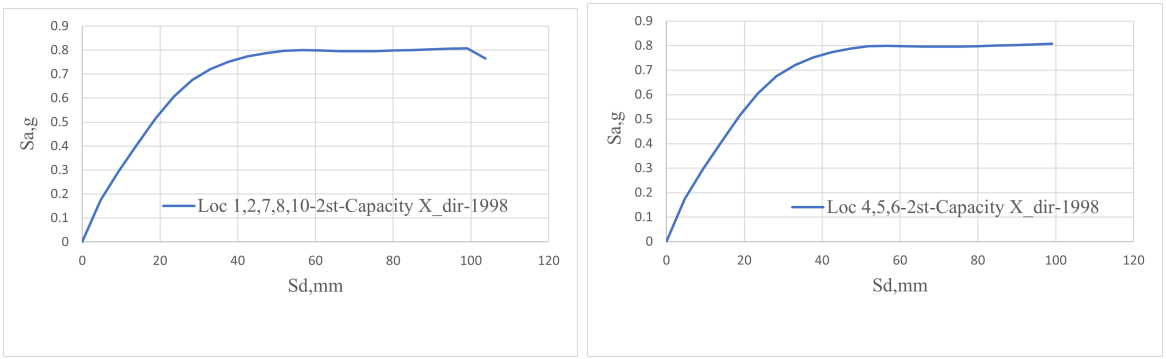

(a) (b)

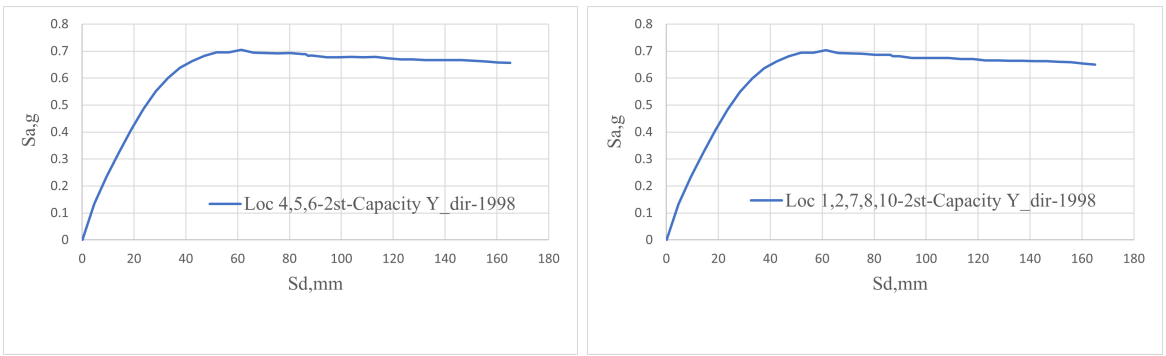

(c) (d)

Figure 3.10. Capacity curves for 2-story buildings.

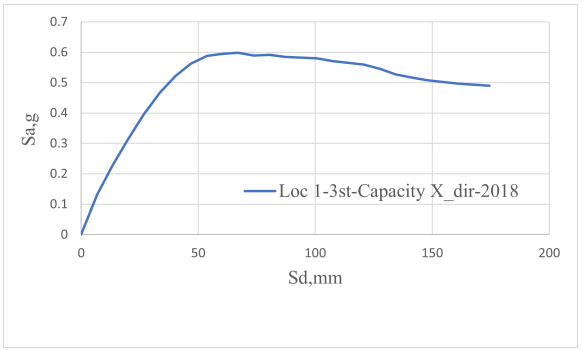

(a)

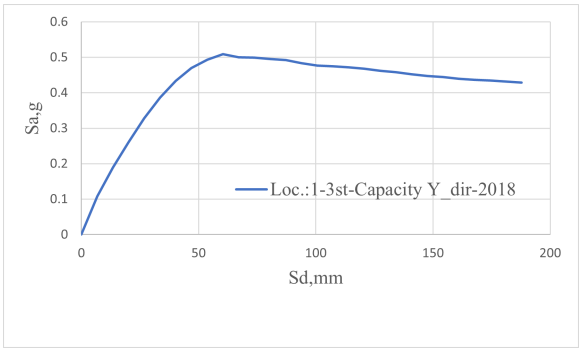

(b)

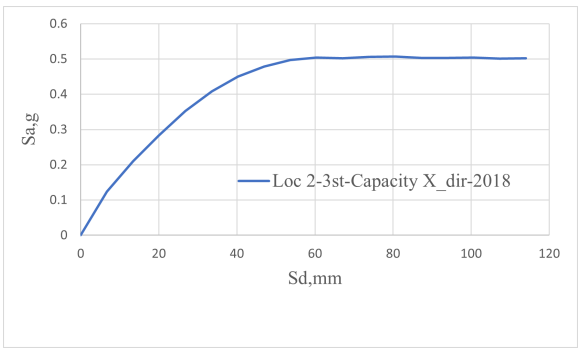

(c)

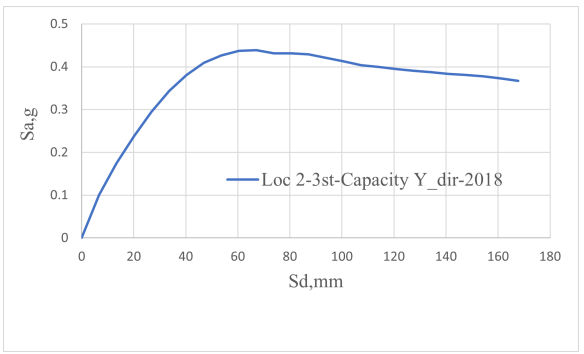

(d)

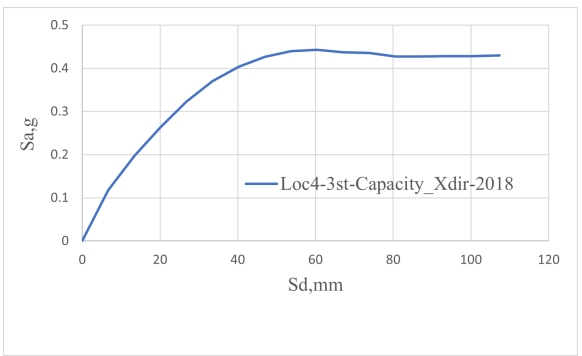

(e)

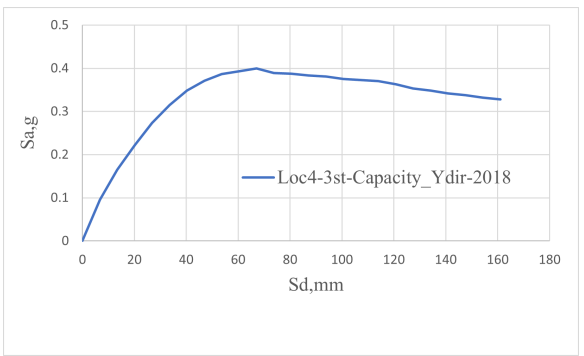

(f)

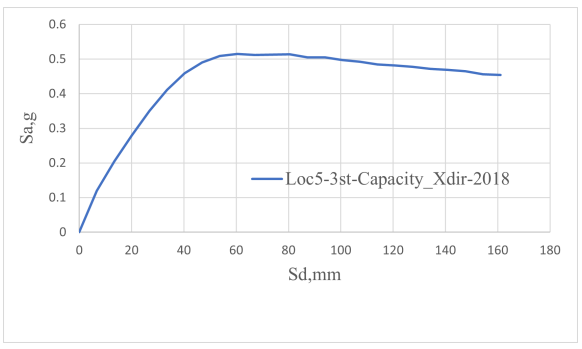

(g)

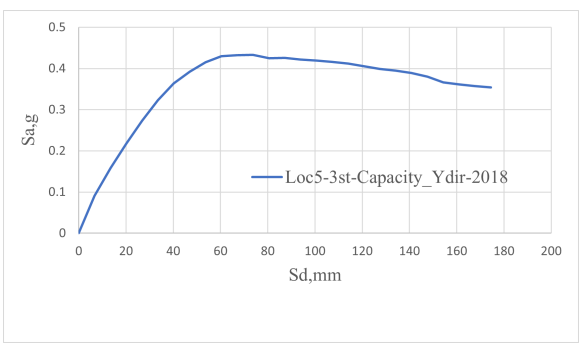

(h)

Figure 3.11. Capacity curves for 3-story buildings. cont.

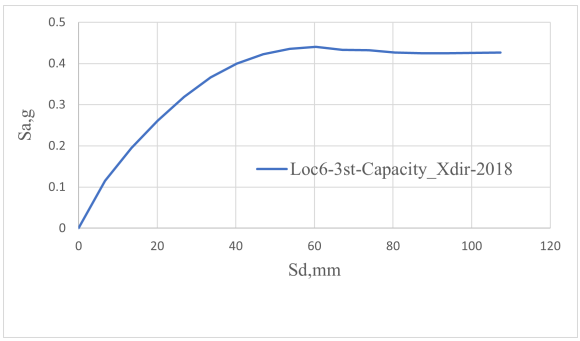

(a)

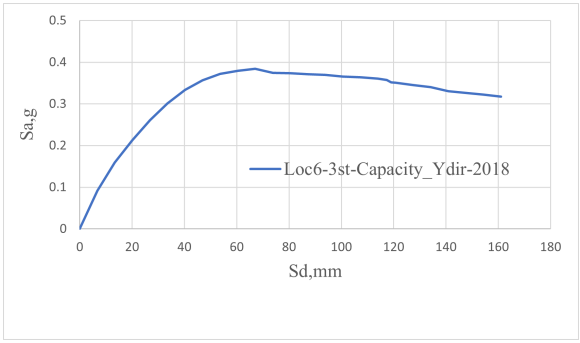

(b)

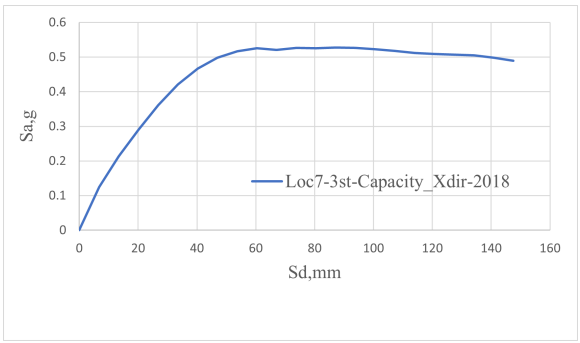

(c)

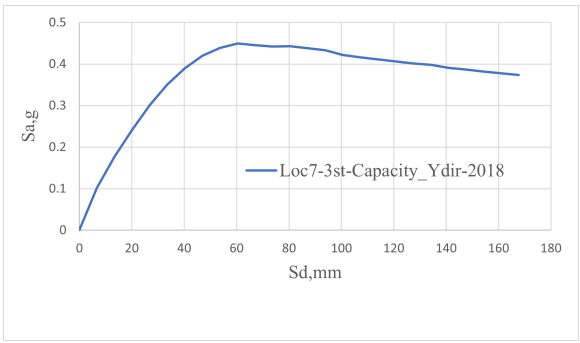

(d)

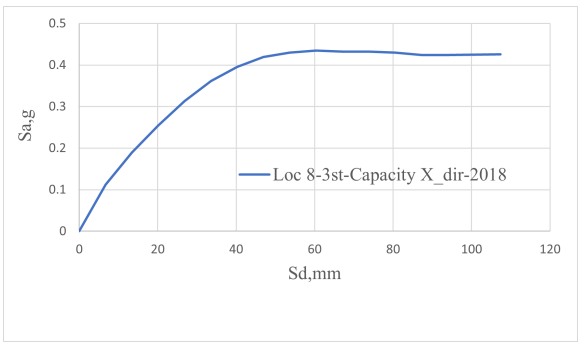

(e)

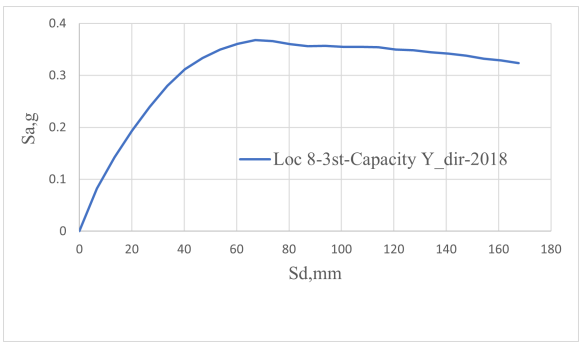

(f)

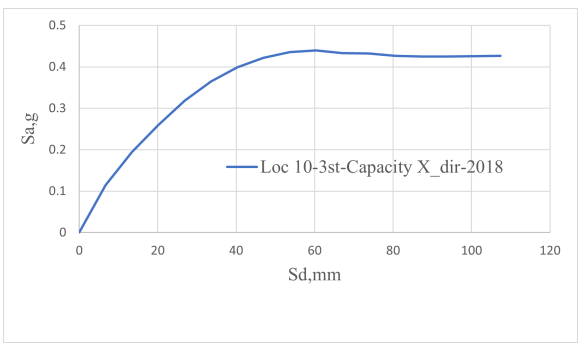

(g)

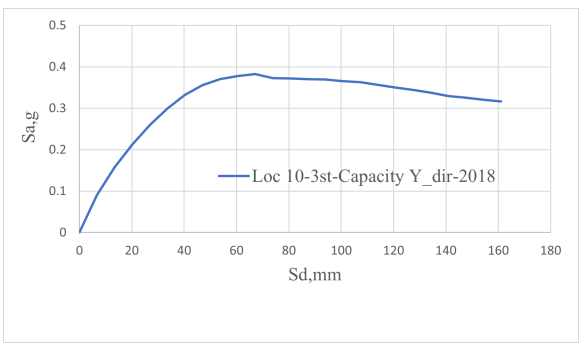

(h)

Figure 3.12. Capacity curves for 3-story buildings. cont.

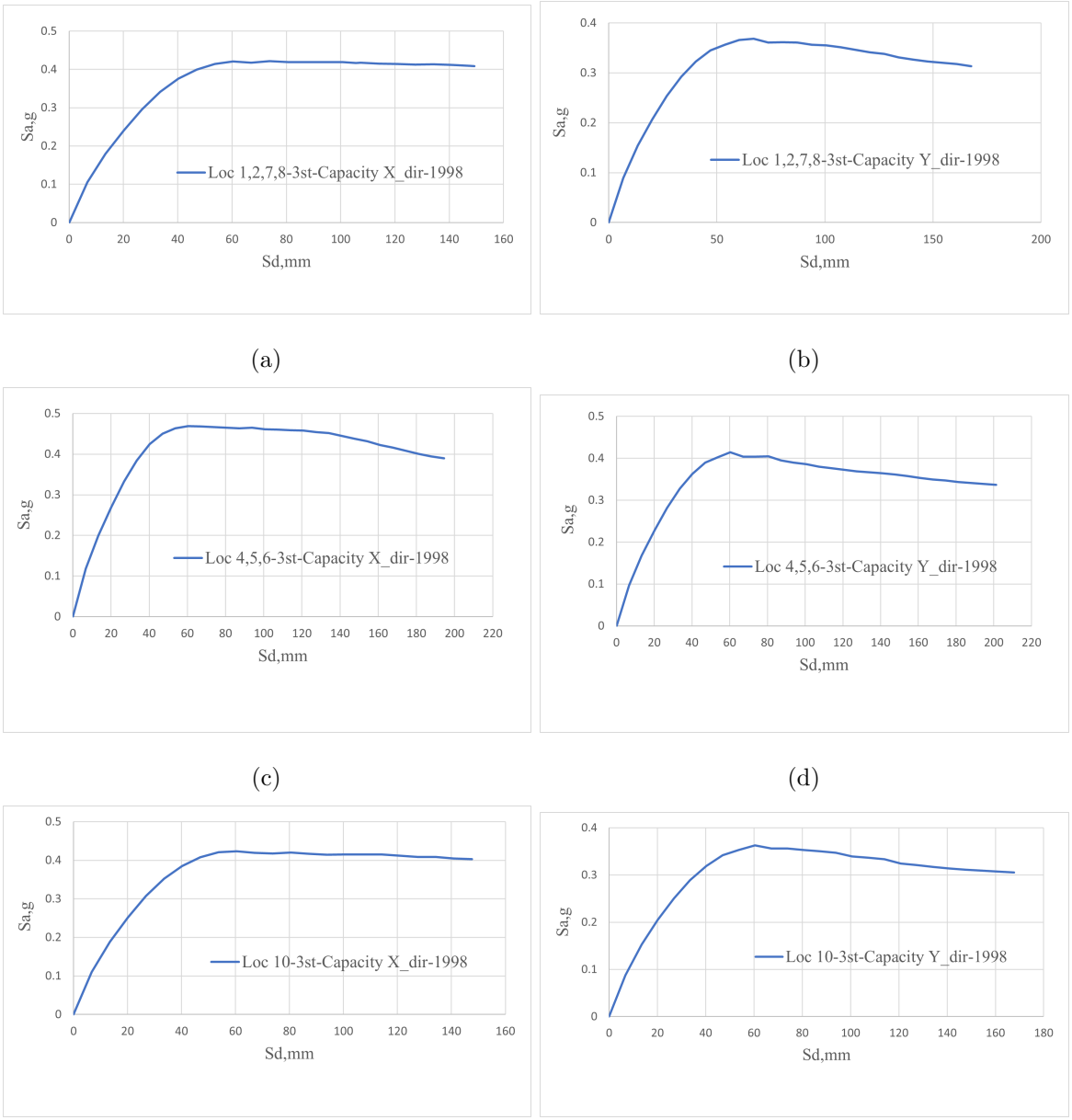

Figure 3.13. Capacity curves for 3-story buildings.

3.2. Selection of the Intensity Measures

There are two different kinds of intensity measures: experimental and instrumental intensity measures. The EMS98 scale, Modified Mercalli Intensity Scale (MMI) are the two examples of the experimental intensity measures. Examples of the instrumental

intensity measures are spectral acceleration (Sa), spectral velocity (Sv), spectral displacement (Sd), peak ground acceleration (PGA), peak ground velocity (PGV), peak ground displacement (PGD), arias intensity (AI) [6]. Instrumental intensity measures are the most useful and effective intensity measures because they give more accurate results, represent the structure's response accurately, and consider ground motion uncertainty. Building type and story number play a big role when selecting an intensity measure.

Intensity measure (IM) is an important fragility parameter, thus, it should be efficient and sufficient. The engineering demand parameter type should be coherent with the selected intensity measure type. Intensity measures should be selected attentively, and the response of structures (EDP) should be well-correlated with intensity measures. For instance, EDPs for low-rise and brittle structures are well-correlated with peak ground acceleration (PGA), while spectral displacement (Sd) and spectral acceleration (Sa) are well-correlated with the response of ductile buildings. If the number of buildings to be analyzed increases, period independent intensity measures (i.e., PGA) are more efficient to use [6].

For the buildings with the intermediate period range like medium height buildings, PGV is a better damage indicator. It correlates well with deformation demands when compared to PGA and Sa [3].

In this study, buildings are ductile, low-rise and first mode vibration periods are dominant. Thus, spectral displacements and spectral accelerations at the first natural vibration periods are used as the intensity measures.

4. MULTIPLE STRIPE ANALYSIS AND DEVELOPMENT OF FRAGILITY CURVES

Fragility functions provide the probability of exceeding a certain damage state versus different intensity measure (IM) levels. In this study, nonlinear dynamic analyses are performed and the results of the analyses are used to generate fragility curves via the statistical method of maximum likelihood estimation (MLE). In this study, a large number of nonlinear dynamic analyses are performed and the analyses results are collected to create the fragility curves. There are different procedures for nonlinear dynamic analyses. Multiple stripes analysis (MSA) and incremental dynamic analysis (IDA) are the two commonly utilized analysis techniques for the development of fragility functions.

For the incremental dynamic analysis (IDA) that is proposed by Vamvatsikos and Cornel (2002), a set of ground motions is scaled incrementally to obtain the response until the structure reaches the dynamic instability, and the intensity measure level that corresponds to the damage level is obtained [17]. One of the biggest drawbacks of this technique is the corruption of the content of the ground motions which is caused by the unrealistic large scaling factors.

For the multiple stripes analysis (MSA), the structural response is obtained for different sets of ground motions that are selected to represent a certain level of intensity measure. For different intensity measures, different sets of ground motions are used instead of scaling the same set of ground motion records multiple times. Since different sets of ground motion can be used for different intensity measure levels (stripes), analysts have the chance to limit the scale factors of ground motion records not to corrupt their content. Also, since different sets of ground motions can be used, the uncertainty resulting from record-to-record variability is accounted for at a certain level.

4.1. Multiple Stripe Analyses of the Buildings

In this study, multiple stripe analysis is used to get credible results. Eleven IM levels (stripes) are defined based on the IM parameter of Sa(T1), and for each stripe, 22 pairs of records are used for the nonlinear dynamic analyses.

For each building type and each IM level (stripe), the respective selected ground motion pairs are applied to the building and the corresponding EDP (MIDR and Dtop) results are saved. There are 16 2-story buildings and 16 3-story buildings (8 different locations and 2 different seismic codes of TSC1998 and TSC2018). The EDP values of all 2-story buildings are collected in 2 pools (designed per TSC1998, designed per TSC2018), similarly, all the EDP values of 3-story buildings are collected in other 2 pools (designed per TSC1998, designed per TSC2018), and they are treated as the results of the 2-story buildings designed per TSC1998, the results of the 2-story buildings designed per TSC2018, the results of the 3-story buildings designed per TSC1998 and the results of the 3-story buildings designed per TSC2018, respectively.

The results of MSA for different IM parameters (Sa and Sd) and different EDPs (MIDR and Dtop) are given in Figures 4.1 to 4.16 which are developed in MATLAB [18]. Also, the damage state limits in terms of the selected EDPs are shown in these figures with vertical red dotted lines. The number of EDP values exceeding the limit values can easily be seen in the figures.

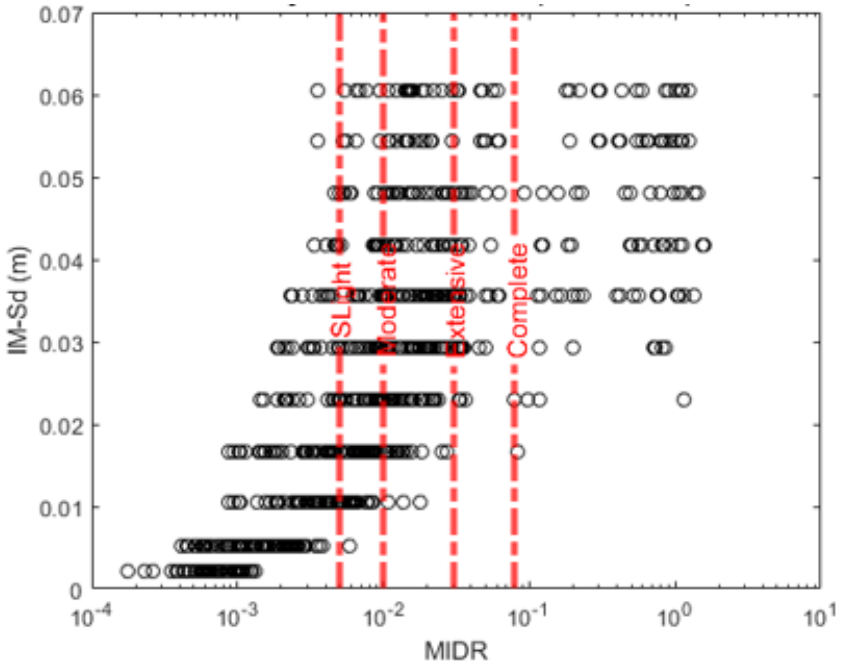

(a) 2-story 1998 in X-direction (EDP=MIDR)

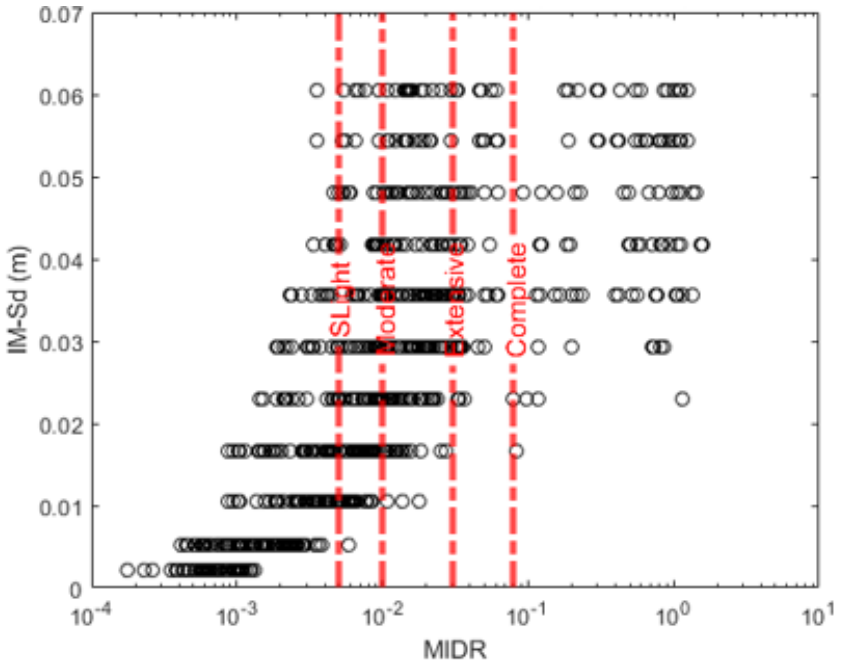

(b) 2-story 1998 in Y-direction (EDP=MIDR)

Figure 4.1. Results of MSA for 2-story buildings designed per TSC 1998, IM(Sd)-EDP(MIDR). The black circles show the MIDR values, and the vertical red dashed lines denote slight, moderate, extensive and complete damage state thresholds from left to the right, respectively.

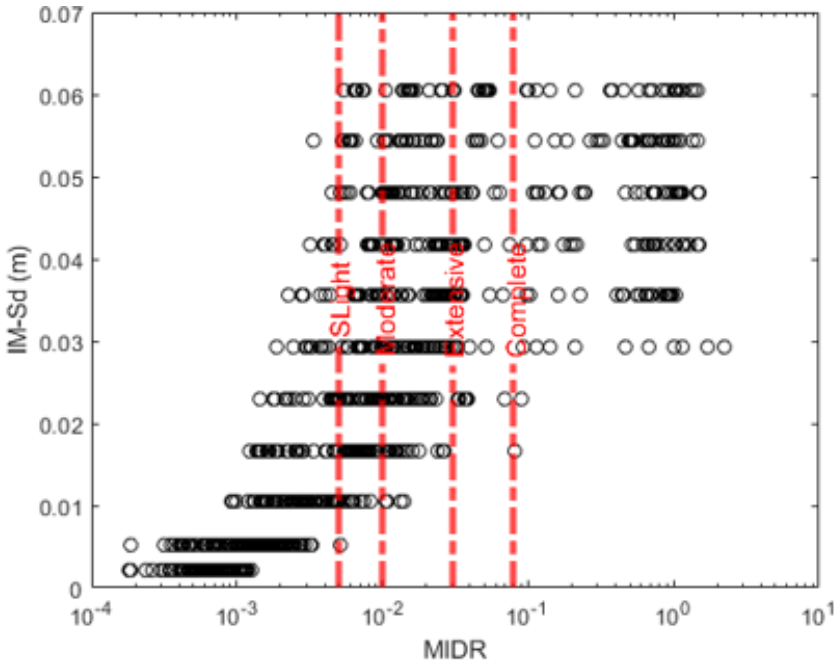

(a) 2-story 2018 in X-direction (EDP=MIDR)

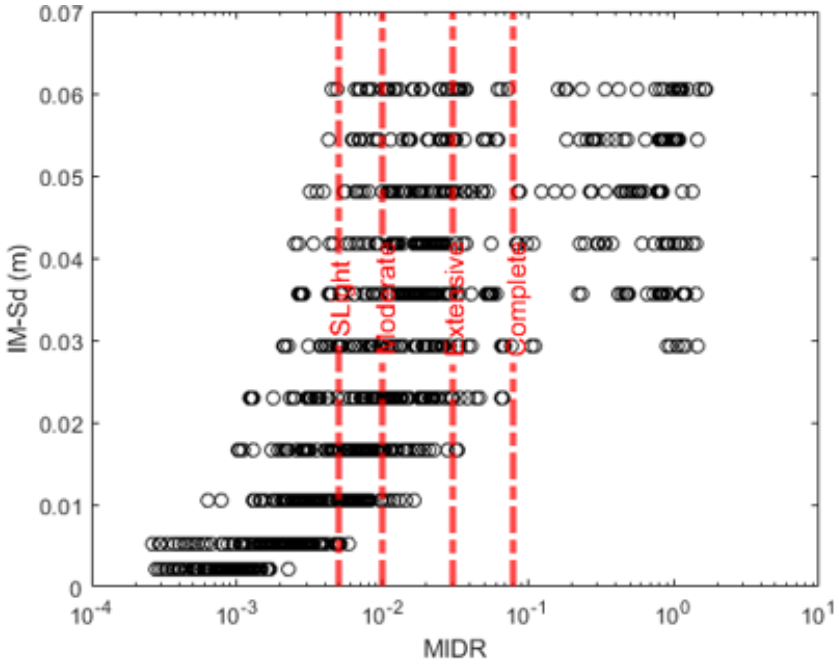

(b) 2-story 2018 in Y-direction (EDP=MIDR)

Figure 4.2. Results of MSA for 2-story buildings designed per TSC 2018, IM(Sd)-EDP(MIDR). The black circles show the MIDR values, and the vertical red dashed lines denote slight, moderate, extensive and complete damage state thresholds from left to the right, respectively.

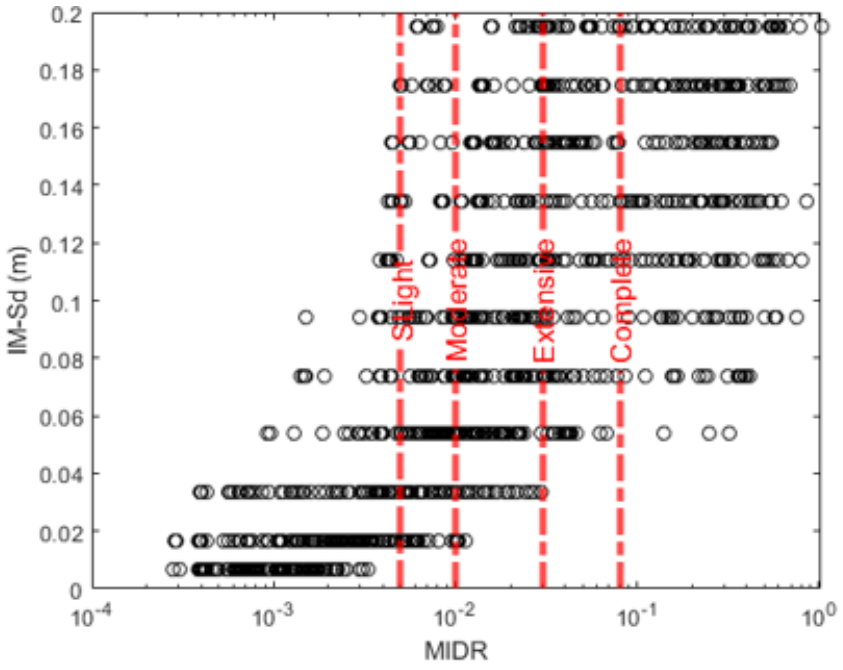

(a) 3-story 1998 in X-direction (EDP=MIDR)

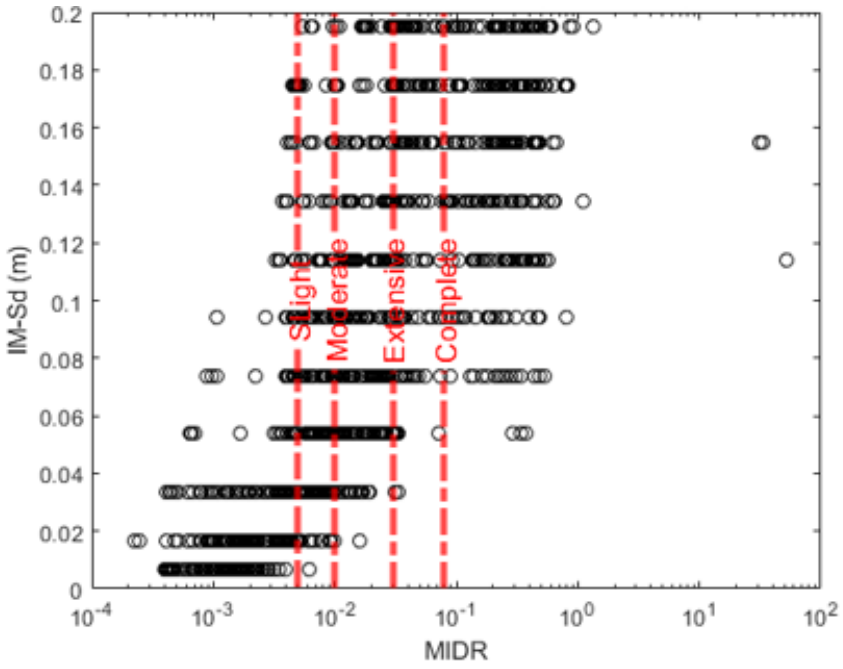

(b) 3-story 1998 in Y-direction (EDP=MIDR)

Figure 4.3. Results of MSA for 3-story buildings designed per TSC 1998, IM(Sd)-EDP(MIDR). The black circles show the MIDR values, and the vertical red dashed lines denote slight, moderate, extensive and complete damage state thresholds from left to the right, respectively.

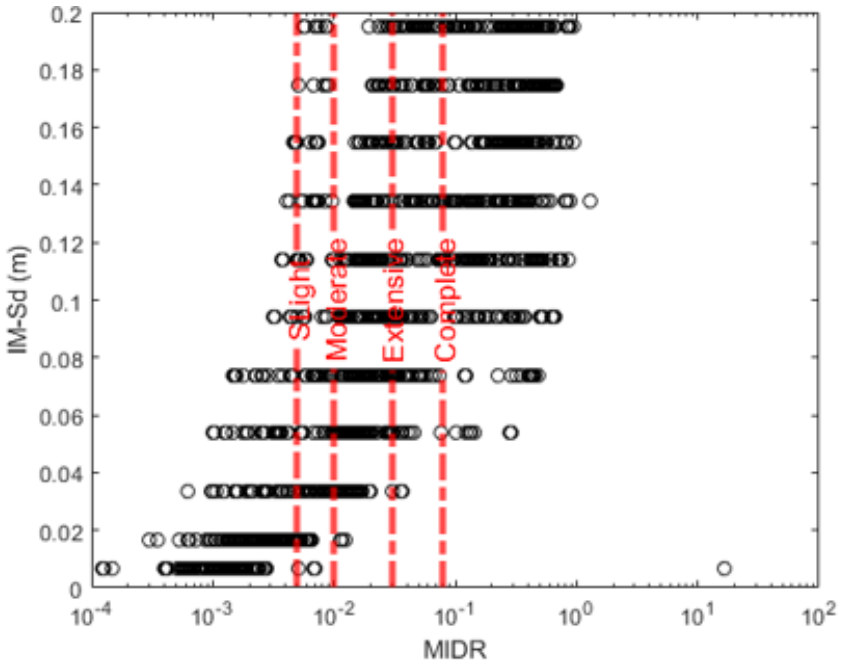

(a) 3-story 2018 in X-direction (EDP=MIDR)

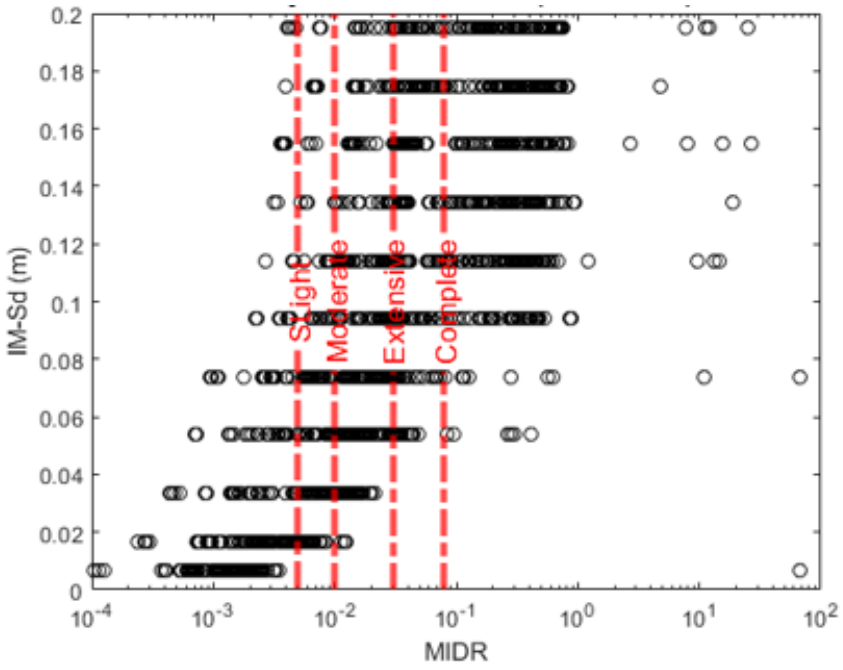

(b) 3-story 2018 in Y-direction (EDP=MIDR)

Figure 4.4. Results of MSA for 3-story buildings designed per TSC 2018, IM(Sd)-EDP(MIDR). The black circles show the MIDR values, and the vertical red dashed lines denote slight, moderate, extensive and complete damage state thresholds from left to the right, respectively.

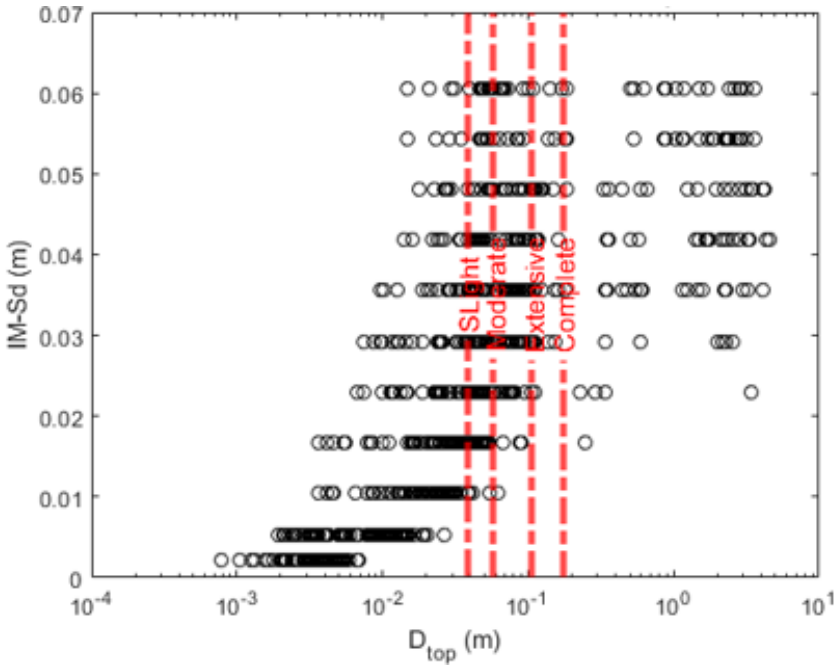

(a) 2-story 1998 in X-direction (EDP=Dtop)

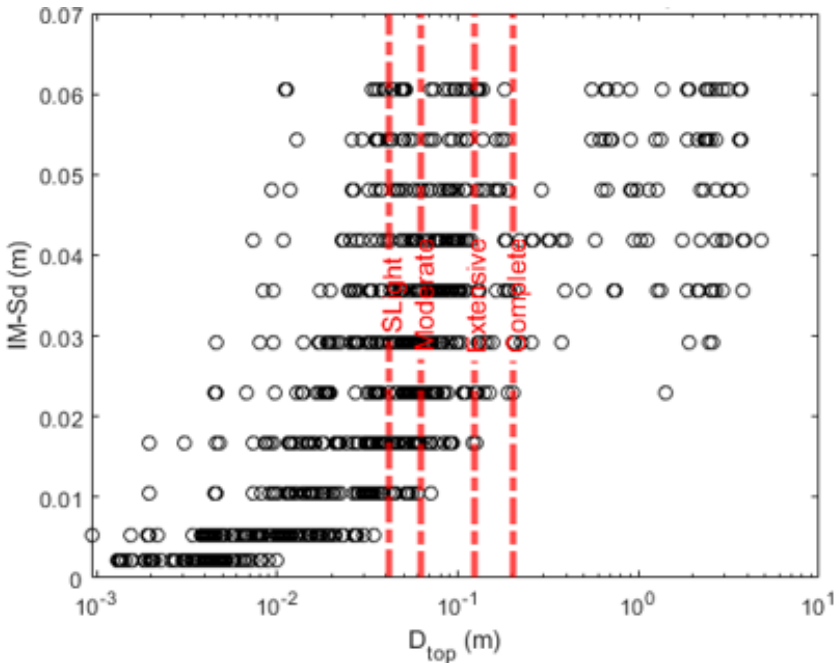

(b) 2-story 1998 in Y-direction (EDP=Dtop)

Figure 4.5. Results of MSA for 2-story buildings designed per TSC 1998, IM(Sd)-EDP(D_{top}). The black circles show the top displacement values, and the vertical red dashed lines denote slight, moderate, extensive and complete damage state thresholds from left to the right, respectively.

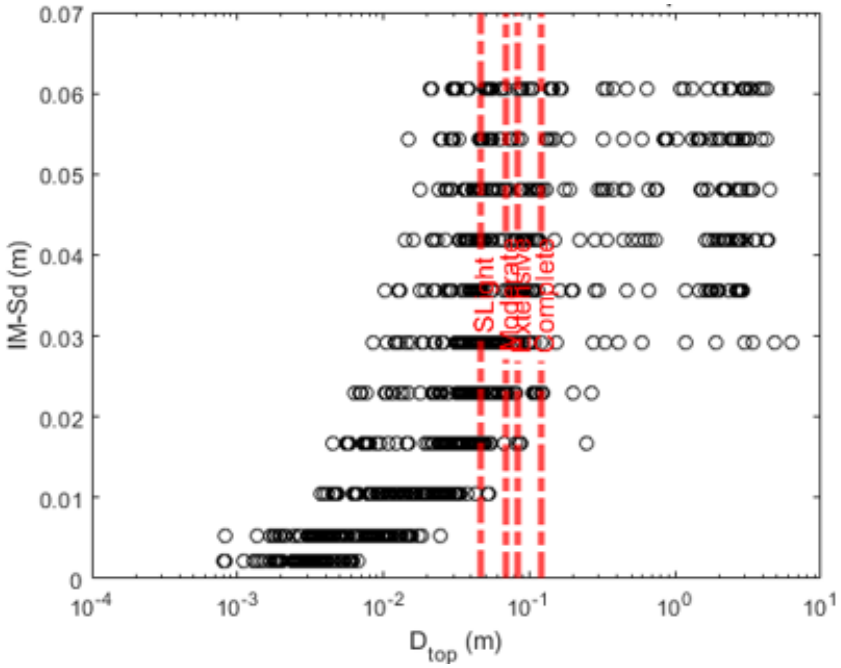

(a) 2-story 2018 in X-direction (EDP=Dtop)

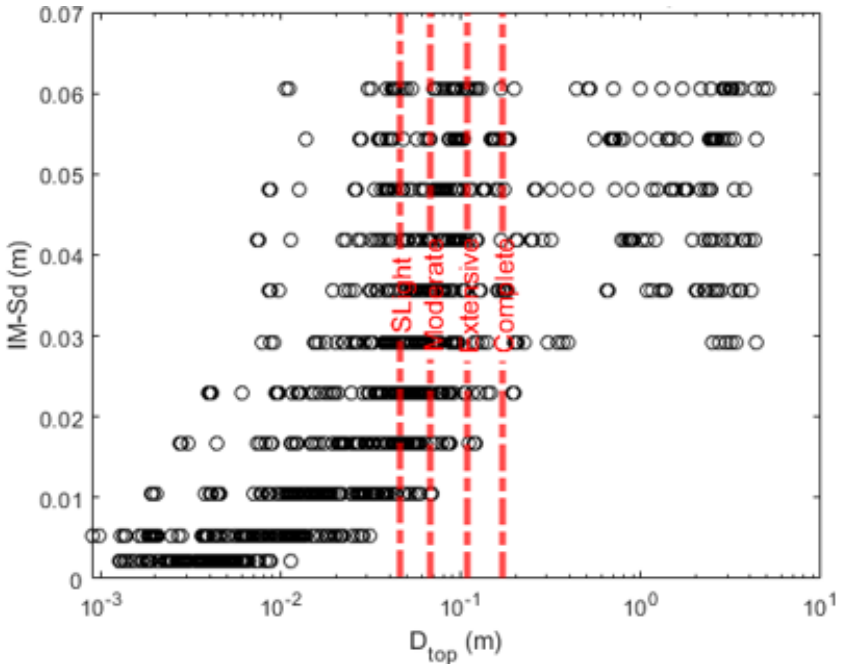

(b) 2-story 2018 in Y-direction (EDP=Dtop)

Figure 4.6. Results of MSA for 2-story buildings designed per TSC 2018, IM(Sd)-EDP(D_{top}). The black circles show the top displacement values, and the vertical red dashed lines denote slight, moderate, extensive and complete damage state thresholds from left to the right, respectively.

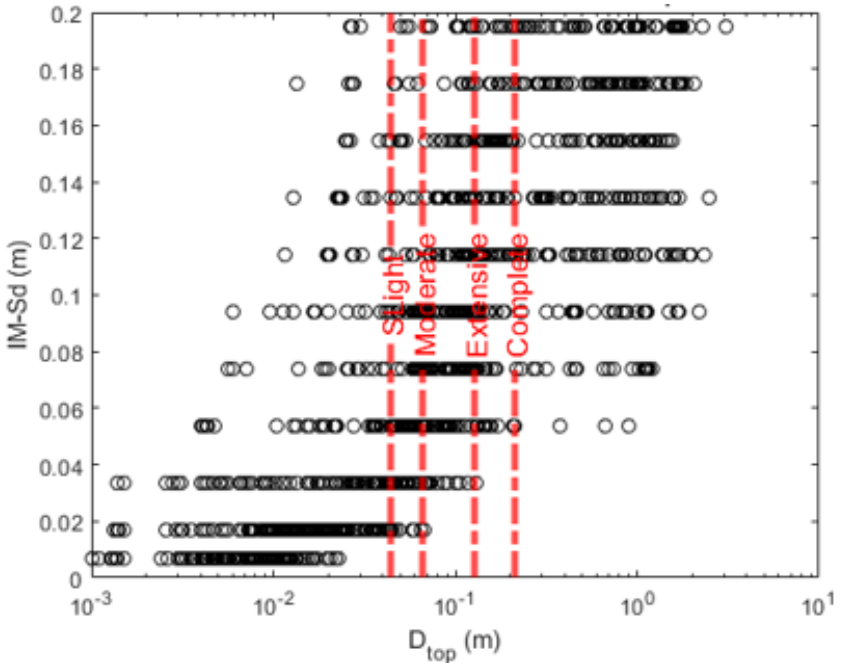

(a) 3-story 1998 in X-direction (EDP=Dtop)

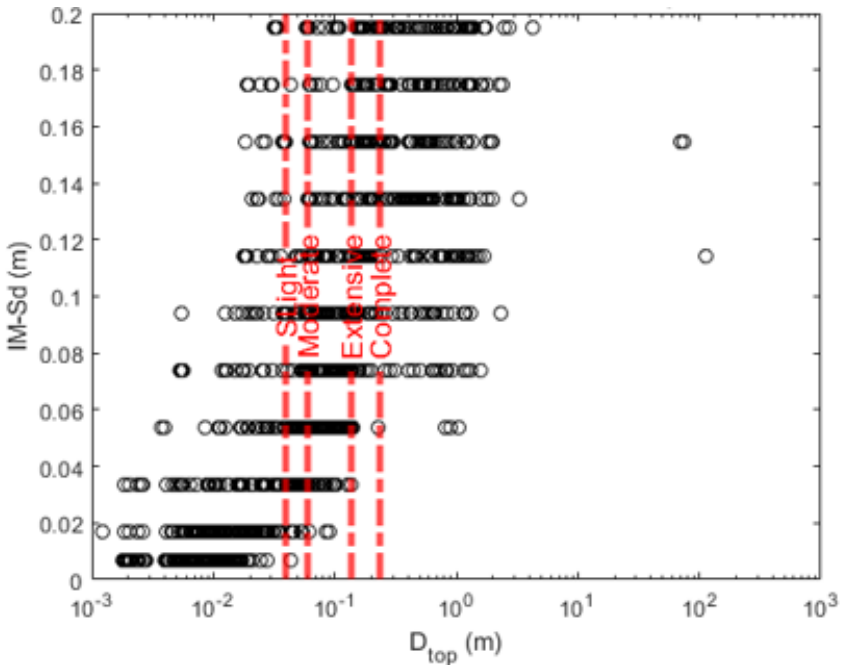

(b) 3-story 1998 in Y-direction (EDP=Dtop)

Figure 4.7. Results of MSA for 3-story buildings designed per TSC 1998, IM(Sd)-EDP(D_{top}). The black circles show the top displacement values, and the vertical red dashed lines denote slight, moderate, extensive and complete damage state thresholds from left to the right, respectively.

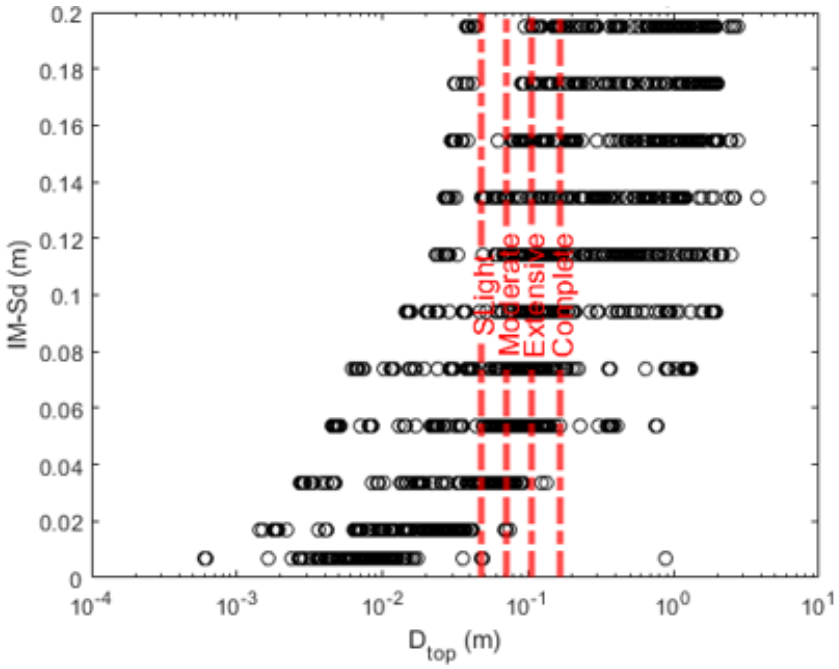

(a) 3-story 2018 in X-direction (EDP=Dtop)

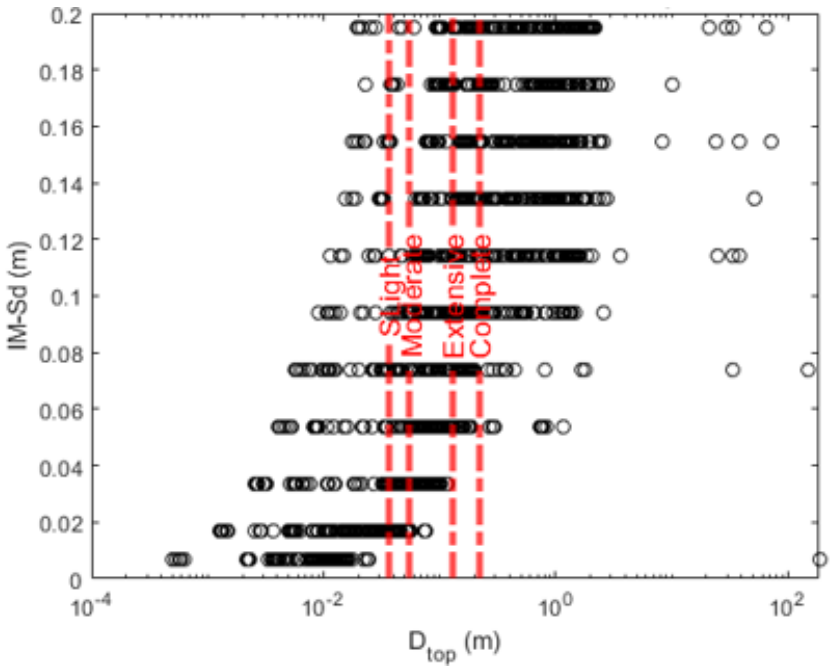

(b) 3-story 2018 in Y-direction (EDP=Dtop)

Figure 4.8. Results of MSA for 3-story buildings designed per TSC 2018, IM(Sd)-EDP(D_{top}). The black circles show the top displacement values, and the vertical red dashed lines denote slight, moderate, extensive and complete damage state thresholds from left to the right, respectively.

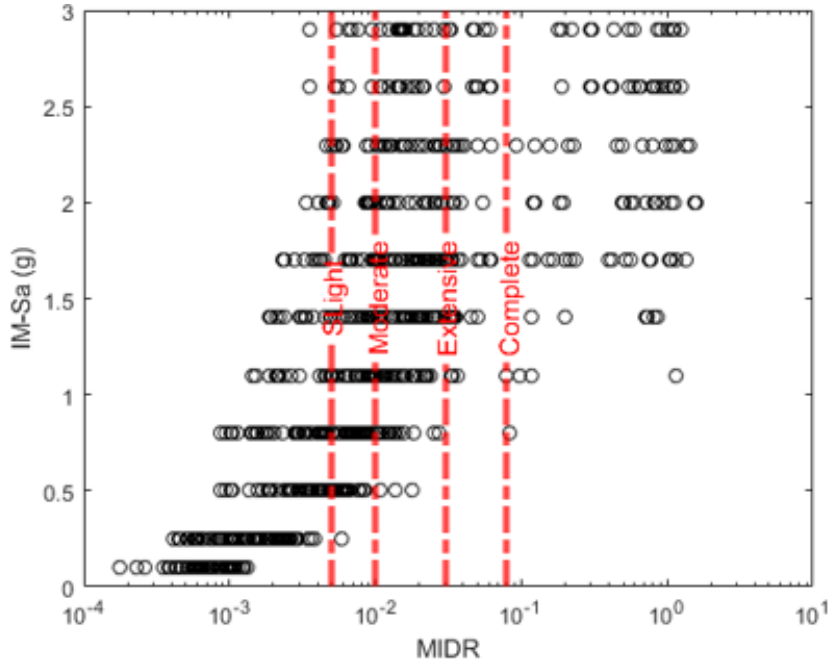

(a) 2-story 1998 in X-direction (EDP=MIDR)

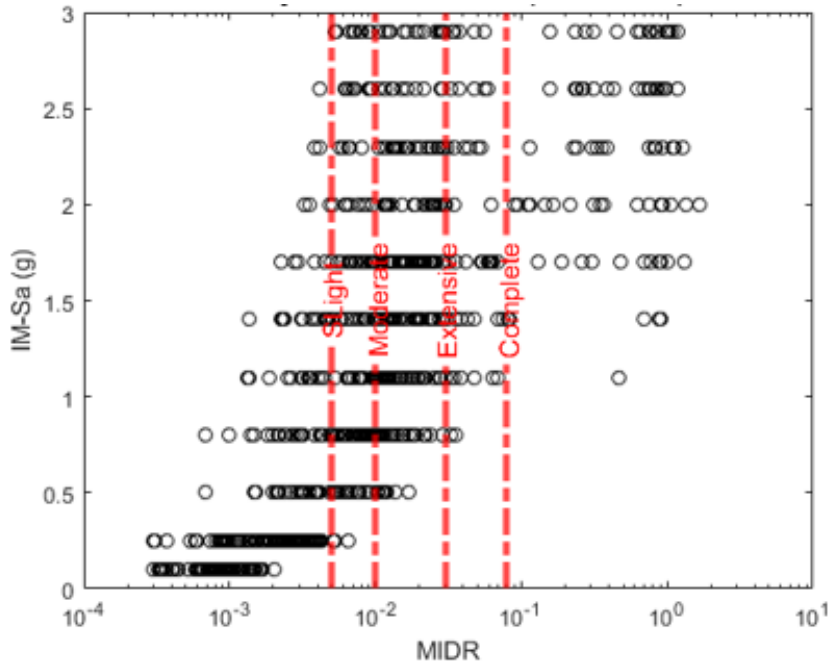

(b) 2-story 1998 in Y-direction (EDP=MIDR)

Figure 4.9. Results of MSA for 2-story buildings designed per TSC 1998, IM(Sa)-EDP(MIDR). The black circles show the MIDR values, and the vertical red dashed lines denote slight, moderate, extensive and complete damage state thresholds from left to the right, respectively.

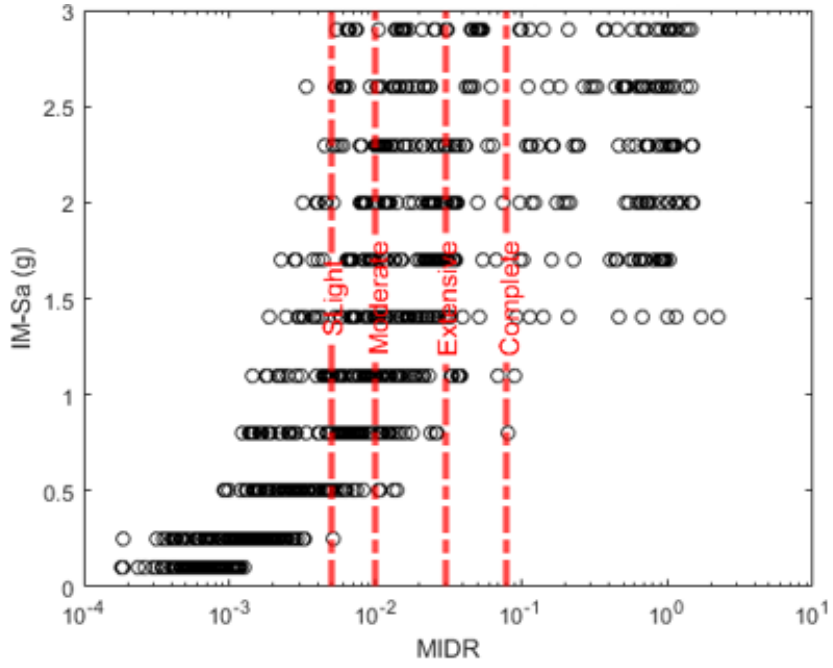

(a) 2-story 2018 in X-direction (EDP=MIDR)

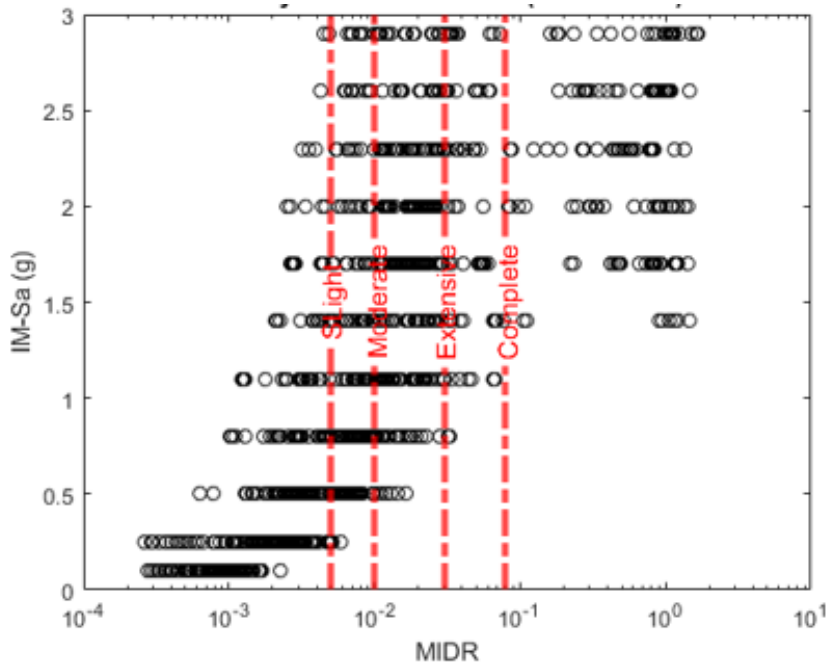

(b) 2-story 2018 in Y-direction (EDP=MIDR)

Figure 4.10. Results of MSA for 2-story buildings designed per TSC 2018, IM(Sa)-EDP(MIDR). The black circles show the MIDR values, and the vertical red dashed lines denote slight, moderate, extensive and complete damage state thresholds from left to the right, respectively.

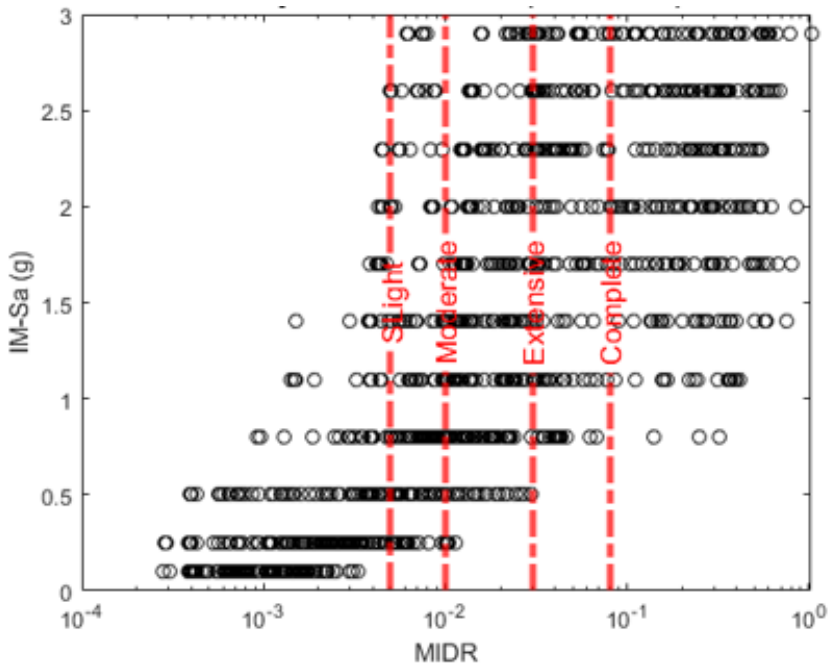

(a) 3-story 1998 in X-direction (EDP=MIDR)

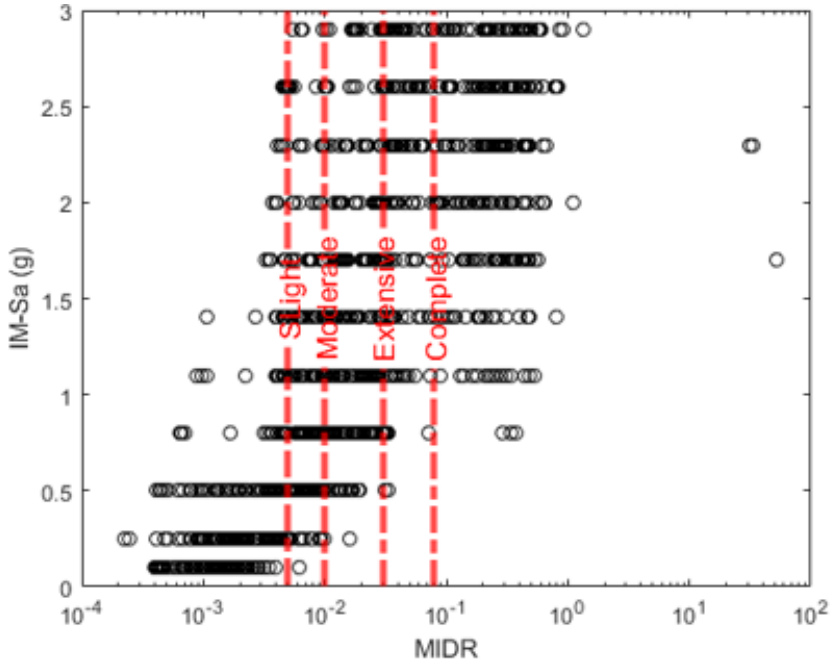

(b) 3-story 1998 in Y-direction (EDP=MIDR)

Figure 4.11. Results of MSA for 3-story buildings designed per TSC 1998, IM(Sa)-EDP(MIDR). The black circles show the MIDR values, and the vertical red dashed lines denote slight, moderate, extensive and complete damage state thresholds from left to the right, respectively.

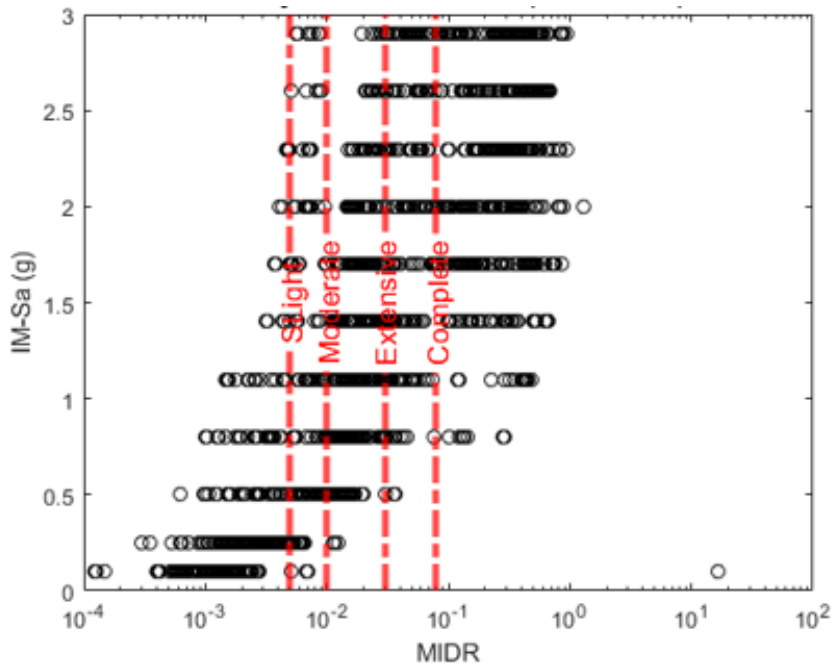

(a) 3-story 2018 in X-direction (EDP=MIDR)

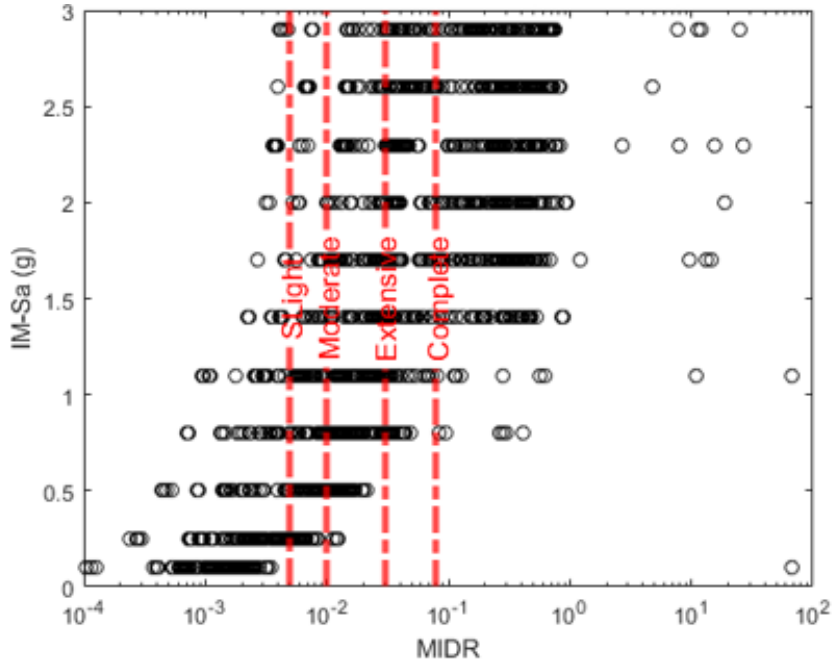

(b) 3-story 2018 in Y-direction (EDP=MIDR)

Figure 4.12. Results of MSA for 3-story buildings designed per TSC 2018, IM(Sa)-EDP(MIDR). The black circles show the MIDR values, and the vertical red dashed lines denote slight, moderate, extensive and complete damage state thresholds from left to the right, respectively.

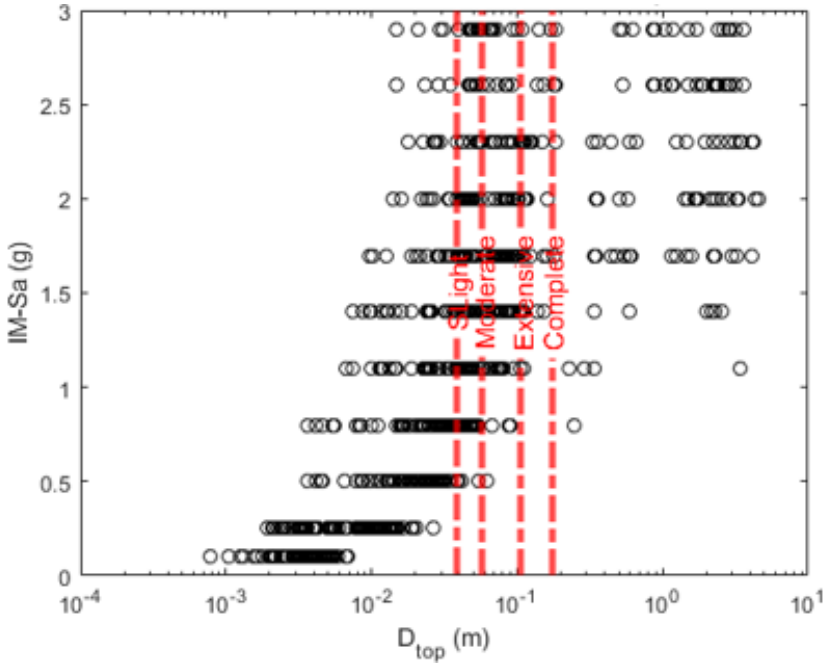

(a) 2-story 1998 in X-direction (EDP=Dtop)

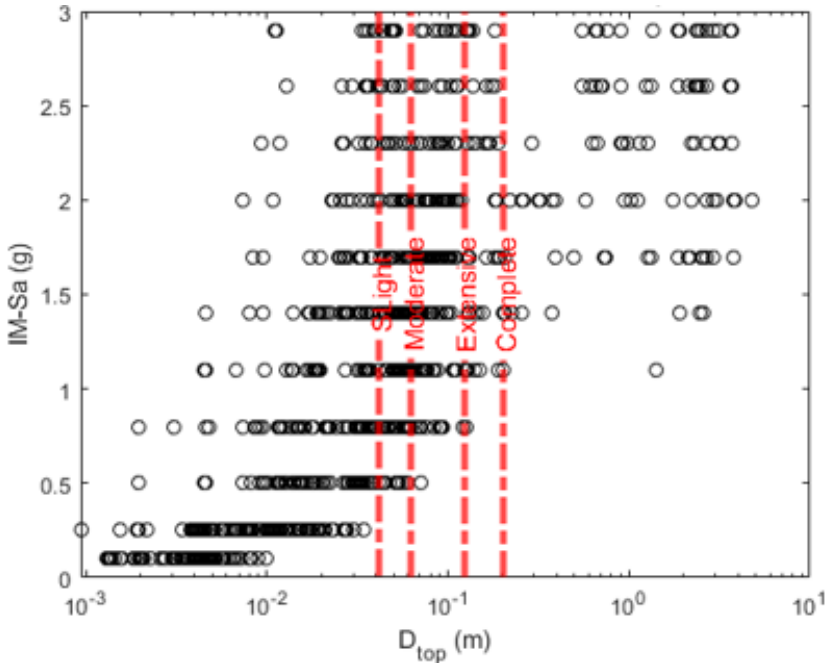

(b) 2-story 1998 in Y-direction (EDP=Dtop)

Figure 4.13. Results of MSA for 2-story buildings designed per TSC 1998, IM(Sa)-EDP(D_{top}). The black circles show the top displacement values, and the vertical red dashed lines denote slight, moderate, extensive and complete damage state thresholds from left to the right, respectively.

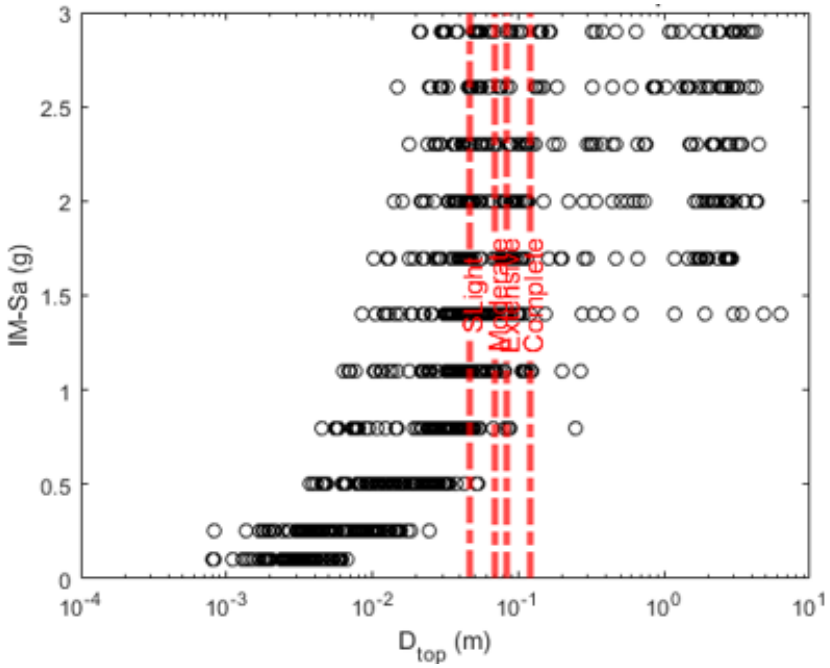

(a) 2-story 2018 in X-direction (EDP=Dtop)

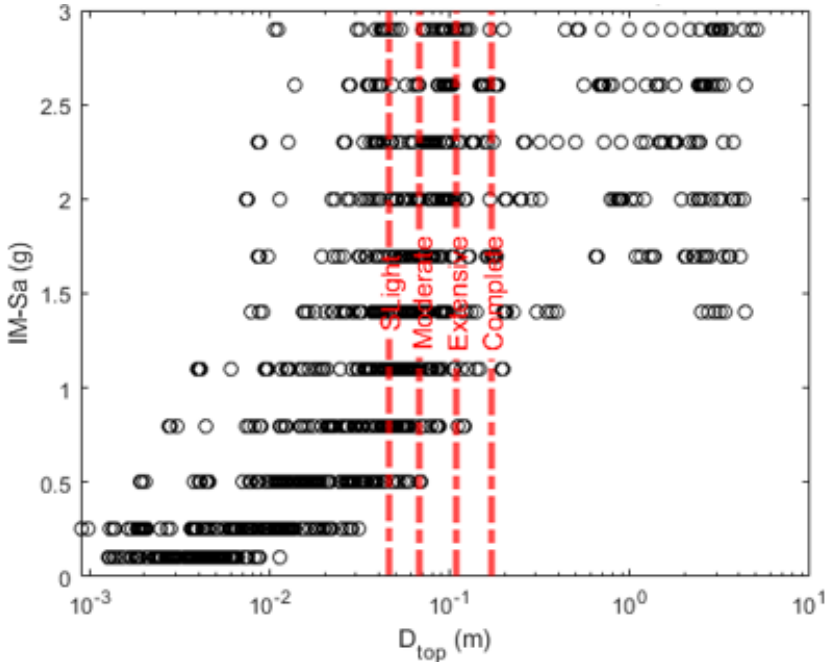

(b) 2-story 2018 in Y-direction (EDP=Dtop)

Figure 4.14. Results of MSA for 2-story buildings designed per TSC 2018, IM(Sa)-EDP(D_{top}). The black circles show the top displacement values, and the vertical red dashed lines denote slight, moderate, extensive and complete damage state thresholds from left to the right, respectively.

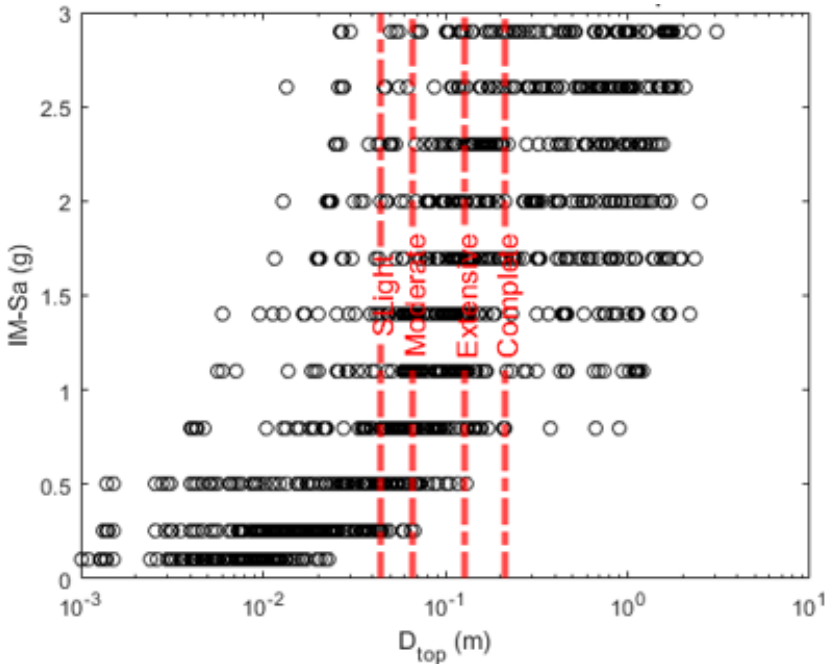

(a) 3-story 1998 in X-direction (EDP=Dtop)

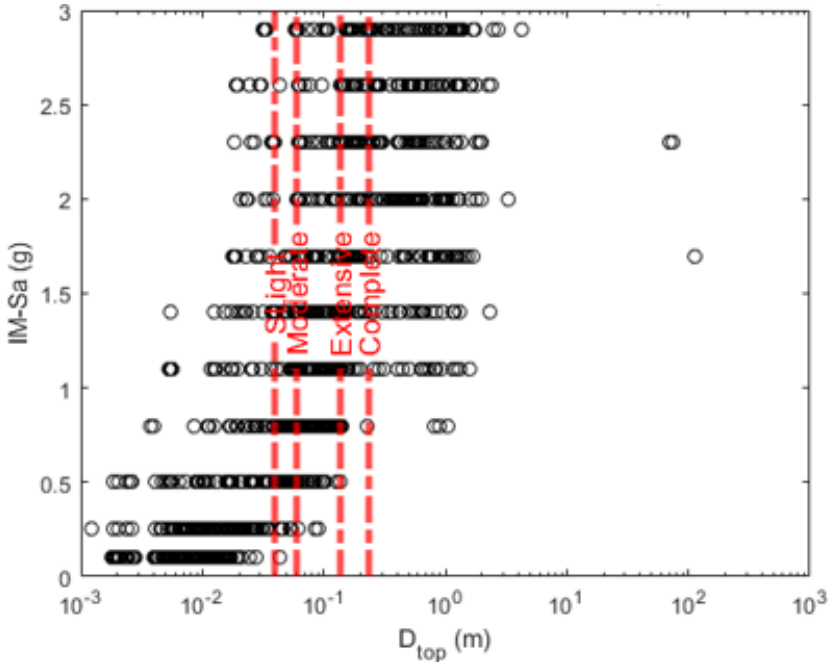

(b) 3-story 1998 in Y-direction (EDP=Dtop)

Figure 4.15. Results of MSA for 3-story buildings designed per TSC 1998, IM(Sa)-EDP(D_{top}). The black circles show the top displacement values, and the vertical red dashed lines denote slight, moderate, extensive and complete damage state thresholds from left to the right, respectively

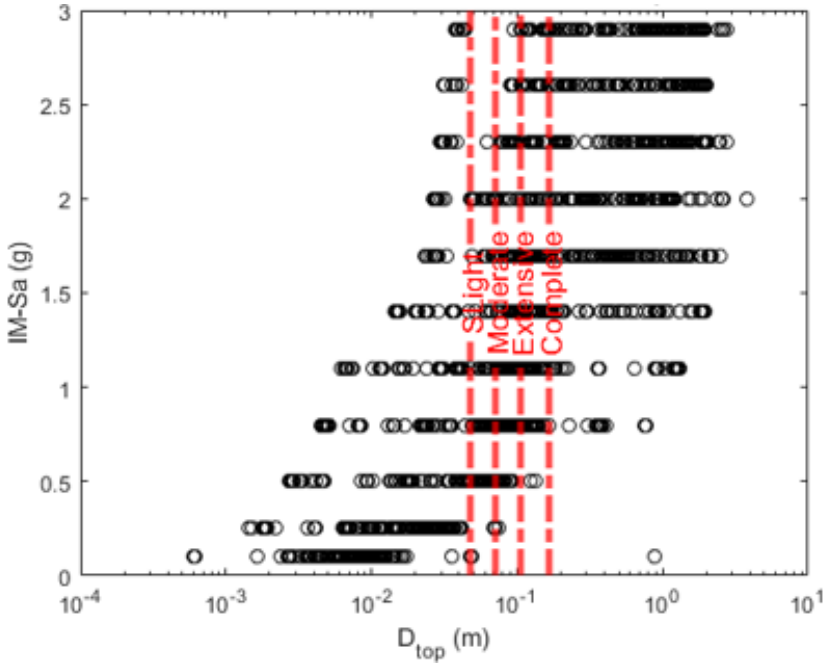

(a) 3-story 2018 in X-direction (EDP=Dtop)

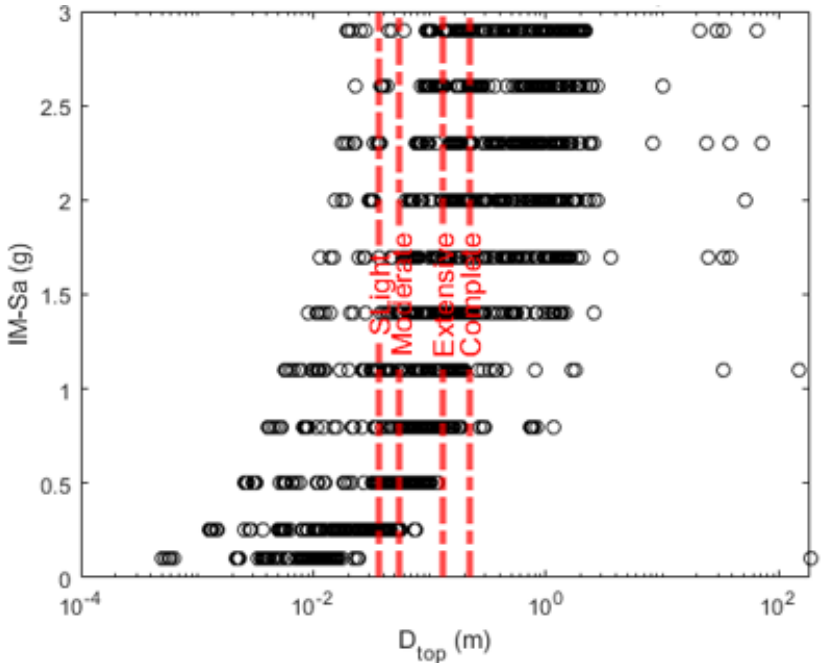

(b) 3-story 2018 in X-direction (EDP=Dtop)

Figure 4.16. Results of MSA for 3-story buildings designed per TSC 2018, IM(Sa)-EDP(D_{top}). The black circles show the top displacement values, and the vertical red dashed lines denote slight, moderate, extensive and complete damage state thresholds from left to the right, respectively.

4.2. Development of Fragility Functions for the Buildings

The maximum likelihood estimation (MSE) method is utilized to generate the fragility functions. The procedure of the MSE method is explained in the article written by Jack Baker (2015) [19]. The study (Baker, 2015) defines the statistical methods to get the fragility functions parameters by using the nonlinear dynamic analyses results. Fragility functions are obtained by using a lognormal cumulative distribution function which is given in Equation 4.1. The goal is to find the best θ and β values which are the median and logarithmic standard deviation of the fragility function, respectively.

$$P(DS/IM \geq x) = \phi\left(\frac{In\,(x/\theta)}{\beta}\right) \tag{4.1}$$

$P(DS/IM \geq x)$ is probability of exceeding a damage state (DS) for a given intensity measure (IM=x). $\phi\,()$ is the standard normal cumulative distribution function and θ , β are the median of IM and the standard deviation of $In(IM)$, respectively.

By using the maximum likelihood estimation (MLE) method, θ and β are predicted. For a given IM level, the probability of observing z_j collapses in n_j ground motions for a certain IM is obtained by the binomial distribution in Equation 4.2.

$$P(z_j collapses in n_j ground motions) = \binom{n_j}{z_j} p_j^{z_j} (1-p_j)^{n_j - z_j} \tag{4.2}$$

In equation 4.2, p_j is the probability of ground motions with IM=xj to exceed a DS for a given building that is previously defined as $P(DS/IM \geq x)$ in Equation 4.1. The maximum likelihood method provides the highest probability of p_j.

When different IM levels are used for the analyses, the likelihood function that is the product of the binomial probabilities (from Equation 4.2) at each IM level is defined by using Equation 4.3.

$$Likelihood = \prod_{j}^{m} \binom{n_j}{z_j} p_j^{z_j} (1 - p_j)^{n_j - z_j} \tag{4.3}$$

If p_j is written in the Likelihood equation, Equation 4.3 is converted to;

$$Likelihood = \prod_{j}^{m} \binom{n_j}{z_j} \phi \left(\frac{In\,(x/\theta)}{\beta} \right)^{z_j} (1 - \phi \left(\frac{In\,(x/\theta)}{\beta} \right))^{n_j - z_j} \tag{4.4}$$

Since it is easier to maximize a sum equation than maximizing a product equation, Equation 4.3 is converted into equation 4.4 by taking the natural logarithm of both sides of Equation 4.4.

The θ and β values which maximize Equation 4.5 are selected as the parameters of the fragility functions.

$$\{\theta, \beta\} = arg_{\theta,\beta} max \sum_{j_1}^{n} \left\{ In \binom{n_j}{z_j} + In\phi \left(\frac{In\,(x/\theta)}{\beta} \right) + (n_j - z_j) In(1 - \phi \left(\frac{In\,(x/\theta)}{\beta} \right) \right\} \tag{4.5}$$

By using the MSA results (Figures 4.1 to 4.8) and the MLE method explained above, the fragility functions are developed for the 2 and 3-story buildings. The fragility curves and the fragility parameters' values are given in Figures 4.17 to 4.24 and Tables

4.1 to 4.8, respectively.

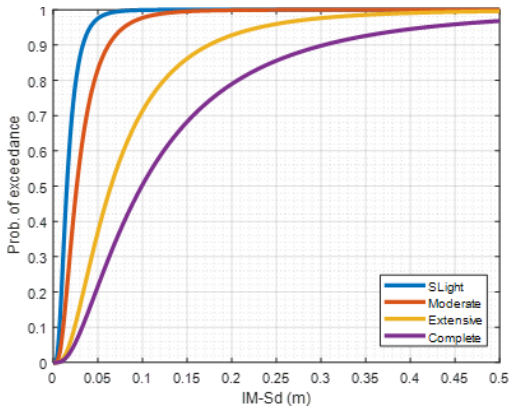

(a) 2-story 1998 in x-direction

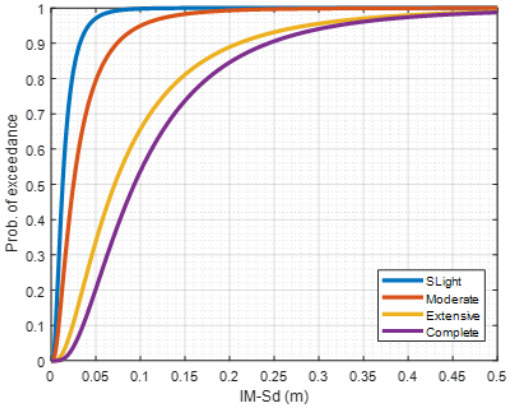

(b) 2-story 1998 in y-direction

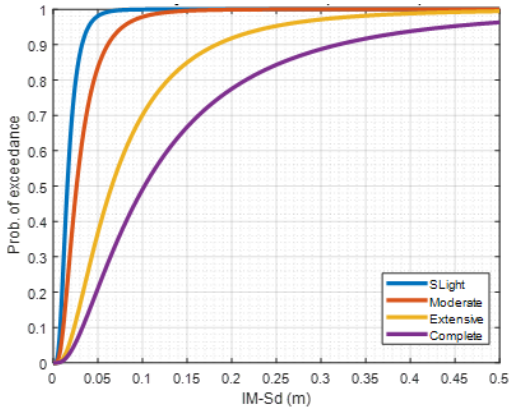

(c) 2-story 2018 in x-direction

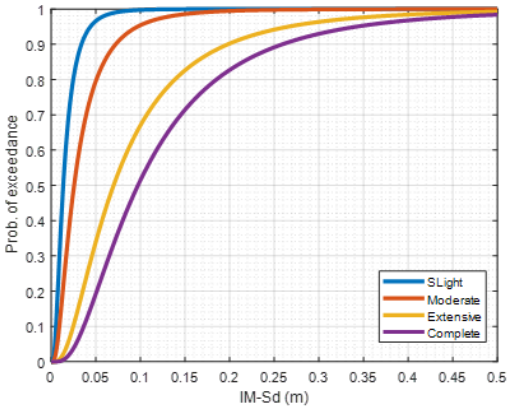

(d) 2-story 2018 in y-direction

Figure 4.17. Fragility curves of 2-story buildings, IM(Sd)-EDP(MIDR).

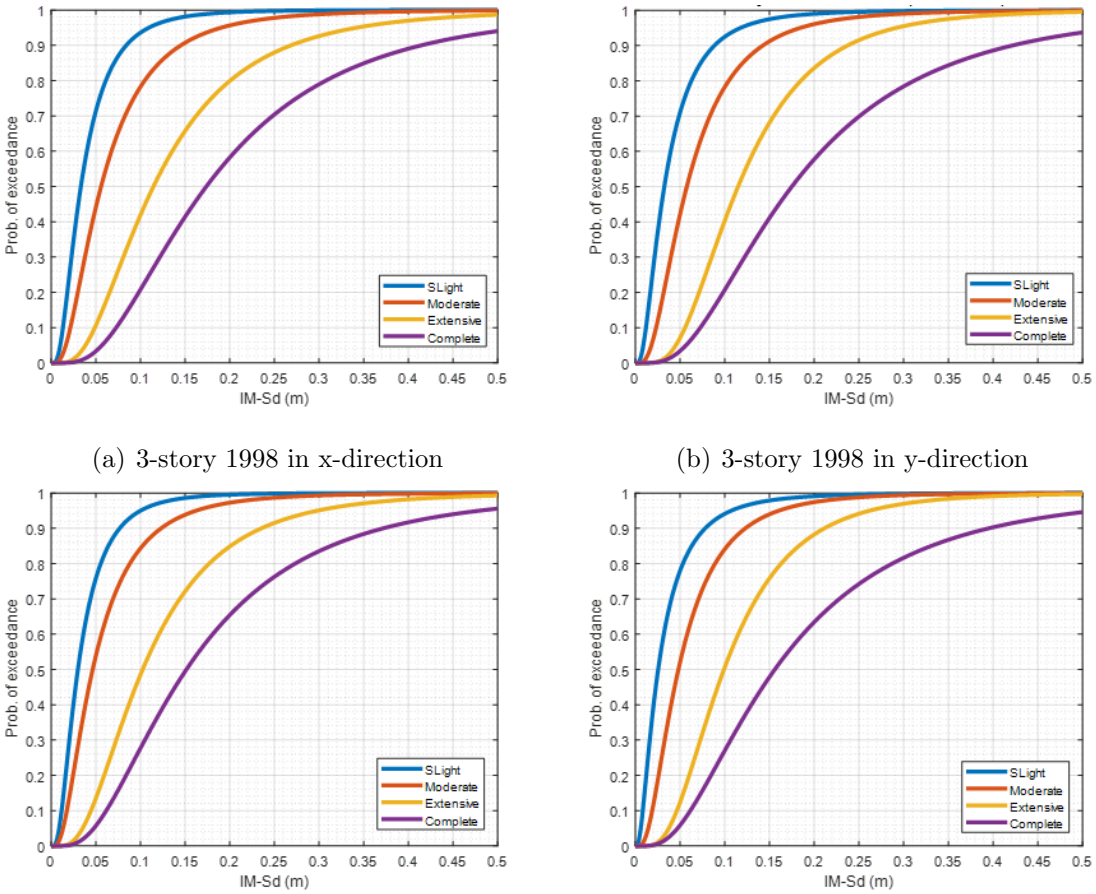

(a) 3-story 1998 in x-direction

(b) 3-story 1998 in y-direction

(c) 3-story 2018 in x-direction

(d) 3-story 2018 in y-direction

Figure 4.18. Fragility curves of 3-story buildings, IM(Sd)-EDP(MIDR).

Table 4.1. Parameters of fragility curves in the x-direction (EDP = MIDR, IM = Sd(m)). (Θ=Sd[m], β=In(Sd[m]))

Building Type	**Slight**		**Moderate**		**Extensive**		**Complete**	
	Θ	β	Θ	β	Θ	β	Θ	β
2-1998	0.0153	0.6027	0.0264	0.6684	0.0647	0.7736	0.0992	0.8712
2-2018	0.0158	0.5544	0.0262	0.6615	0.0656	0.7997	0.1022	0.8879
3-1998	0.0332	0.7242	0.0559	0.7456	0.1145	0.6652	0.1738	0.6787
3-2018	0.0299	0.7343	0.0465	0.7604	0.1025	0.6494	0.1515	0.7011

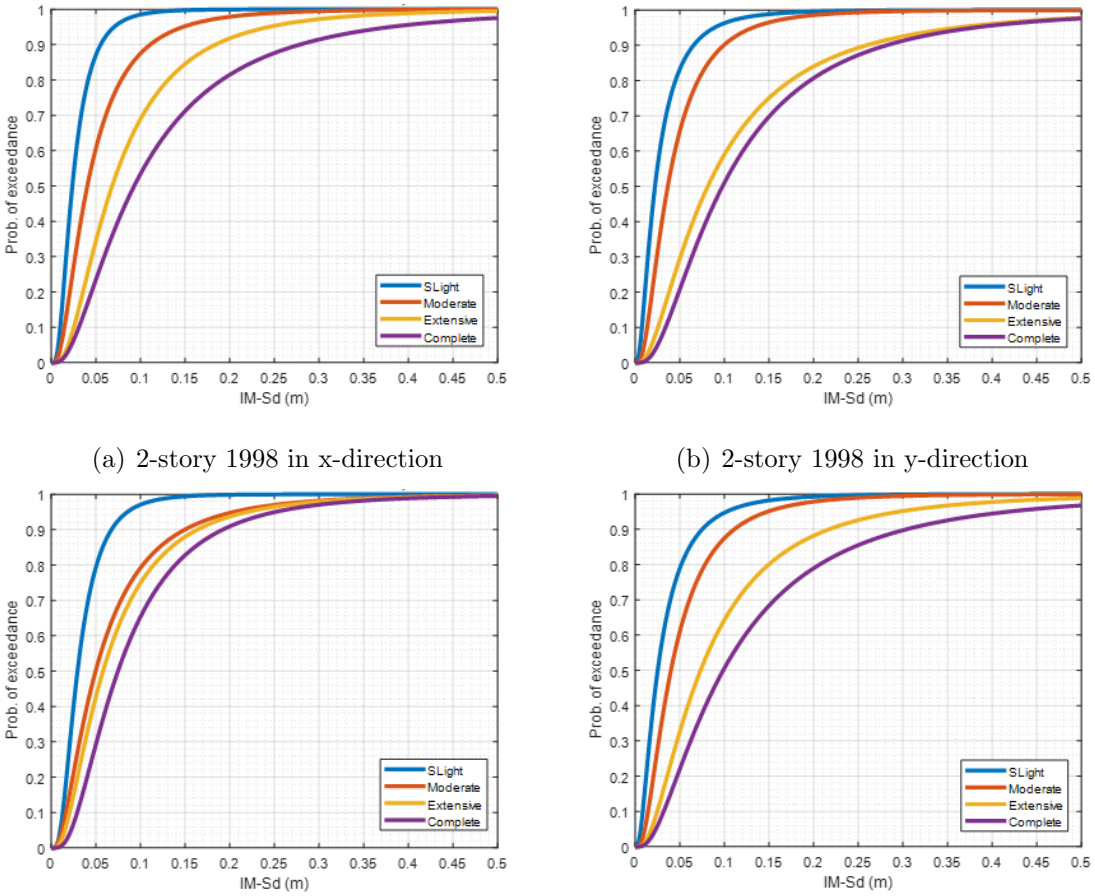

(a) 2-story 1998 in x-direction

(b) 2-story 1998 in y-direction

(c) 2-story 2018 in x-direction

(d) 2-story 2018 in y-direction

Figure 4.19. Fragility curves of 2-story buildings, IM(Sd)-EDP(D_{top}).

Table 4.2. Parameters of fragility curves in the x-direction (EDP = Dtop, IM = Sd(m)). (Θ=Sd[m], β=In(Sd[m]))

Building Type	**Slight**		**Moderate**		**Extensive**		**Complete**	
	Θ	β	Θ	β	Θ	β	Θ	β
2-1998	0.0237	0.6630	0.0405	0.7860	0.0683	0.7732	0.0930	0.8557
2-2018	0.0295	0.6463	0.0498	0.8590	0.0581	0.8083	0.0748	0.7358
3-1998	0.0432	0.7668	0.0625	0.7402	0.1140	0.6554	0.1573	0.6479
3-2018	0.0385	0.8256	0.0562	0.6932	0.0891	0.5829	0.1249	0.6299

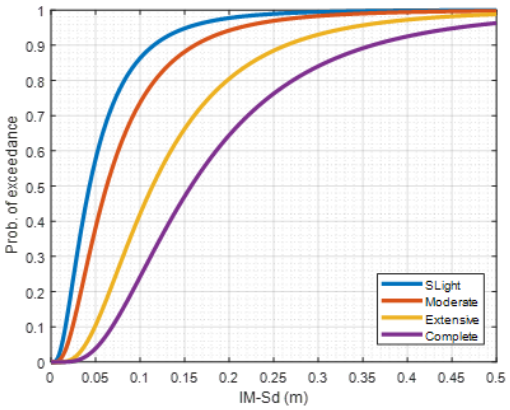

(a) 3-story 1998 in x-direction

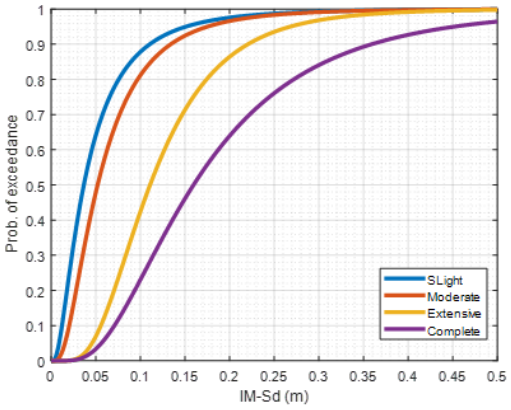

(b) 3-story 1998 in y-direction

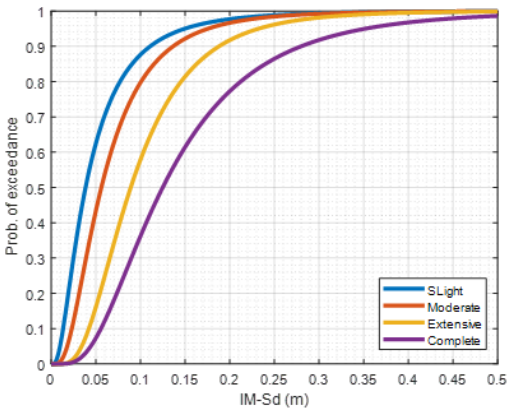

(c) 3-story 2018 in x-direction

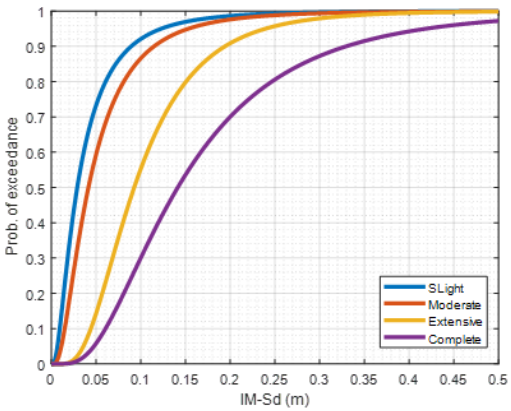

(d) 3-story 2018 in y-direction

Figure 4.20. Fragility curves of 3-story buildings, IM(Sd)-EDP(D_{top}).

Table 4.3. Parameters of fragility curves in the x-direction (EDP = MIDR, IM = Sa(g)). (Θ=Sa[g], β=In(Sa[g]))

Building Type	**Slight**		**Moderate**		**Extensive**		**Complete**	
	Θ	β	Θ	β	Θ	β	Θ	β
2-1998	0.7339	0.6027	1.2620	0.6683	3.0964	0.7736	4.7494	0.8712
2-2018	0.7582	0.5544	1.2544	0.6614	3.1401	0.7998	4.8921	0.8879
3-1998	0.4948	0.7242	0.8317	0.7456	1.7047	0.6652	2.5863	0.6787
3-2018	0.4453	0.7343	0.6915	0.7605	1.5249	0.6493	2.2542	0.7011

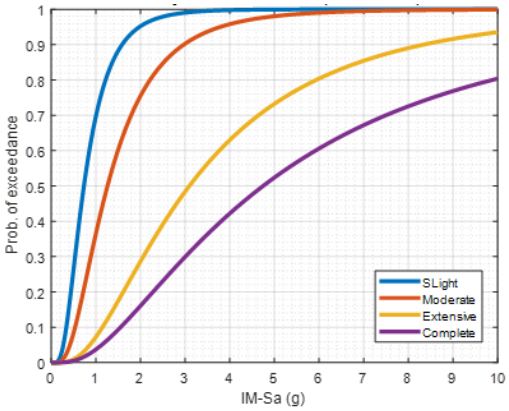

(a) 2-story 1998 in x-direction

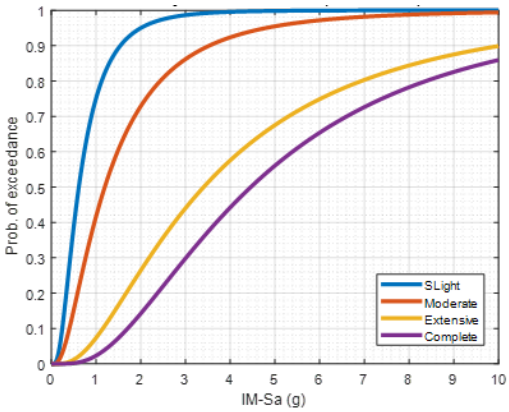

(b) 2-story 1998 in y-direction

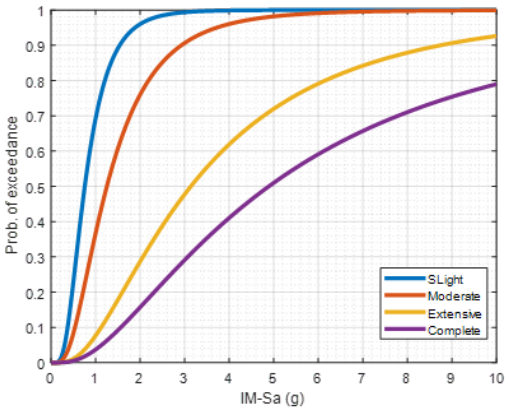

(c) 2-story 2018 in x-direction

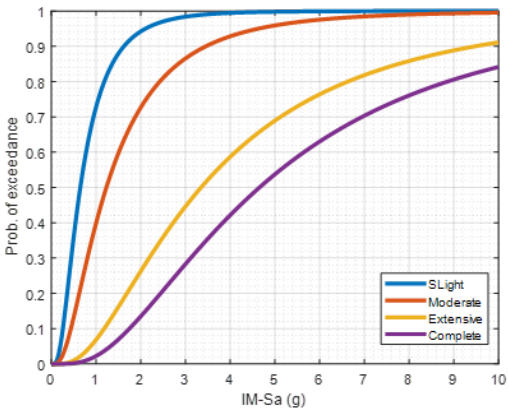

(d) 2-story 2018 in y-direction

Figure 4.21. Fragility curves of 2-story buildings, IM(Sa)-EDP(MIDR).

Table 4.4. Parameters of fragility curves in the x-direction (EDP = Dtop, IM = Sa(g)). (Θ=Sa[g], β=In(Sa[g]))

Building Type	**Slight**		**Moderate**		**Extensive**		**Complete**	
	Θ	β	Θ	β	Θ	β	Θ	β
2-1998	1.1335	0.6629	1.9381	0.7860	3.2679	0.7732	4.4487	0.8556
2-2018	1.4109	0.6463	2.3813	0.8591	2.7796	0.8082	3.5796	0.7358
3-1998	0.6429	0.7668	0.9307	0.7402	1.6961	0.6554	2.3414	0.6479
3-2018	0.5729	0.8256	0.8362	0.6932	1.3259	0.5828	1.8588	0.6299

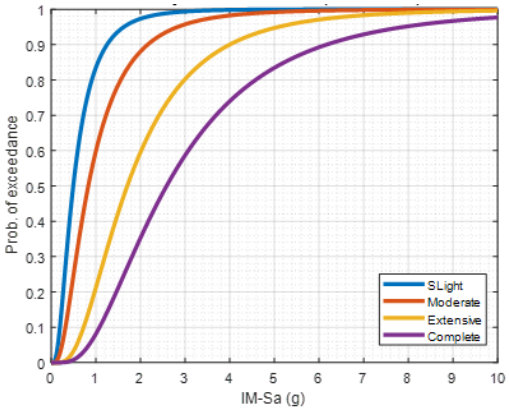

(a) 3-story 1998 in x-direction

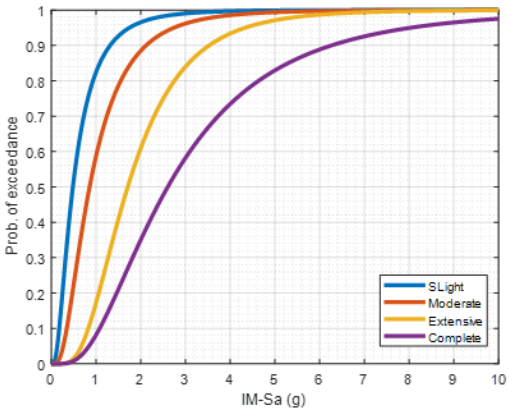

(b) 3-story 1998 in y-direction

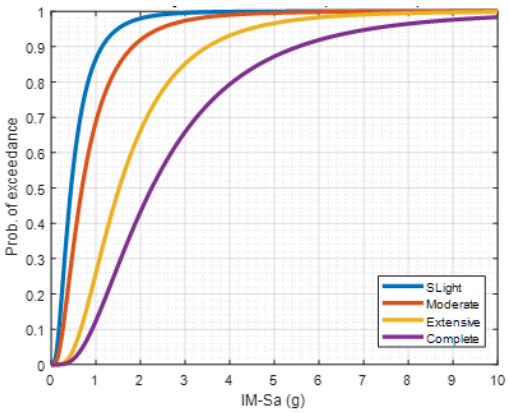

(c) 3-story 2018 in x-direction

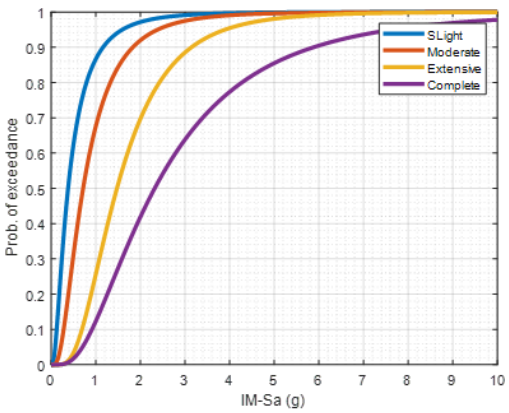

(d) 3-story 2018 in y-direction

Figure 4.22. Fragility curves of 2-story buildings, IM(Sa)-EDP(MIDR).

Table 4.5. Parameters of fragility curves in the y-direction (EDP = MIDR, IM = Sd(m). (Θ=Sd[m], β=In(Sd[m]))

Building Type	**Slight**		**Moderate**		**Extensive**		**Complete**	
	Θ	β	Θ	β	Θ	β	Θ	β
2-1998	0.0129	0.7176	0.0250	0.8458	0.0712	0.8444	0.0932	0.7491
2-2018	0.0136	0.7163	0.0257	0.8056	0.0700	0.8116	0.0973	0.7646
3-1998	0.0324	0.7832	0.0575	0.7078	0.1149	0.5662	0.1750	0.6857
3-2018	0.0255	0.8731	0.0482	0.7316	0.0991	0.5912	0.1560	0.7256

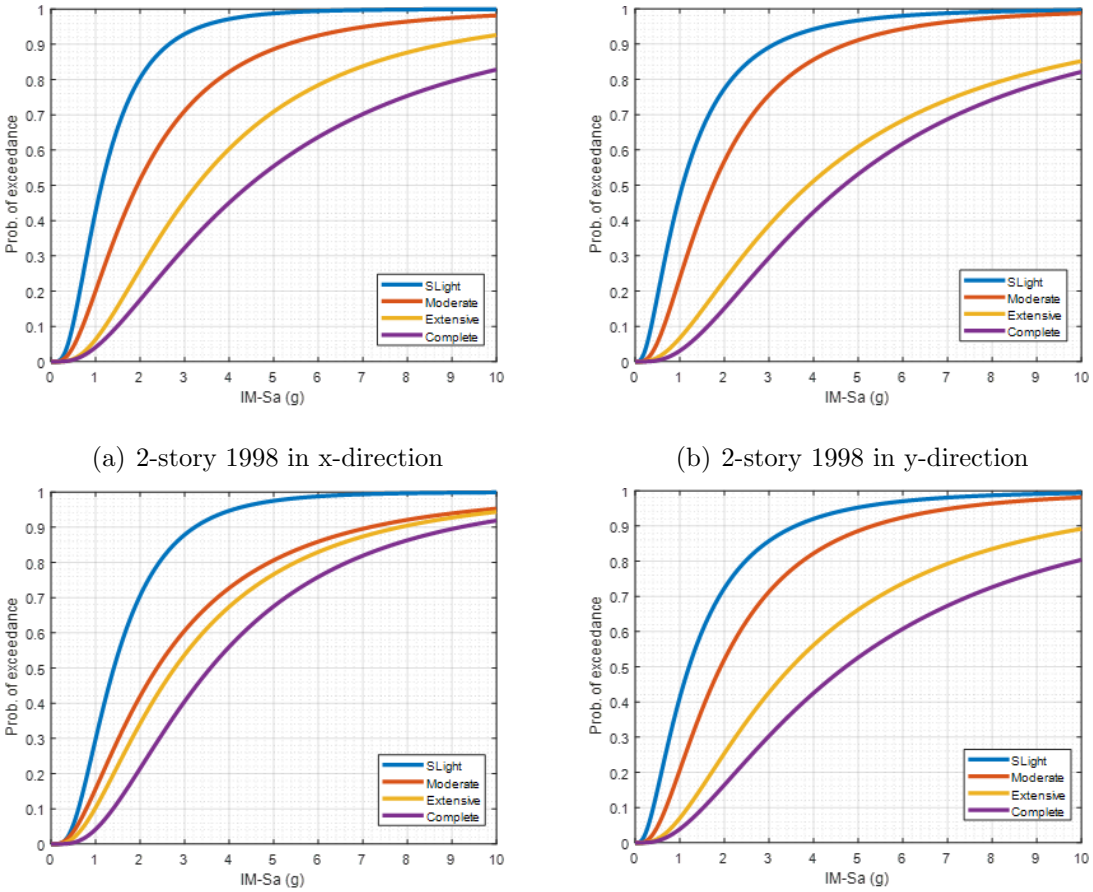

(a) 2-story 1998 in x-direction

(b) 2-story 1998 in y-direction

(c) 2-story 2018 in x-direction

(d) 2-story 2018 in y-direction

Figure 4.23. Fragility curves of 2-story buildings, IM(Sa)-EDP(D_{top}).

Table 4.6. Parameters of fragility curves in the y-direction (EDP = Dtop, IM = Sd(m). (Θ=Sd[m], β=In(Sd[m]))

Building Type	**Slight**		**Moderate**		**Extensive**		**Complete**	
	Θ	β	Θ	β	Θ	β	Θ	β
2-1998	0.0222	0.8426	0.0366	0.7795	0.0814	0.9043	0.0979	0.8246
2-2018	0.0253	0.8514	0.0401	0.7952	0.0733	0.8481	0.0987	0.8786
3-1998	0.0366	0.8619	0.0521	0.7382	0.1108	0.5370	0.1596	0.6333
3-2018	0.0290	0.8788	0.0415	0.7950	0.0927	0.5776	0.1414	0.6609

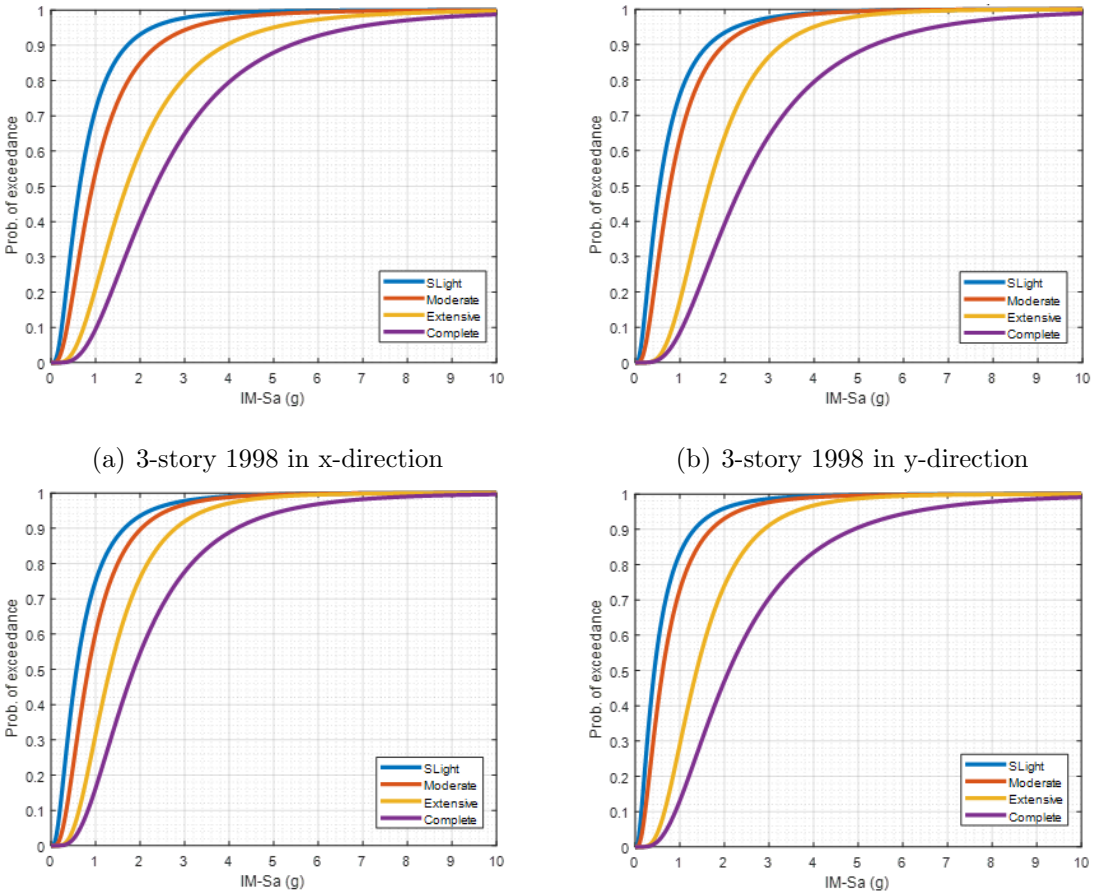

(a) 3-story 1998 in x-direction

(b) 3-story 1998 in y-direction

(c) 3-story 2018 in x-direction

(d) 3-story 2018 in y-direction

Figure 4.24. Fragility curves of 3-story buildings, IM(Sa)-EDP(D_{top}).

Table 4.7. Parameters of fragility curves in the y-direction (EDP = MIDR, IM = Sa(g). (Θ=Sa[g], β=In(Sa[g]))

Building Type	**Slight**		**Moderate**		**Extensive**		**Complete**	
	Θ	β	Θ	β	Θ	β	Θ	β
2-1998	0.6156	0.7177	1.1956	0.8458	3.4078	0.8445	4.4622	0.7491
2-2018	0.6485	0.7162	1.2314	0.8055	3.3494	0.8117	4.6557	0.7646
3-1998	0.4824	0.7832	0.8563	0.7078	1.7096	0.5662	2.6043	0.6857
3-2018	0.3798	0.8732	0.7170	0.7316	1.4750	0.5911	2.3211	0.7257

Table 4.8. Parameters of fragility curves in the y-direction (EDP = Dtop, IM = Sa(g). (Θ=Sa[g], β=In(Sa[g]))

Building Type	**Slight**		**Moderate**		**Extensive**		**Complete**	
	Θ	β	Θ	β	Θ	β	Θ	β
2-1998	1.0637	0.8426	1.7495	0.7795	3.8947	0.9043	4.6855	0.8246
2-2018	1.2084	0.8514	1.9193	0.7953	3.5075	0.8481	4.7207	0.8785
3-1998	0.5452	0.8619	0.7749	0.7381	1.6496	0.5370	2.3746	0.6333
3-2018	0.4314	0.8788	0.6175	0.7950	1.3789	0.5776	2.1041	0.6609

5. RESULTS AND DISCUSSIONS

In this study, fragility functions are derived for low-rise (2 and 3-stories) MRF RC buildings which are designed by considering the minimum conditions of Turkish Seismic Codes released in 1998 and 2018. To increase the reliability of the study, eight different locations in Istanbul are selected and the buildings are designed according to the seismic hazard parameters defined for these locations. The buildings' responses are obtained by performing multiple stripes analyses (MSA). The fragility curves are compared conveniently in Figures 5.1 to 5.8.

As can be seen from Figures 5.1 to 5.8, the 2-story buildings that are designed per TSC 2018 have lower exceeding probabilities than the 2-story buildings that are designed per TSC 1998. However, the 3-story buildings that are designed per TSC 1998 have lower exceeding probabilities than the 3-story buildings that are designed per TSC 2018. This results from the new seismic hazard map released with the 2018 Turkish Seismic Code. In the new seismic hazard map, instead of the seismic zones, Ss and S_1 values, which are the spectral acceleration coefficients corresponding to the T=0.2-second-short period and T=1.0-second-long period, are defined. When designing the 3-story buildings per TSC1998, due to the use of the same seismic acceleration coefficients given in TSC1998, higher base shear forces are calculated than the base shear forces calculated per TSC 2018. This situation gives rise to a higher reinforcement amount in the structural elements of the 3-story buildings designed per TSC 1998. In Table 5.1, the base shear forces are listed as the average of the base shear forces in the X and Y directions for each building.

In Figures 5.9 to 5.12, fragility curves, which are derived in the scope of this thesis, are compared with different studies. In Figure 5.9, fragility curves in the scope of this study are compared with the low-rise(1-4 story) RC-MRF buildings(B513). Fragility curves for this building type(B513) were created with the study that was done by Istanbul Metropolitan Municipality and nonlinear static analyses were used to generate the fragility curves. In this study, for the estimation of building damages

by analytical methods, the spectral capacity-based damage estimation method that was developed within the framework of the HAZUS project (1999), was used. For this method, capacity spectrum and earthquake demand spectrum for each building class were determined. Capacity spectrum and earthquake demand spectrum curves are intersected mathematically and spectral displacement value which corresponds to the building capacity was obtained as a performance point. In this study, four damage states were considered as slight, moderate, extensive, and complete. In this study, B513 is the building type and represents the low-rise buildings constructed post-2000. In Figure 5.9, the probability of exceedance for buildings designed per TSC 1998 and TSC 2018 is lower than the B513 buildings for slight, moderate, and extensive damage states. However, the probability of exceedance for buildings designed per TSC 1998 and TSC 2018 is higher than the B513 buildings for complete damages states. This is probably due to taking the high damage limit value for buildings B513.

In Figures 5.10 to 5.12, fragility curves, which are derived in the scope of this thesis, are compared with other studies that were derived by using nonlinear dynamic analyses. In Figures 5.10 to 5.11, four damage states were considered as slight, moderate, extensive, and complete. In Figure 5.12, three damage states were considered as immediate occupancy, life safety, and collapse prevention. Damage thresholds were determined by using the Turkish Seismic Code 2007. Three performance levels as immediate occupancy, life safety, and collapse prevention were considered as specified in Turkish Seismic Code 2007. Fragility curves for 3-story buildings designed per TSC 1999 and TSC 2018 have a lower probability of exceedance than fragility curves that are obtained for different studies by using nonlinear analyses.

Table 5.1. Base shear forces for 2-story and 3-story buildings, kN

	2 story buildings		**3 story buildings**	
	TSC 1998	**TSC 2018**	**TSC 1998**	**TSC 2018**
Location 1	242.25	547.11	896.76	1528.91
Location 2	242.25	412.34	896.76	1101.83
Location 4	323.00	401.52	1195.68	874.24
Location 5	323.00	536.74	1195.68	1159.42
Location 6	323.00	254.84	1195.68	523.14
Location 7	242.25	436.52	896.76	1152.27
Location 8	242.25	306.70	896.76	684.39
Location 10	161.50	176.26	501.70	362.32

Moreover, two types of IMs (Sd and Sa), and two types of EDPs (MIDR and Dtop) are used. When Sd is selected as the IM, the 3-story buildings have less probability of exceedance than the 2-story buildings. However, when Sa is selected as IM, the probability of exceedance of the 2-story buildings is less than that of the 3-story buildings. This is because when Sa is used as IM, all Sa values for IM levels (stripes) are the same for the two types of buildings (2 and 3 story). However, when Sd is used as IM, Sd values for IM levels (stripes) for the two types of buildings are different since the natural period of the two types of building are different. When converting the Sa values to the Sd values, Equation 5.1 is used. Since the value of T (period) is different for the 2 and 3-story buildings, Sd values for IM levels (stripes) differ.

$$S_d = \frac{T^2}{4\Pi^2} S_a \tag{5.1}$$

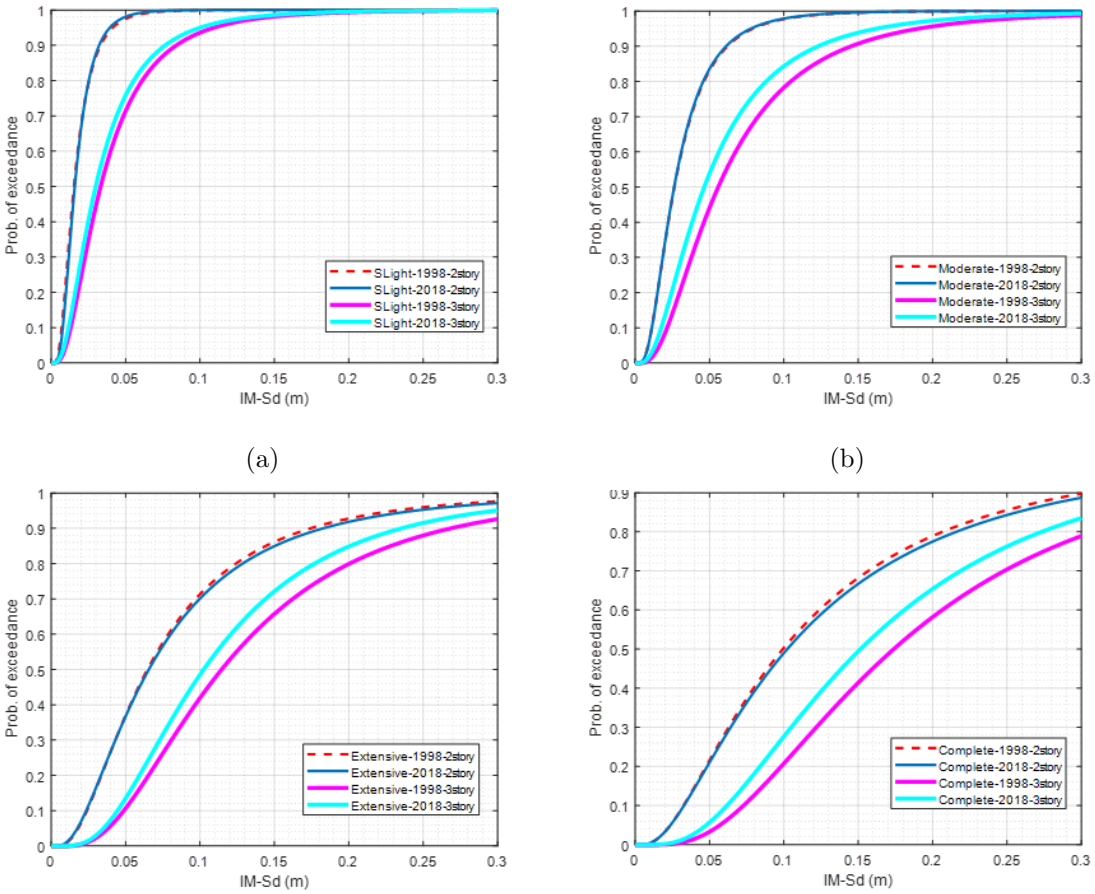

Figure 5.1. Comparison of fragility curves of 2 and 3-story buildings in the x-direction according to the TSC 1998 and TSC 2018 for different damage states (a) slight damage state, (b) moderate damage state, (c) extensive damage state, (d) complete damage state, IM(Sd)-EDP(MIDR).

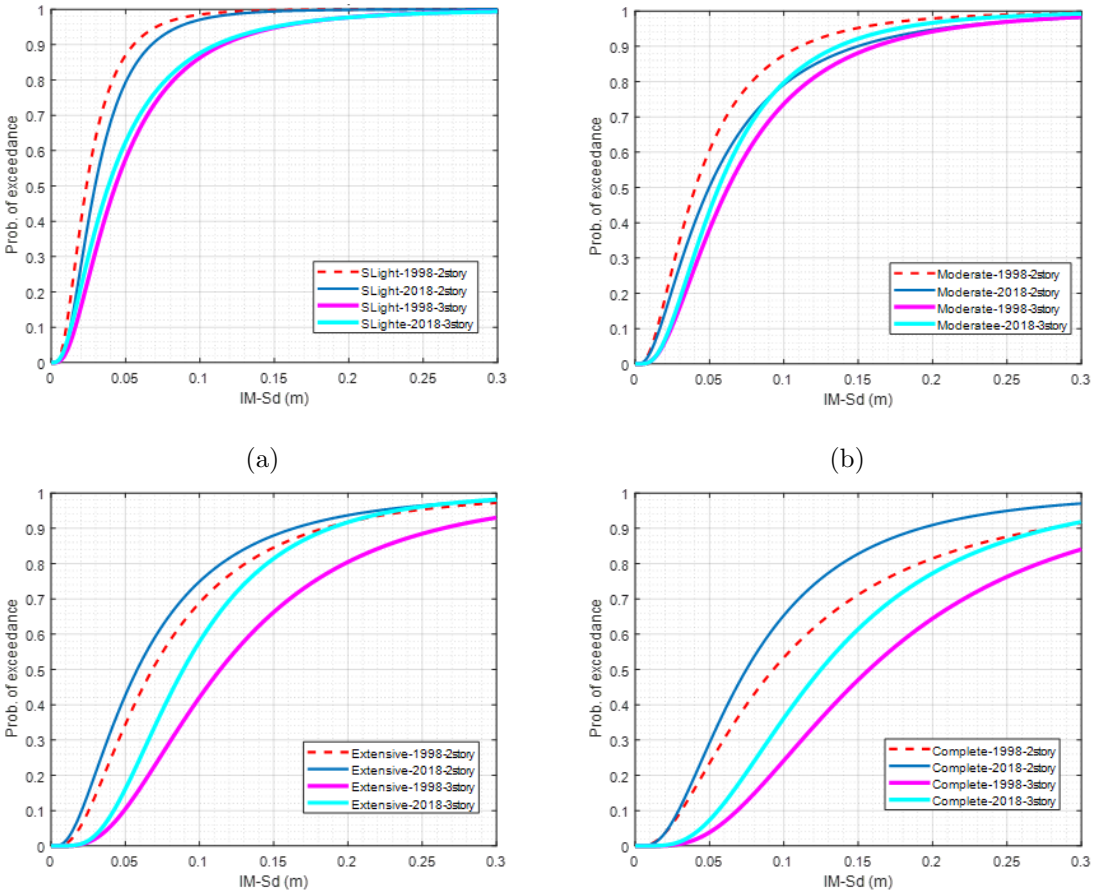

Figure 5.2. Comparison of fragility curves of 2 and 3-story buildings in the x-direction according to the TSC 1998 and TSC 2018 for different damage states (a) slight damage state, (b) moderate damage state, (c) extensive damage state, (d) complete damage state, IM(Sd)-EDP(D_{top}).

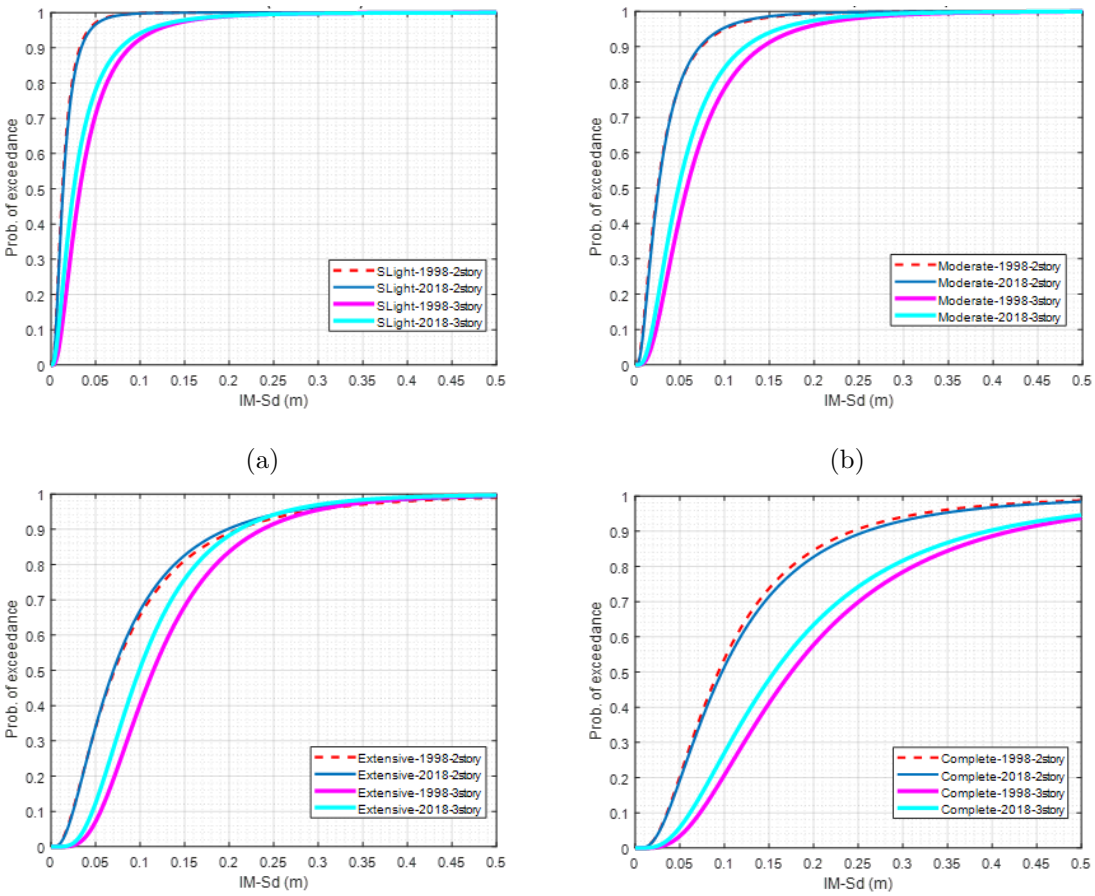

Figure 5.3. Comparison of fragility curves of 2 and 3-story buildings in the y-direction according to the TSC 1998 and TSC 2018 for different damage states (a) slight damage state, (b) moderate damage state, (c) extensive damage state, (d) complete damage state, IM(Sd)-EDP(MIDR).

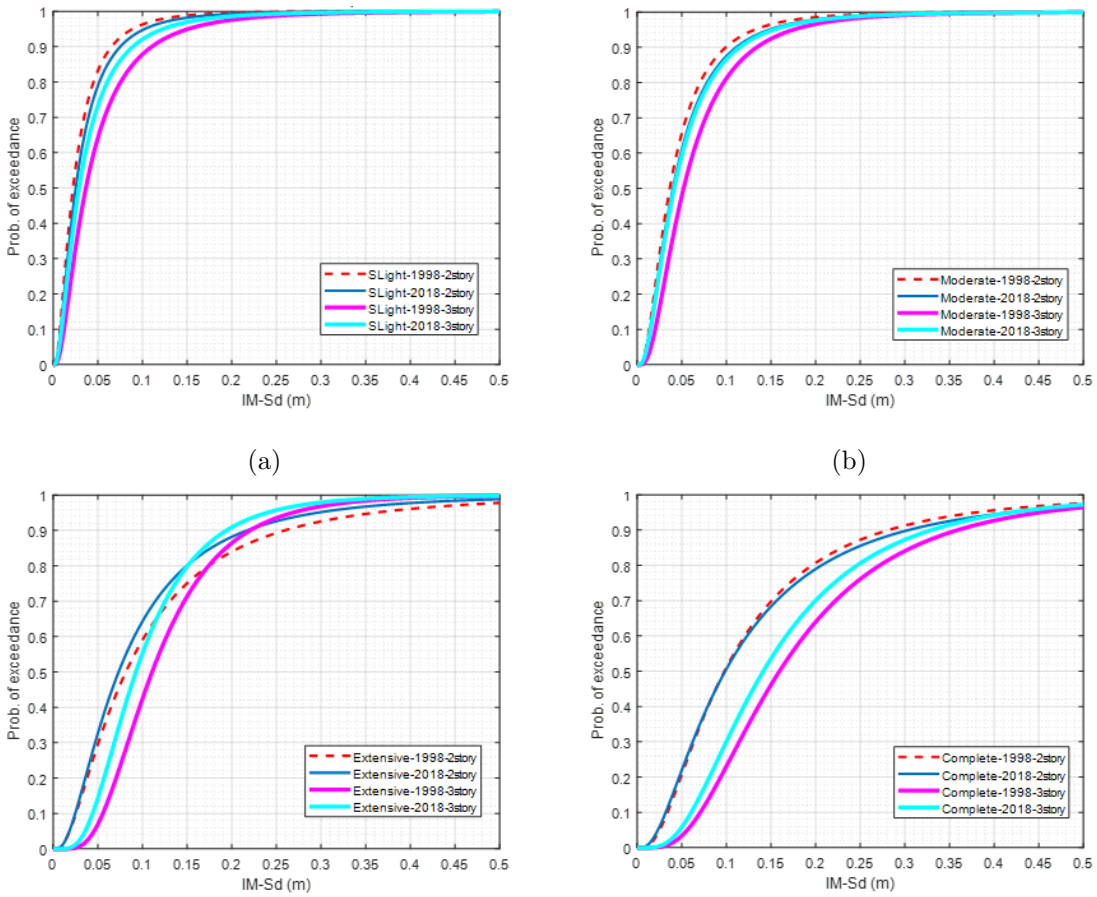

Figure 5.4. Comparison of fragility curves of 2 and 3-story buildings in the y-direction according to the TSC 1998 and TSC 2018 for different damage states (a) slight damage state, (b) moderate damage state, (c) extensive damage state, (d) complete damage state, IM(Sd)-EDP(D_{top}).

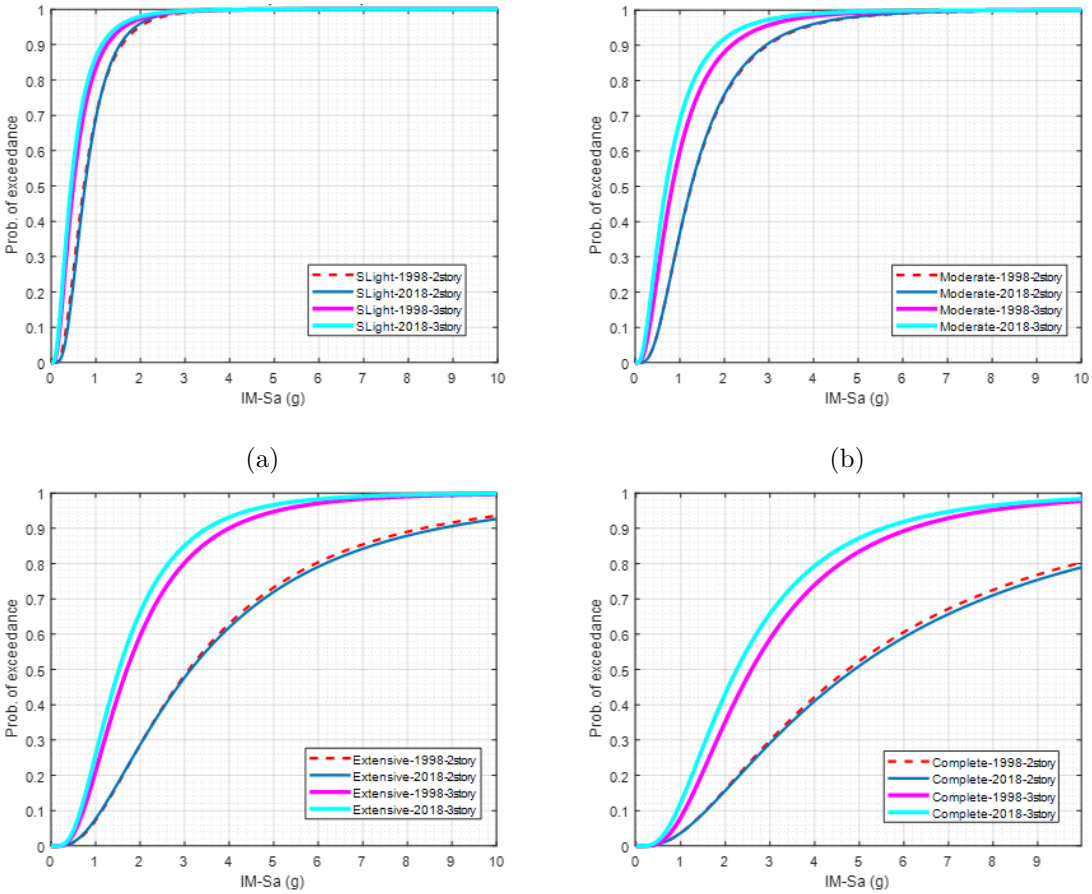

Figure 5.5. Comparison of fragility curves of 2 and 3-story buildings in the x-direction according to the TSC 1998 and TSC 2018 for different damage states (a) slight damage state, (b) moderate damage state, (c) extensive damage state, (d) complete damage state, IM(Sa)-EDP(MIDR).

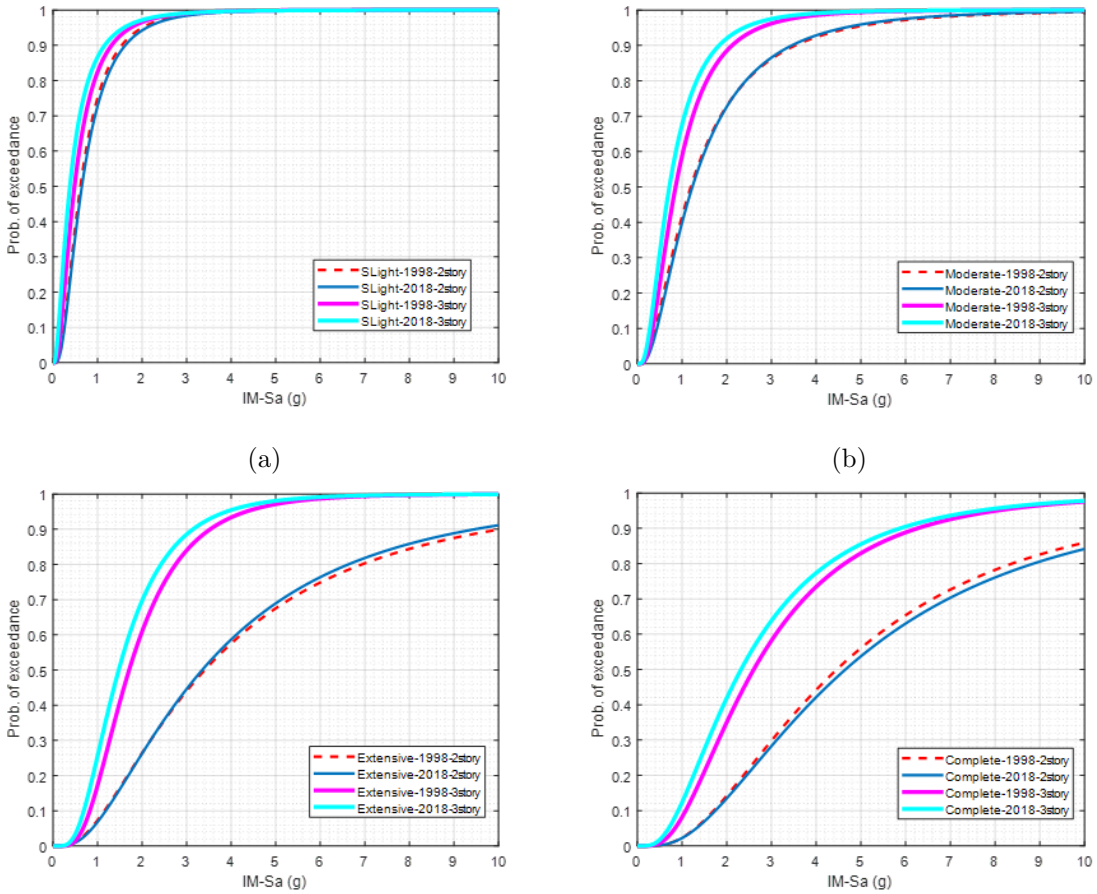

Figure 5.6. Comparison of fragility curves of 2 and 3-story buildings in the y-direction according to the TSC 1998 and TSC 2018 for different damage states (a) slight damage state, (b) moderate damage state, (c) extensive damage state, (d) complete damage state, IM(Sa)-EDP(MIDR).

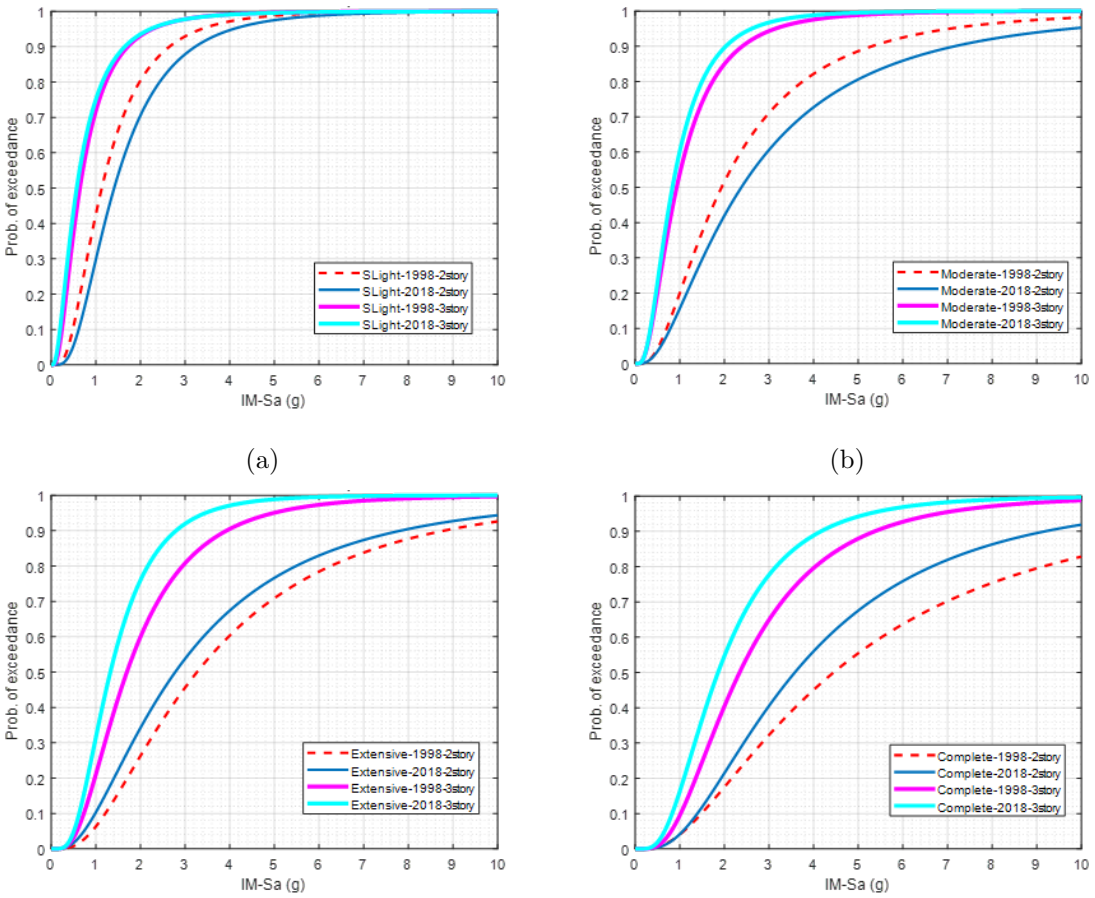

Figure 5.7. Comparison of fragility curves of 2 and 3-story buildings in the x-direction according to the TSC 1998 and TSC 2018 for different damage states (a) slight damage state, (b) moderate damage state, (c) extensive damage state, (d) complete damage state, IM(Sa)-EDP(D_{top}).

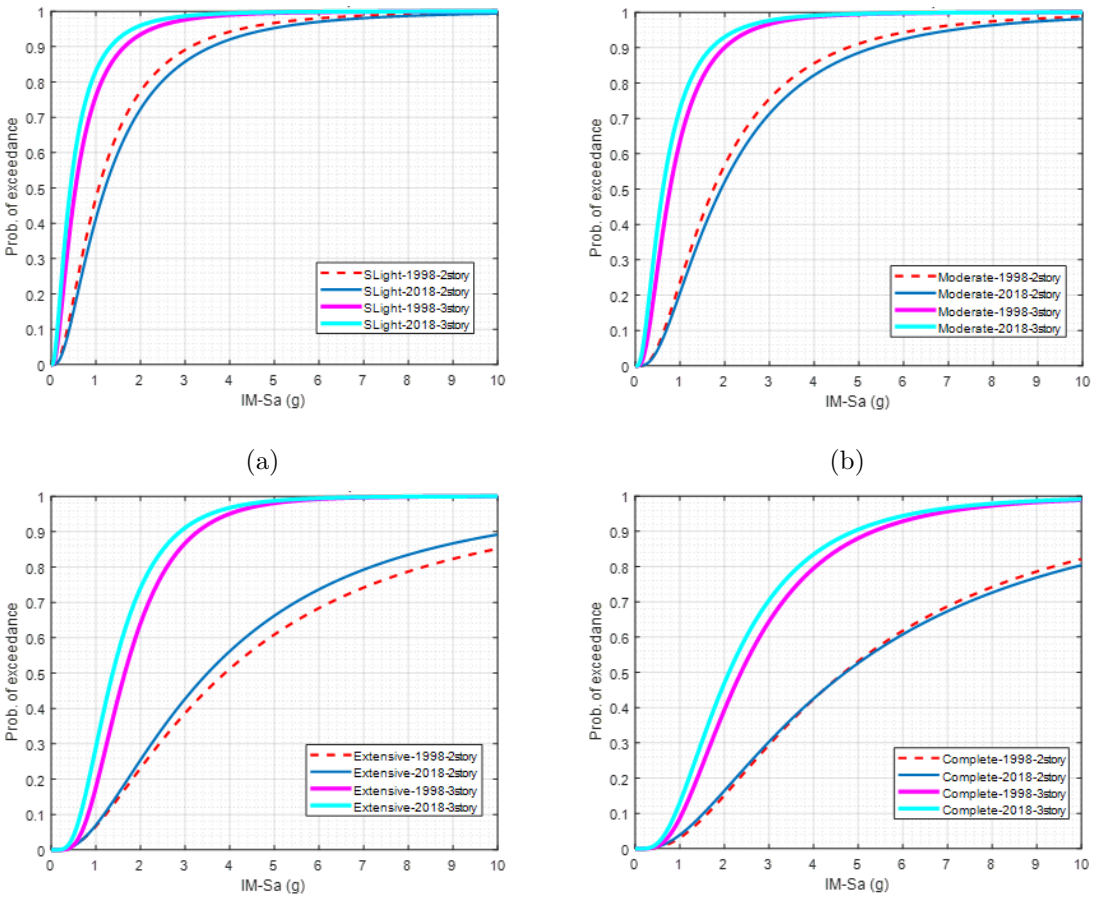

Figure 5.8. Comparison of fragility curves of 2 and 3-story buildings in the y-direction according to the TSC 1998 and TSC 2018 for different damage states (a) slight damage state, (b) moderate damage state, (c) extensive damage state, (d) complete damage state, IM(Sa)-EDP(D_{top}).

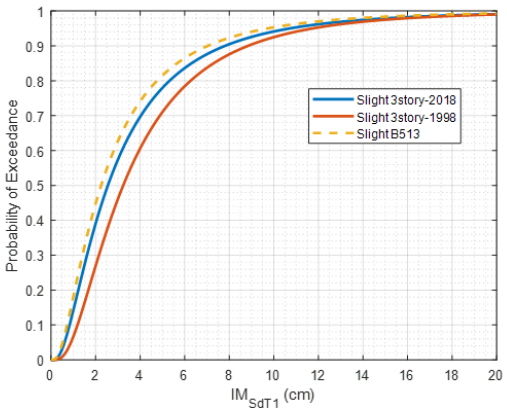

(a) Fragility curves for slight damage state

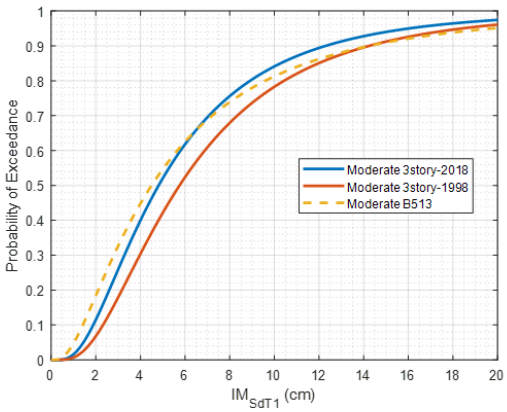

(b) Fragility curves for moderate damage state

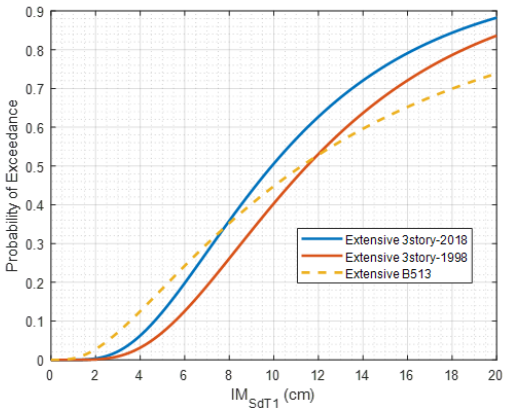

(c) Fragility curves for extensive damage state

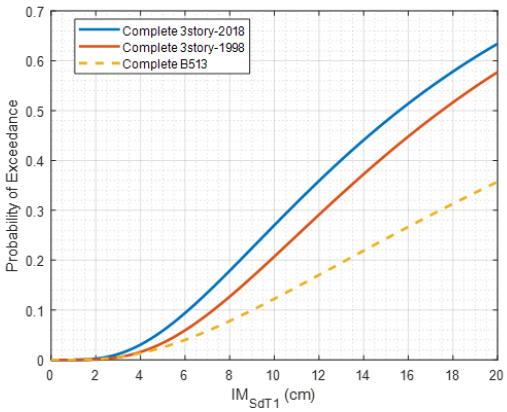

(d) Fragility curves for complete damage state

Figure 5.9. Comparison of fragility curves for different damage states for buildings which are 3-story buildings designed per TSC 2018, 3-story buildings per TSC 1998, and B513 buildings for different damage states, IM(Sd)-EDP(MIDR).

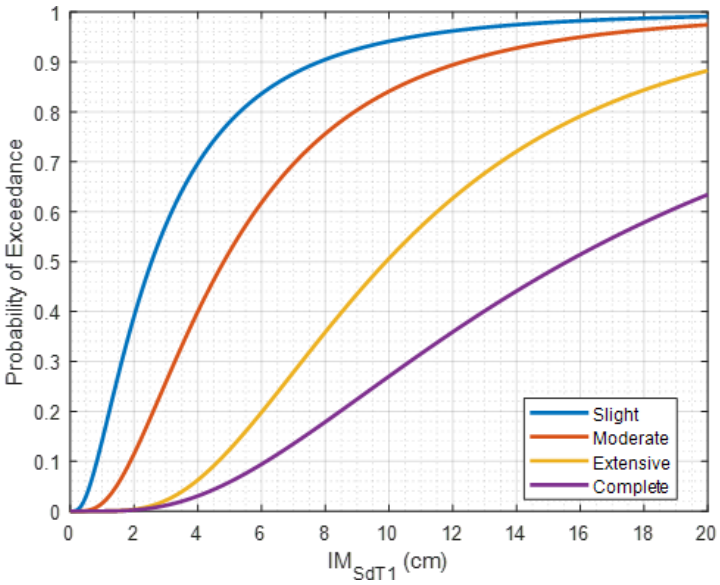

(a)

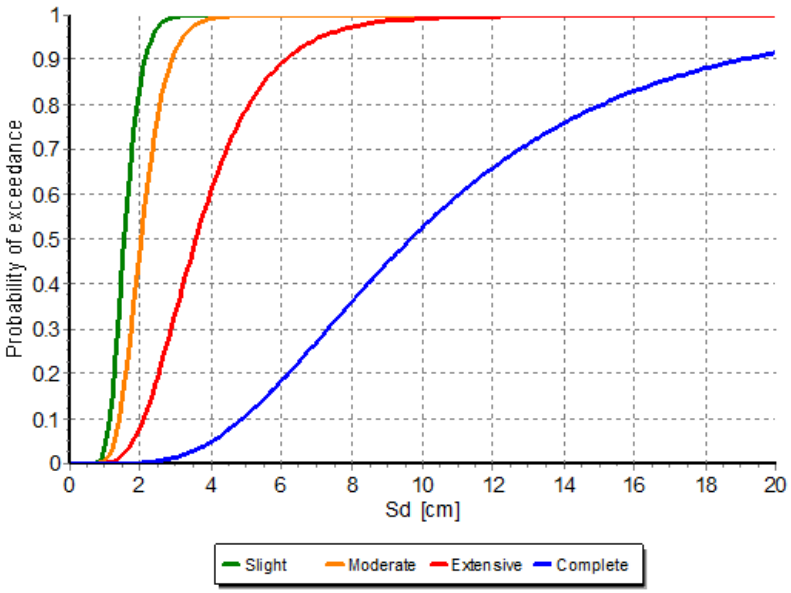

(b)

Figure 5.10. Comparison of fragility curves for different damage states,(a) Fragility curves for 3-story buildings designed per TSC 2018, (b) Fragility curves for prototype buildings designed to simulate the existing Euro-Mediterranean buildings (Greece, Italy, Turkey in particular) (source: Ahmed at al. 2010,RC).

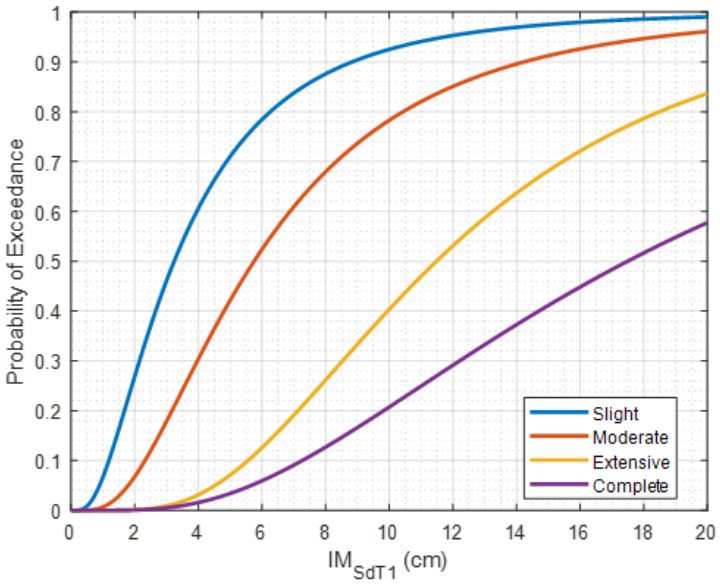

(a)

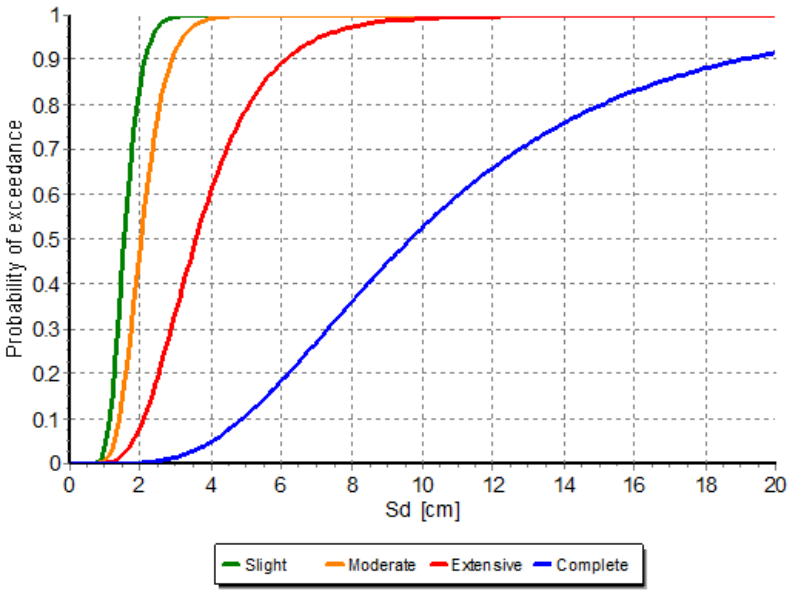

(b)

Figure 5.11. Comparison of fragility curves for different damage states, (a) Fragility curves for 3-story buildings designed per TSC 1998,(b) Fragility curves for prototype buildings designed to simulate the existing Euro-Mediterranean buildings (Greece, Italy, Turkey in particular) (source: Ahmed at al. 2010,RC).

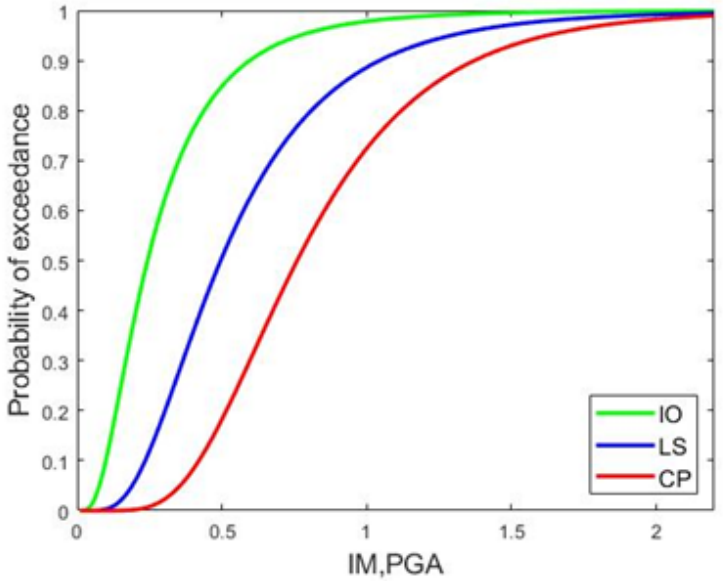

(a)

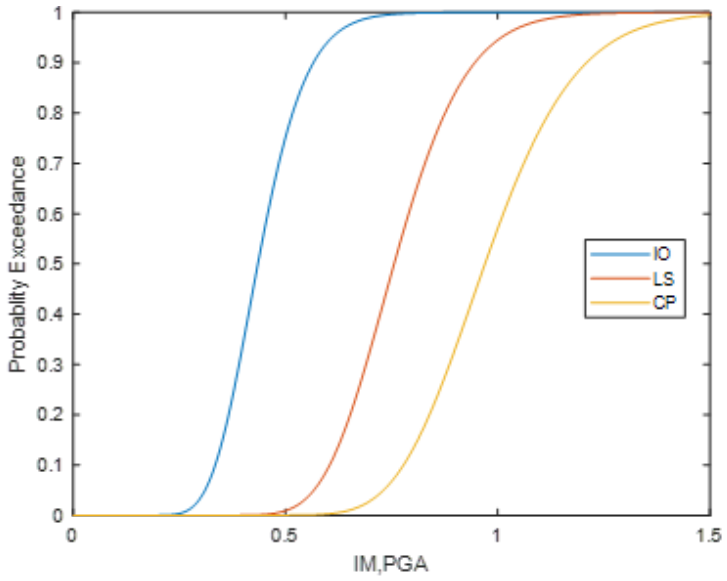

(b)

Figure 5.12. Comparison of fragility curves for different damage states,(a) Fragility curves for 3-story building at location-1 designed per TSC 2018, (b) Fragility curves for 4 storeys building designed per TSC 1998, 25MPa concrete strength, lateral reinforcement detailing conforms the corresponding code (source: H.B. Ozmen, M. Inel, E. Meral and M. Bucakli, "Vulnerability of Low and Mid-Rise Reinforced Concrete Buildings in Turkey", 14ECEE, Ohrid, 2010).

6. CONCLUSION

In this study, fragility functions are developed and compared for low-rise (2 and 3-story), reinforced concrete (RC), moment-resisting frame (MRF) buildings, which are designed per the Turkish Seismic Codes (TSC) released in 1998 and 2018, at eight different locations in Istanbul, Turkey.

To generate the fragility functions for the buildings, multiple stripe analysis (MSA) together with the maximum likelihood estimation (MLE) method is utilized. Spectral displacement (Sd) and spectral acceleration (Sa) are selected as the intensity measure (IM) parameters whereas the maximum inter-story drift ratio (MIDR) and top displacement (Dtop) are used as engineering demand parameters (EDP). The fragility functions are developed for four damage states which are defined as slight damage, moderate damage, extensive damage, and complete damage.

With regards to the comparison of fragility functions in terms of the seismic codes, the developed fragility functions show that 2-story buildings designed per TSC 1998 have a higher probability of exceedance than the 2-story buildings designed per TSC 2018, however, the 3-story buildings designed per TSC 2018 have a larger probability of exceedance than the 3-story buildings designed per TSC 1998 for all damage states (slight, moderate, extensive and complete). The reason for the 3-story buildings designed per TSC 2018 have a higher probability of exceedance is because TSC 1998 resulted in higher design base shear forces in the preliminary design of 3-story buildings which, in turn, gave rise to a higher amount of reinforcement in the structural members (beams and columns) of the 3-story buildings designed per TSC 1998. This means that TSC 2018 gives lower base shear forces at some locations due to its grid-based spectral parameters for short and long periods (Ss and S1). However, in TSC 1998, a single acceleration coefficient is considered for a wide region which, in turn, gives rise to high base shear forces at the locations where TSC 2018 gives lower base shear forces.

Regarding the comparison of the fragility curves in terms of different IMs (Sd

and Sa), when Sd is selected as the IM, the 3-story buildings have less probability of exceedance than the 2-story buildings. However, when Sa is selected as IM, the probability of exceedance for the 2-story buildings is less than that of the 3-story buildings. This is because when Sa is used as IM, all the Sa values for IM levels (stripes) are the same for the two types of buildings (2 and 3 story). However, when Sd is used as IM, Sd values for IM levels (stripes) for the two types of buildings are different since the natural vibration periods of the two types of buildings are different.

REFERENCES

1. Erdik, M., "Earthquake risk assessment", *Bulletin of Earthquake Engineering*, Vol. 15, No. 12, pp. 5055–5092, 2017.

2. Porter, K., "A beginner's guide to fragility, vulnerability, and risk", *Encyclopedia of earthquake engineering*, Vol. 2015, pp. 235–260, 2015.

3. Duran, H. İ., "PGV Based No-Code Mid-Rise Reinforced Concrete Frame-Type Building Fragilities in İstanbul", *M.Sc. Thesis, Department of Earthquake Engineering, Bogazici University, İstanbul, Turkey,*, 2020.

4. Akkar, S. and Ö. Özen, "Effect of peak ground velocity on deformation demands for SDOF systems", *Earthquake engineering & structural dynamics*, Vol. 34, No. 13, pp. 1551–1571, 2005.

5. FEMA-356, N., *NEHRP, Prestandard and commentary for the seismic rehabilitation of buildings*, Tech. rep., Report, 2000.

6. Hancilar, U. and E. Çaktı, "Fragility functions for code complying RC frames via best correlated IM–EDP pairs", *Bulletin of Earthquake Engineering*, Vol. 13, No. 11, pp. 3381–3400, 2015.

7. D'Ayala, D., A. Meslem, D. Vamvatsikos, K. Porter, T. Rossetto and V. Silva, "Guidelines for analytical vulnerability assessment—Low/mid-rise (GEM Technical Report No. 2014–12 V1. 0.0).", , 2019.

8. Hancilar, U., E. Çaktı, M. Erdik, G. E. Franco and G. Deodatis, "Earthquake vulnerability of school buildings: Probabilistic structural fragility analyses", *Soil Dynamics and Earthquake Engineering*, Vol. 67, pp. 169–178, 2014.

9. Kirçil, M. S. and Z. Polat, "Fragility analysis of mid-rise R/C frame buildings",

Engineering Structures, Vol. 28, No. 9, pp. 1335–1345, 2006.

10. Tüzün, C., "A Seismic Vulnerability Analysis Procedure for Urban Loss Assessment", *M.Sc. Thesis, Department of Earthquake Engineering, Bogazici University, İstanbul, Turkey,*, 2008.

11. Dolağan, İ., "Development of Peak Ground Acceleration (PGA) Based Pre-Code Reinforced Concrete Frame Building Fragilities for İstanbul", *M.Sc. Thesis, Department of Earthquake Engineering, Bogazici University, İstanbul, Turkey,*, 2019.

12. Ozmen, H., M. Inel, S. Senel and A. Kayhan, "Load carrying system characteristics of existing Turkish RC building stock", *International Journal of Civil Engineering*, Vol. 13, No. 1, pp. 76–91, 2015.

13. Computer and Structures, Inc., (2019). ETABS V18, *ETABS V18*, 2019.

14. Filippou, F. C., E. P. Popov and V. V. Bertero, "Effects of bond deterioration on hysteretic behavior of reinforced concrete joints", , 1983.

15. (ATC), A. T. C., "Preliminary Evaluation of Methods for Defining Performance, ATC-58-2", , 2003.

16. FEMA, "HAZUS MH MR4 Earthquake Technical Manual Multi-hazard Loss Estimation Methodology", *Prepared by the National Institute of Building Sciences for FEMA*, 2003.

17. Vamvatsikos, D. and C. A. Cornell, "Incremental dynamic analysis", *Earthquake engineering & structural dynamics*, Vol. 31, No. 3, pp. 491–514, 2002.

18. The Mathworks, Inc., Natick, Massachusetts, *MATLAB version (R2019a)*, 2019.

19. Baker, J. W., "Efficient analytical fragility function fitting using dynamic structural analysis", *Earthquake Spectra*, Vol. 31, No. 1, pp. 579–599, 2015.

APPENDIX A: BUILDING REINFORCEMENT RATIO FOR LOAD CARRYING MEMBERS

The examples of designed buildings for location 1 are given in this section. The following tables summarize the selected amount of steel bars for buildings at location 1.

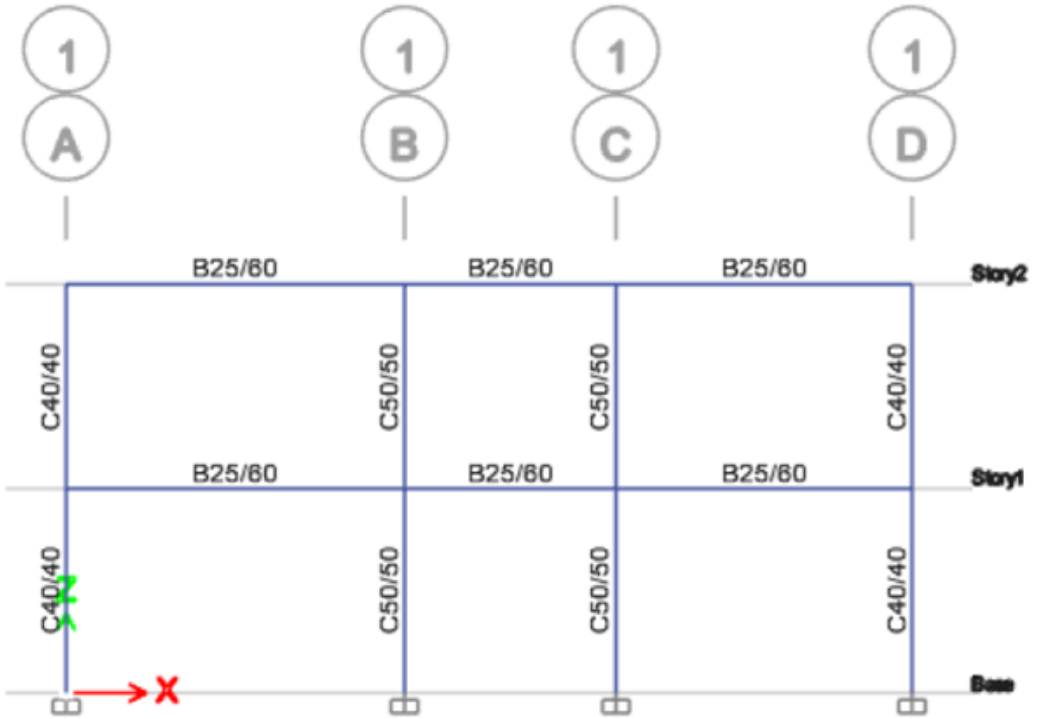

(a)

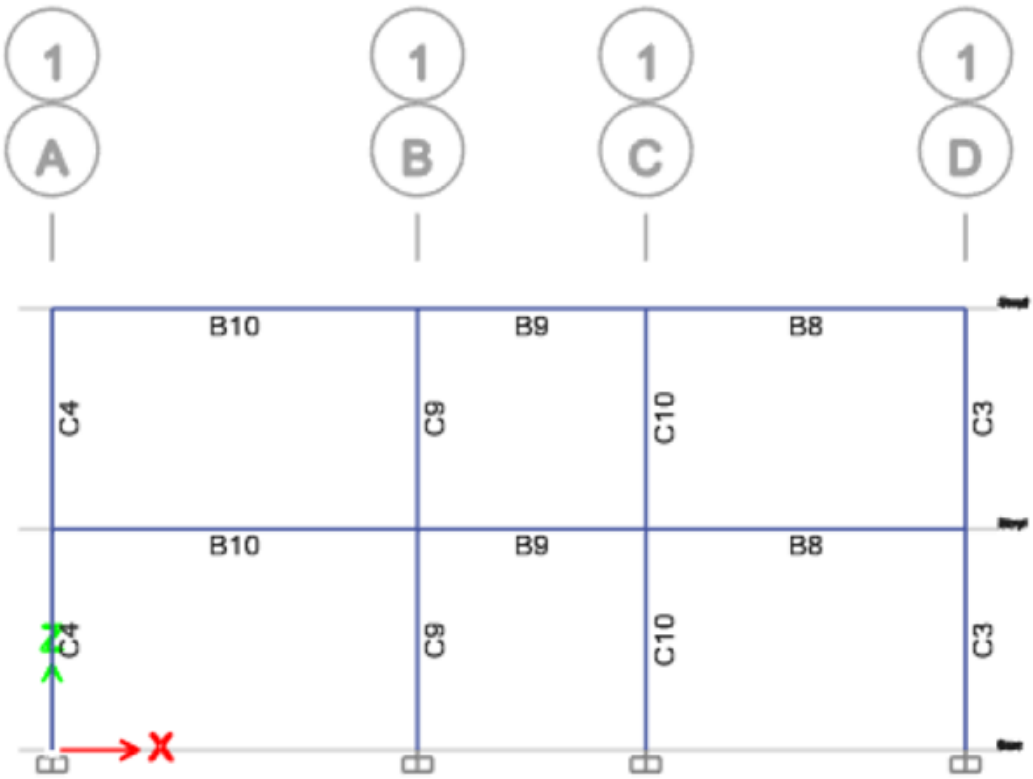

(b)

Figure A.1. 2-story building model.

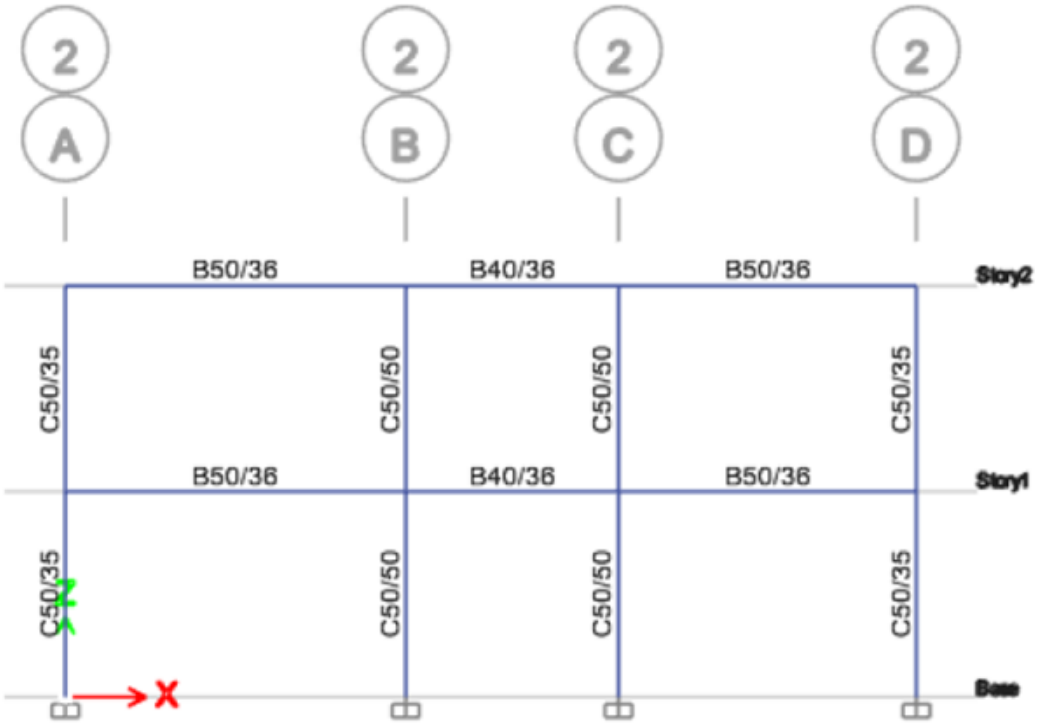

(a)

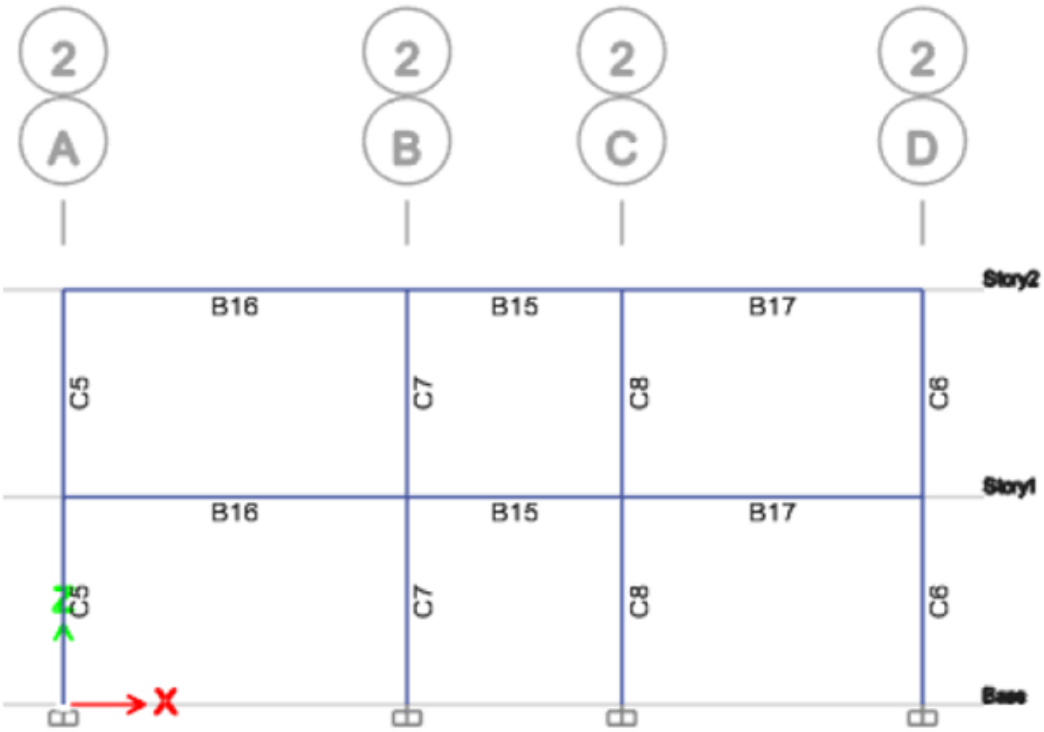

(b)

Figure A.2. 2-story building model. cont.

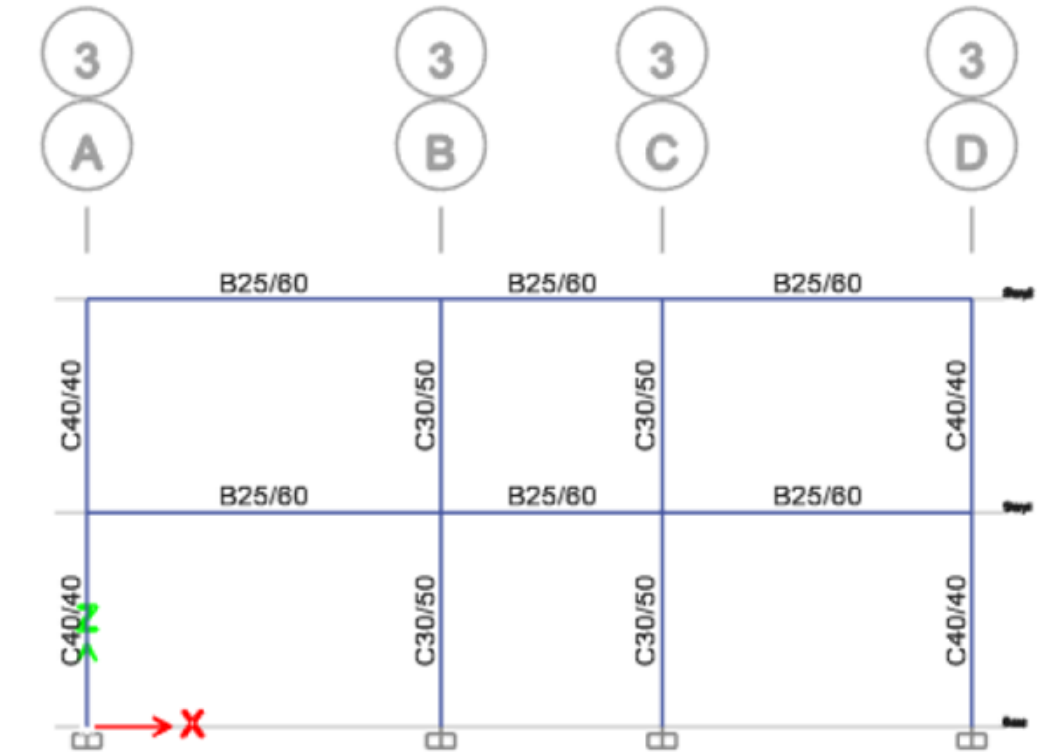

(a)

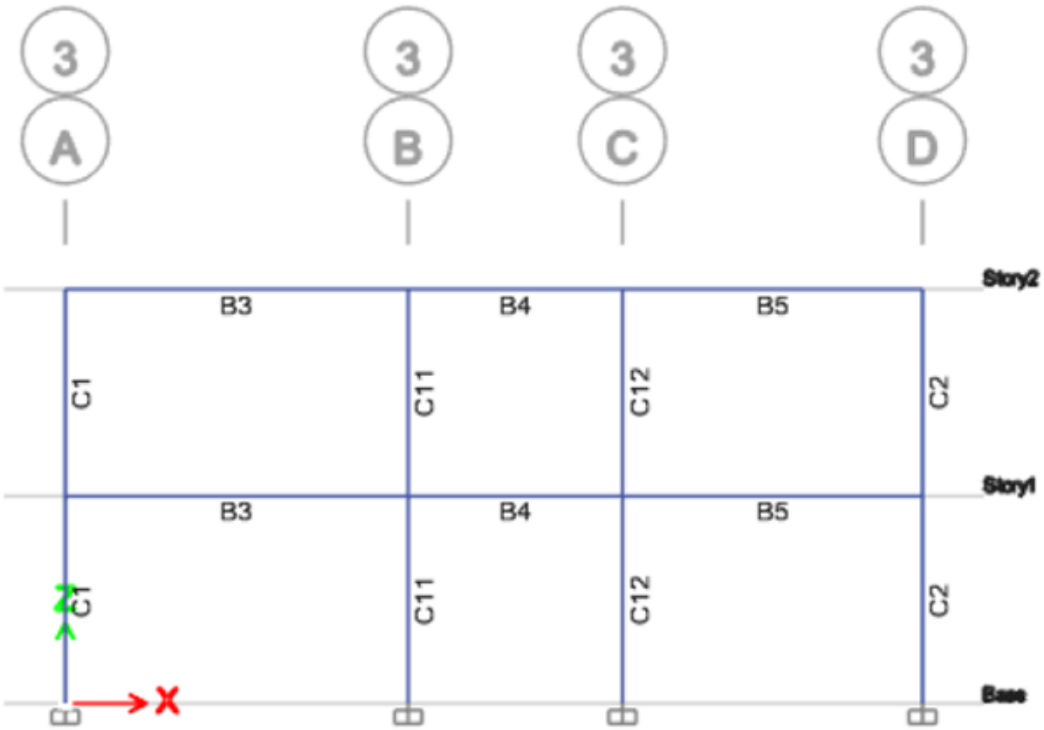

(b)

Figure A.3. 2-story building model. cont.

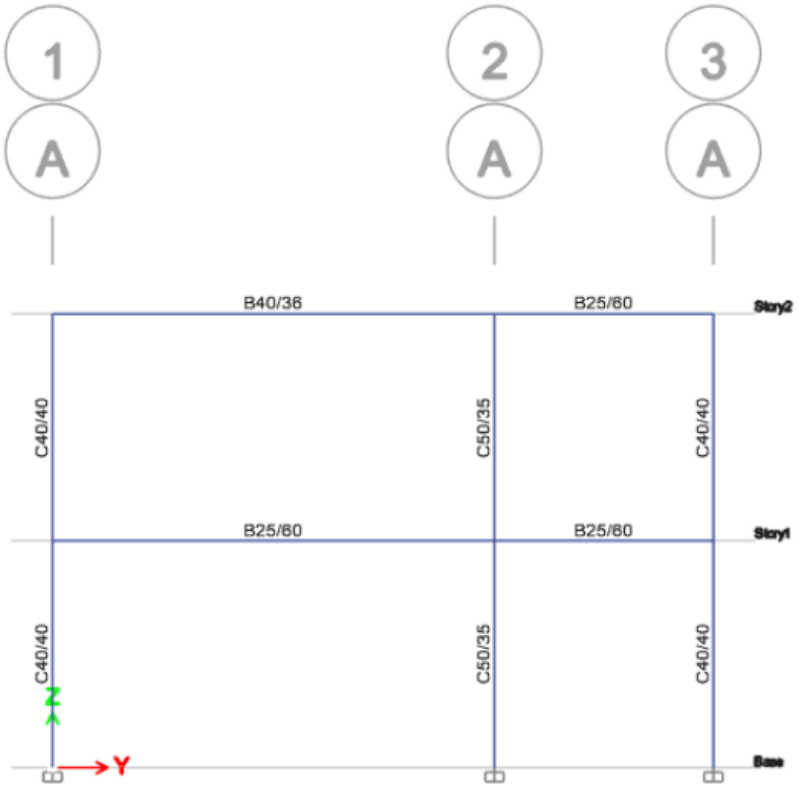

(a)

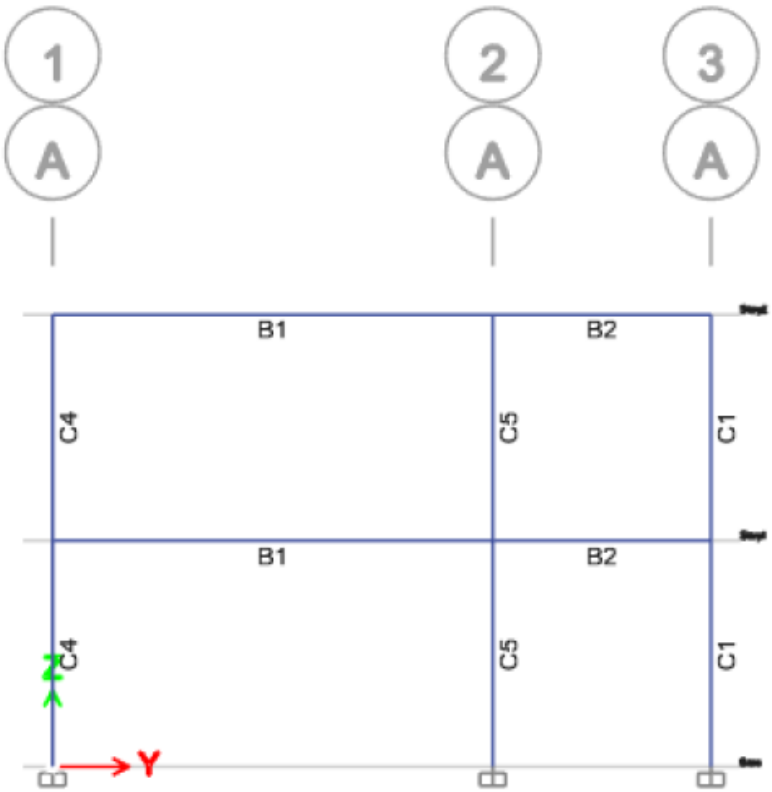

(b)

Figure A.4. 2-story building model. cont.

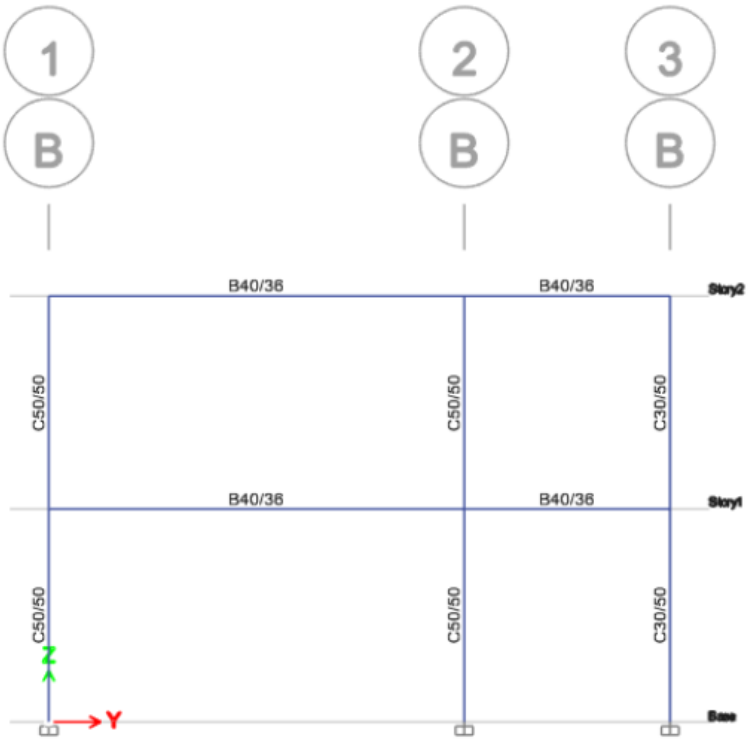

(a)

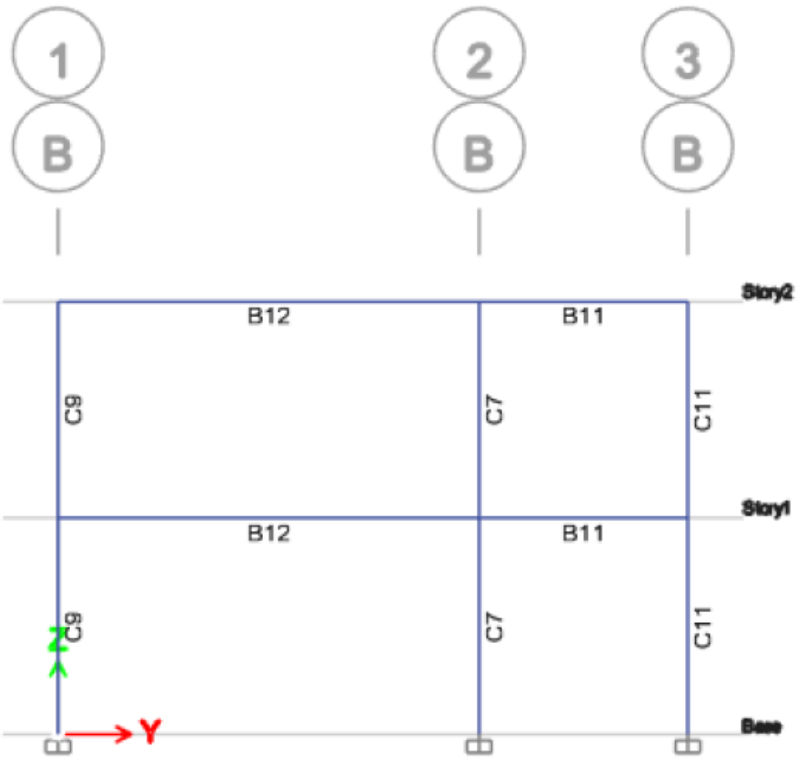

(b)

Figure A.5. 2-story building model. cont.

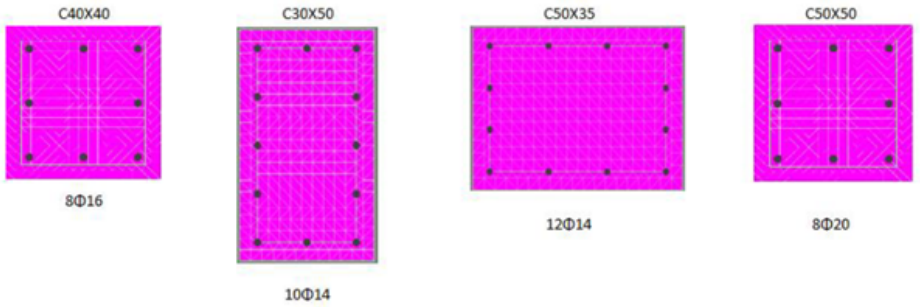

(a)

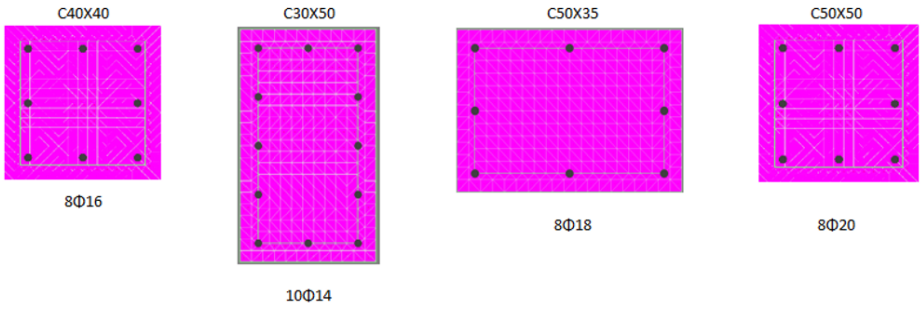

(b)

Figure A.6. (a) 2-story building model designed per TSC 1998, (b) 2-story building model designed per TSC 2018

B10	
Top	Bottom
4Φ12	2Φ12
0	1Φ14

B8	
Top	Bottom
4Φ12	2Φ12
0	1Φ14

B9	
Top	Bottom
4Φ12	2Φ12
0	1Φ14

(a)

B16	
Top	Bottom
2Φ12	2Φ12
2Φ14	1Φ16

B17	
Top	Bottom
2Φ12	2Φ12
2Φ14	1Φ16

B15	
Top	Bottom
2Φ12	2Φ12
1Φ16	1Φ12

(b)

Figure A.7. Reinforcement for 2-story building model designed per TSC 1998.

B3

Top	Bottom
4Φ12	2Φ12
0	1Φ14

B5

Top	Bottom
4Φ12	2Φ12
0	1Φ14

B4

Top	Bottom
4Φ12	2Φ12
0	1Φ14

(a)

B1

Top	Bottom
2Φ12	2Φ12
1Φ16	1Φ12

B2

Top	Bottom
4Φ12	2Φ12
1Φ16	1Φ14

B1-B25/60

Top	Bottom
4Φ12	2Φ12
0	1Φ14

(b)

Figure A.8. Reinforcement for 2-story building model designed per TSC 1998. cont.

B12	
Top	Bottom
2Φ12	2Φ14
3Φ12	1Φ12

B11	
Top	Bottom
2Φ12	2Φ12
1Φ16	1Φ12

(a)

Figure A.9. Reinforcement for 2-story building model designed per TSC 1998. cont.

B10	
Top	Bottom
4Φ12	2Φ16
0	0

B8	
Top	Bottom
4Φ12	2Φ16
0	0

B9	
Top	Bottom
4Φ12	2Φ16
0	0

(a)

B16	
Top	Bottom
2Φ16	3Φ14
1Φ16	0

B17	
Top	Bottom
2Φ16	3Φ14
1Φ16	0

B15	
Top	Bottom
2Φ12	2Φ12
1Φ14	1Φ14

(b)

Figure A.10. Reinforcement for 2-story building model designed per TSC 2018.

B3

Top	Bottom
2Φ16	2Φ16
0	0

B5

Top	Bottom
2Φ16	2Φ16
0	0

B4

Top	Bottom
2Φ16	2Φ16
0	0

(a)

B1

Top	Bottom
2Φ12	2Φ16
1Φ16	0

B2

Top	Bottom
2Φ14	2Φ16
1Φ16	0

B1-B25/60

Top	Bottom
2Φ14	2Φ16
1Φ16	0

(b)

Figure A.11. Reinforcement for 2-story building model designed per TSC 2018. cont.

B12	
Top	Bottom
2Φ14	2Φ12
3Φ14	1Φ16

B11	
Top	Bottom
2Φ12	2Φ12
1Φ16	1Φ14

(a)

Figure A.12. Reinforcement for 2-story building model designed per TSC 2018. cont.

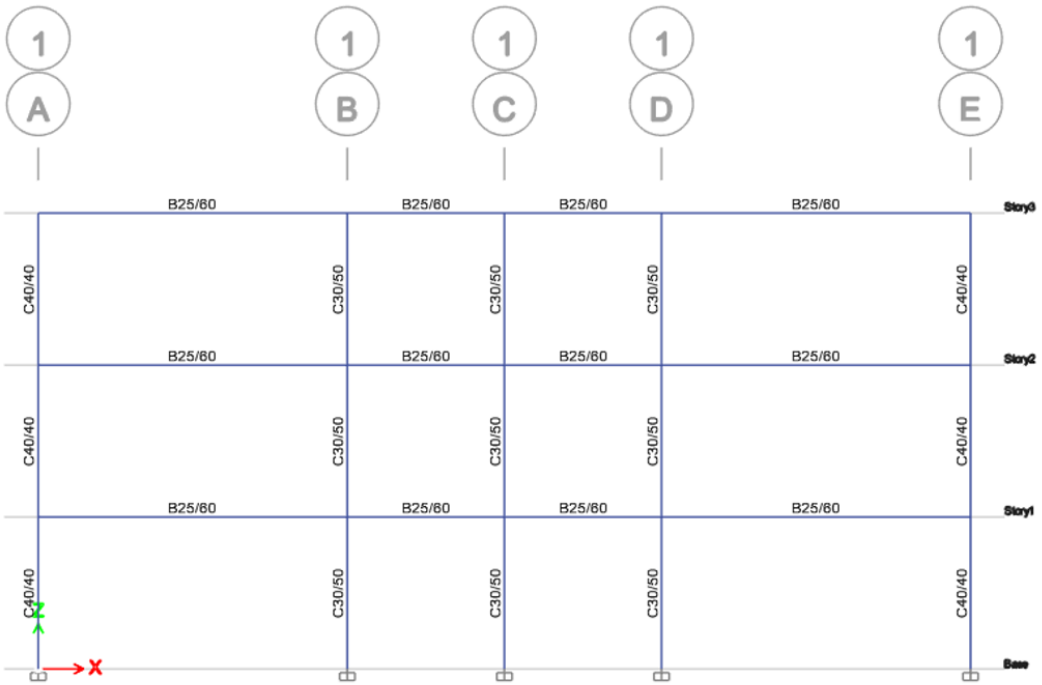

(a)

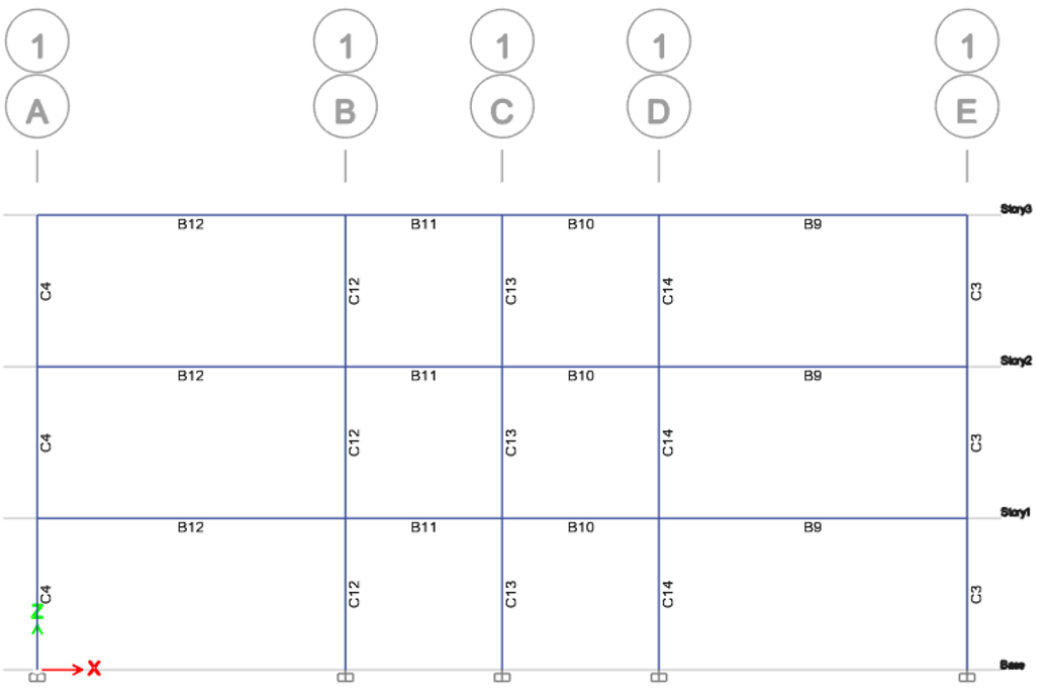

(b)

Figure A.13. 3-story building model.

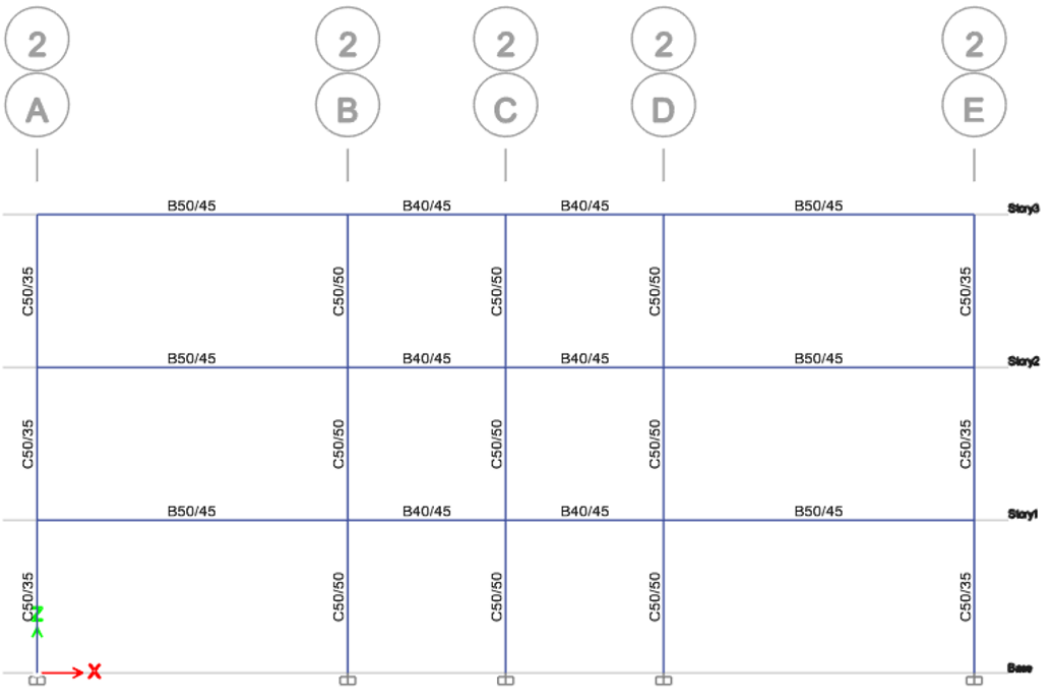

(a)

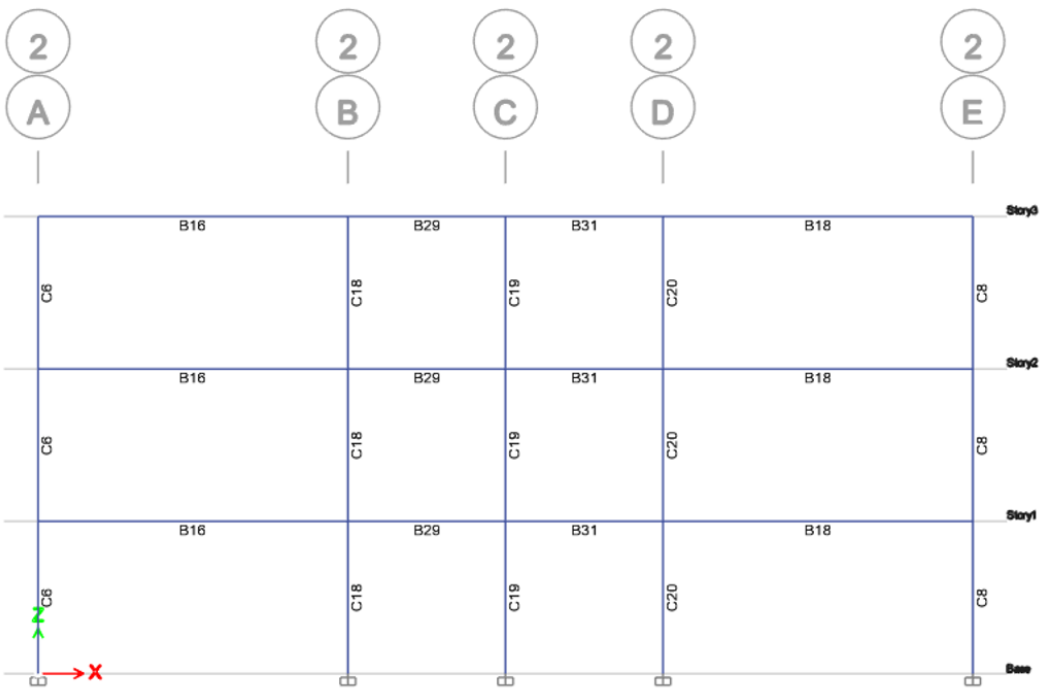

(b)

Figure A.14. 3-story building model. cont.

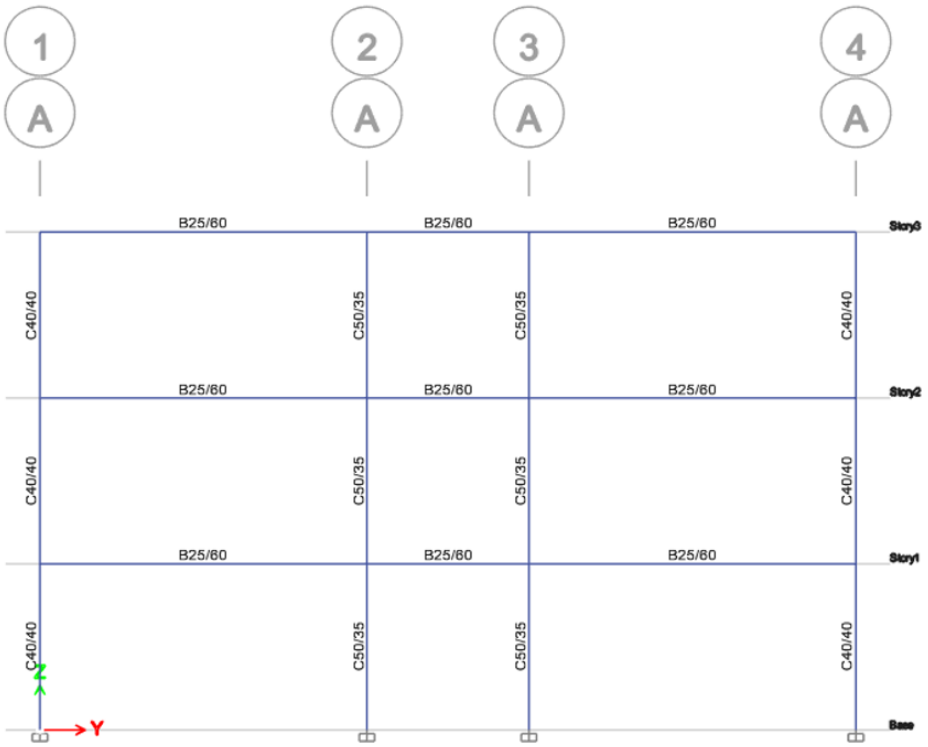

(a)

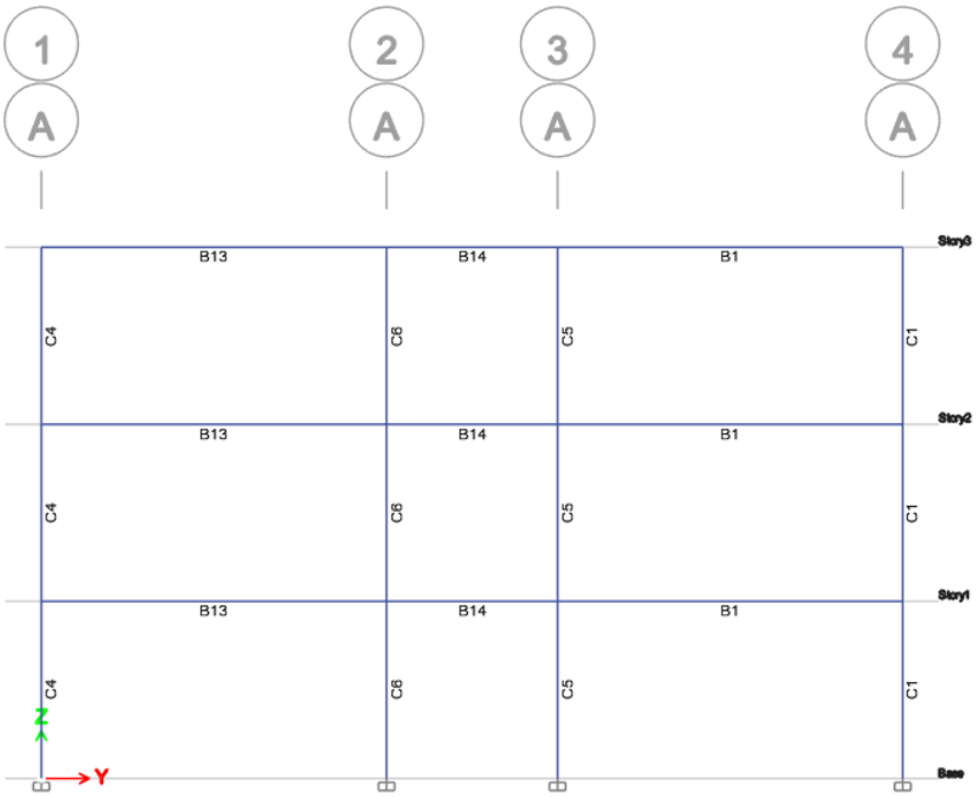

(b)

Figure A.15. 3-story building model. cont.

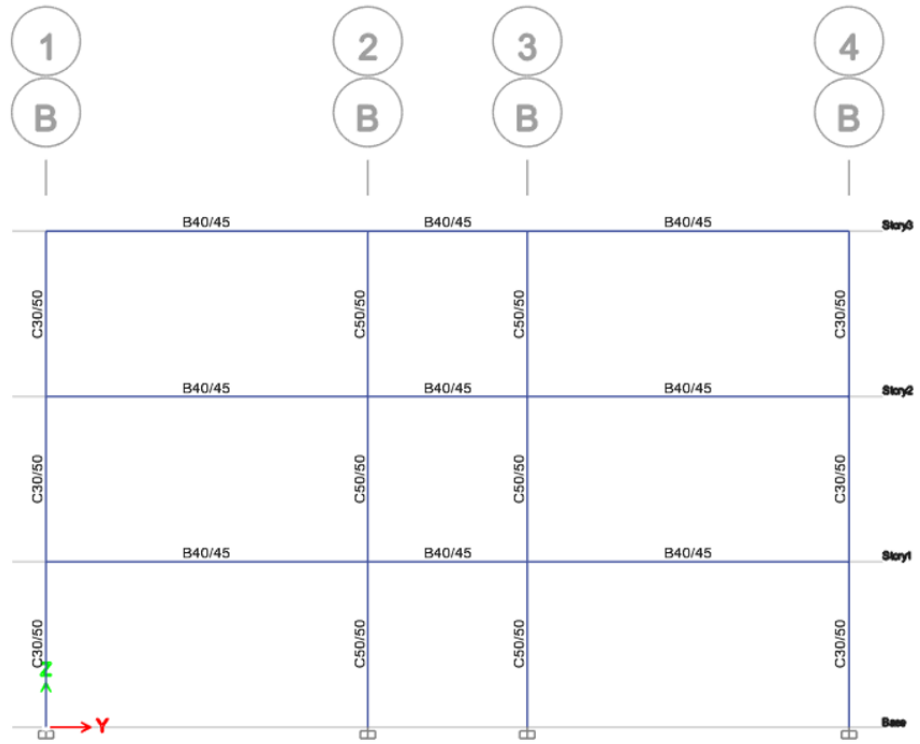

(a)

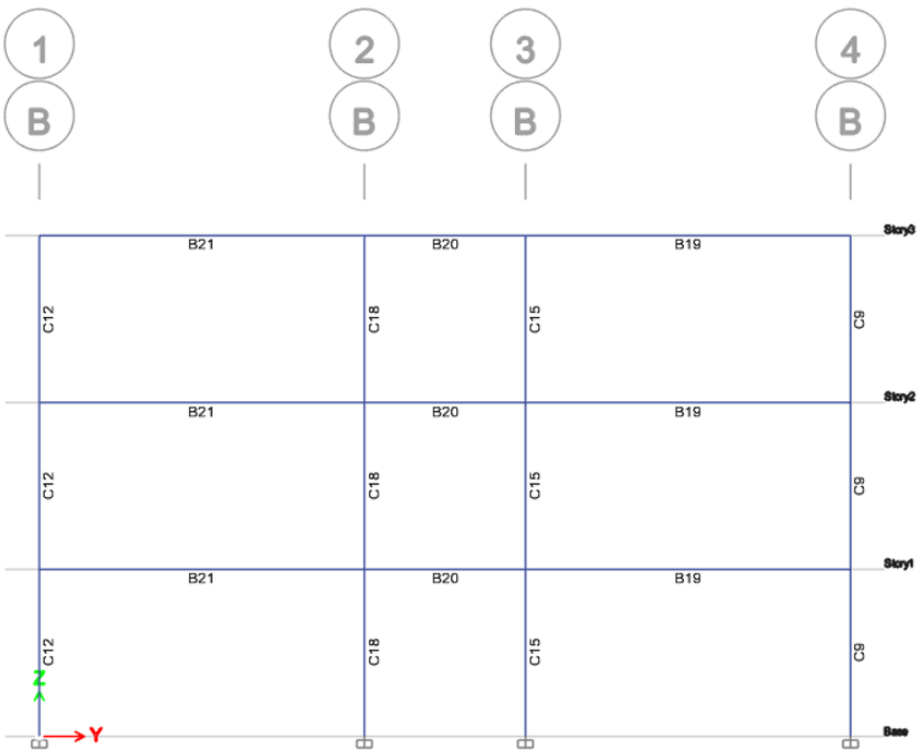

(b)

Figure A.16. 3-story building model. cont.

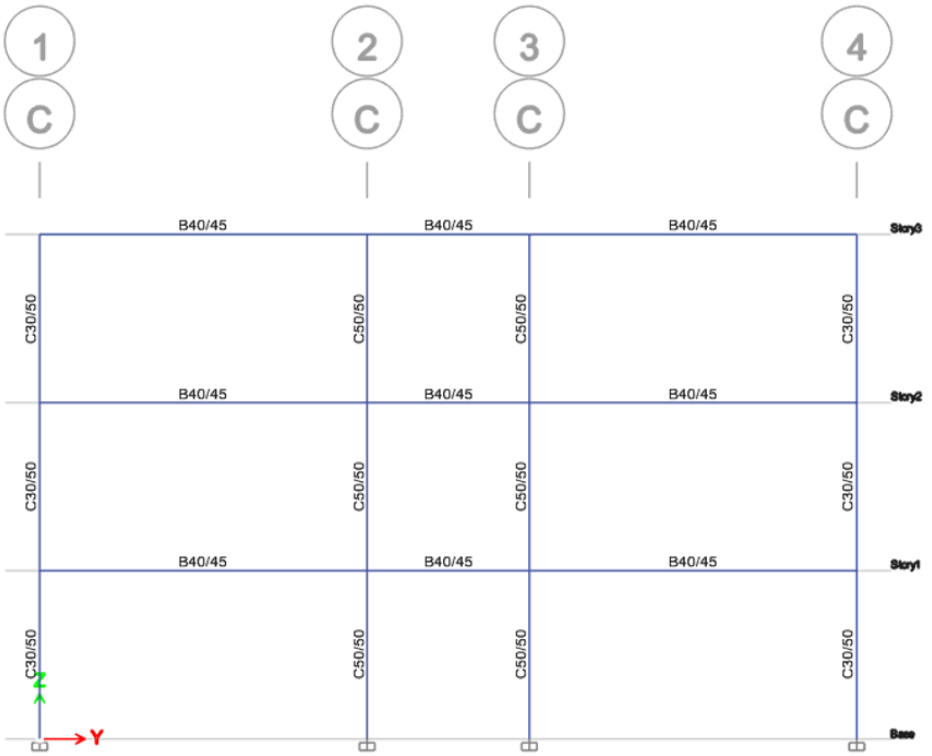

(a)

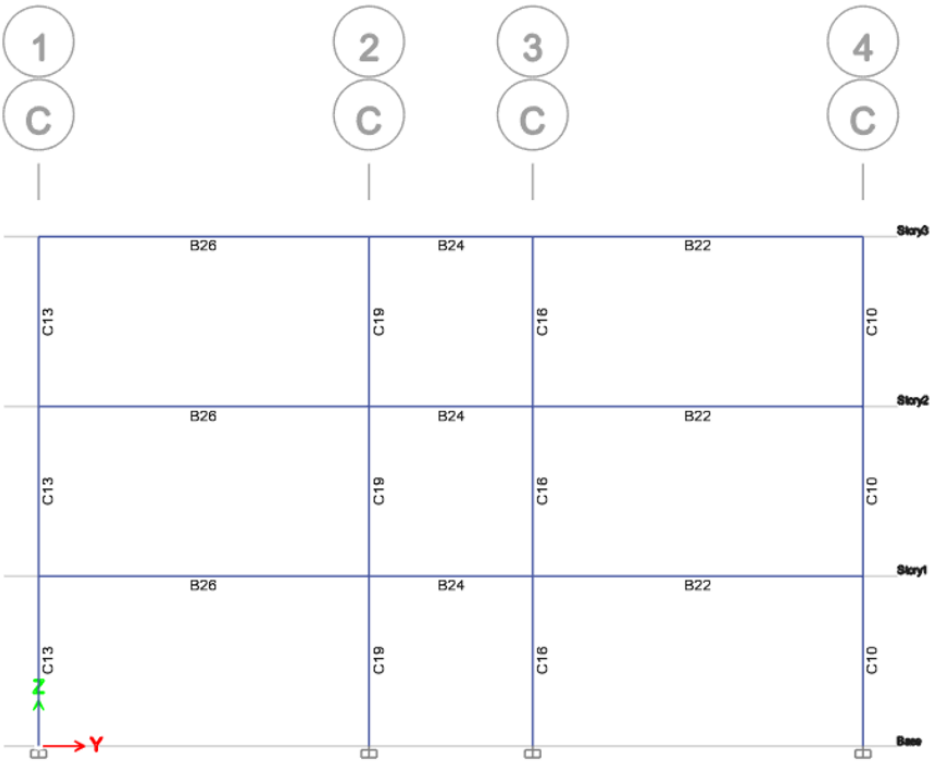

(b)

Figure A.17. 3-story building model. cont.

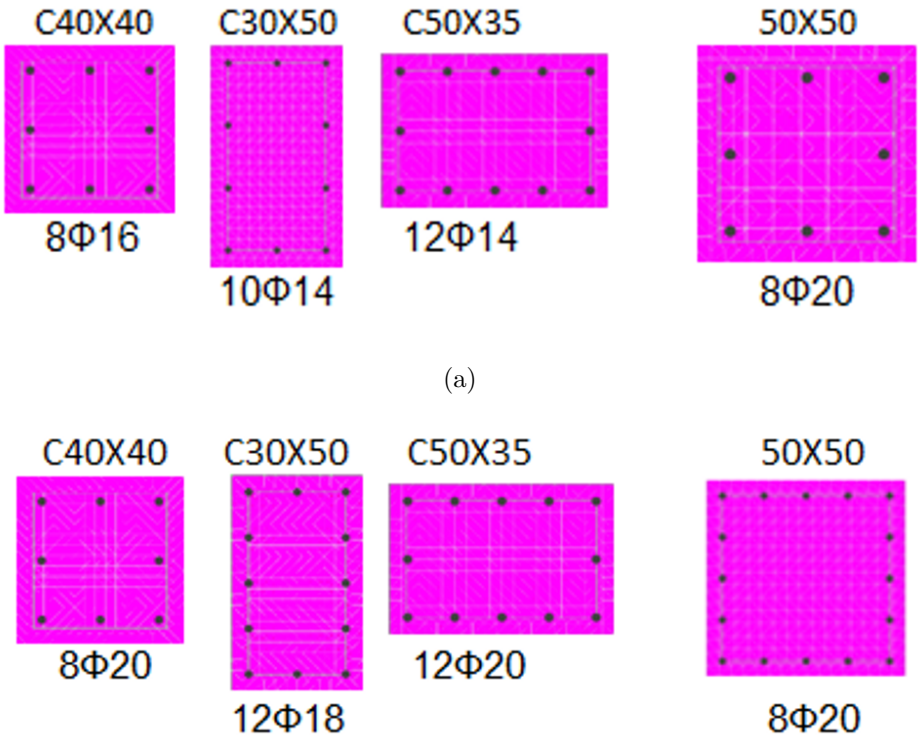

Figure A.18. (a) 3-story building model designed per TSC 1998, (b) 3-story building model designed per TSC 2018

B9	
Top	Bottom
2Φ14	2Φ16
2Φ12	0

B10	
Top	Bottom
2Φ14	2Φ16
1Φ14	0

B11	
Top	Bottom
2Φ14	2Φ16
1Φ14	0

B12	
Top	Bottom
2Φ14	2Φ16
2Φ12	0

(a)

B16	
Top	Bottom
2Φ14	2Φ16
2Φ18	1Φ14

B29	
Top	Bottom
2Φ16	2Φ14
1Φ16	1Φ12

B31	
Top	Bottom
2Φ16	2Φ14
1Φ16	1Φ12

B18	
Top	Bottom
2Φ14	2Φ16
2Φ18	1Φ14

(b)

Figure A.19. Reinforcement for 3-story building model designed per TSC 1998.

B13

Top	Bottom
2Φ14	2Φ16
2Φ14	0

B1

Top	Bottom
2Φ14	2Φ16
2Φ14	0

B14

Top	Bottom
2Φ16	2Φ16
1Φ14	0

(a)

B21

Top	Bottom
2Φ16	2Φ16
2Φ16	1Φ12

B19

	Top	Bottom
Montage	2Φ16	2Φ16
Additional	2Φ16	1Φ12

B20

Top	Bottom
2Φ16	2Φ16
2Φ14	1Φ12

(b)

Figure A.20. Reinforcement for 3-story building model designed per TSC 1998. cont.

B21	
Top	Bottom
2Φ16	2Φ14
2Φ14	1Φ12

B19	
Top	Bottom
2Φ16	2Φ14
2Φ14	1Φ12

B20	
Top	Bottom
2Φ14	2Φ14
3Φ12	1Φ12

(a)

Figure A.21. Reinforcement for 3-story building model designed per TSC 1998. cont.

B9

Top	Bottom
2Φ14	2Φ16
3Φ14	0

B10

Top	Bottom
2Φ14	2Φ16
3Φ14	0

B11

Top	Bottom
2Φ14	2Φ16
3Φ14	0

B12

Top	Bottom
2Φ14	2Φ16
3Φ14	0

(a)

B16

Top	Bottom
2Φ18	2Φ16
3Φ16	1Φ16

B29

Top	Bottom
2Φ16	2Φ16
3Φ14	1Φ14

B31

Top	Bottom
2Φ16	2Φ16
3Φ14	1Φ14

B18

Top	Bottom
2Φ18	2Φ16
3Φ16	1Φ16

(b)

Figure A.22. Reinforcement for 3-story building model designed per TSC 2018.

B13	
Top	Bottom
2Φ16	2Φ16
2Φ16	0

B1	
Top	Bottom
2Φ16	2Φ16
2Φ16	0

B14	
Top	Bottom
2Φ14	3Φ16
3Φ16	0

(a)

B21	
Top	Bottom
2Φ16	3Φ16
3Φ16	0

B19	
Top	Bottom
2Φ16	3Φ16
3Φ16	0

B20	
Top	Bottom
2Φ16	3Φ16
3Φ16	0

(b)

Figure A.23. Reinforcement for 3-story building model designed per TSC 2018. cont.

B21	
Top	Bottom
2Φ16	3Φ16
3Φ16	0

B19	
Top	Bottom
2Φ16	3Φ16
3Φ16	0

B20	
Top	Bottom
2Φ16	3Φ16
3Φ16	0

(a)

Figure A.24. Reinforcement for 3-story building model designed per TSC 2018. cont.